INNOVATIVE ULTRA-LIGHT STRUCTURAL TIMBER SANDWICH PANELS

Mr Siavash Darzi

B.Eng., MEng

School of Engineering and Built Environment

Griffith University

Submitted in Fulfilment of the requirements of the degree of

Doctor of Philosophy

March 2020

Abstract

Sandwich panels are utilized extensively in many industries such as marine, aerospace, and automotive industries due to their high strength-to-weight and stiffness-to-weight ratios. However, sandwich panels have only just started to be utilized in the building industry. Most sandwich panels today consist of two thin and stiff skins and a low-strength foam core, which makes the panels vulnerable under bending action. Furthermore, with the recent global trend towards mid-rise to high-rise timber buildings, more attention is given to lightweight, cost-effective, and particularly sustainable wood products. This study aims to investigate the appropriateness of composite timber sandwich panels made by combining existing commercial wood products with affordable and sustainable local timber and wood waste, to manufacture sandwich panels for building purposes. These composite sandwich panels are manufactured by gluing commercial plywood skins to either bamboo rings to produce Bamboo Core Sandwich (BCS) panels or to peeler core rings to produce Peeler Core Sandwich (PCS) panels.

In the first part of this thesis, a modified Ritz method is developed that can predict the flexural response of a sandwich panel with thick skins and thick-stiff core in one-way and two-way bending configurations. The proposed Ritz formulation is used to evaluate the flexural responses of the proposed BCS and PCS panels with different aspect ratios. To provide comparison, the results are compared with an engineered wood product, Cross-laminated Timber (CLT) panels with almost similar depths. A Finite Element Analysis (FEA) is then developed, validated against Ritz and previous experimental work, to capture the ultimate capacity and failure modes of the panels.

In the second part of this thesis, the proposed panels are manufactured and physically tested in standard bending (using four-point) and shear (using three-point) tests. The optimum adhesive spread rate is identified through conducting shear bond tests. Results are compared to the test results of conventional CLT panels with almost similar depths. The experimental results are interpreted using analytical equations.

In the third part of this thesis, single and double core layer BCS panels are manufactured and tested under axial compressive load. The capacity and failure

modes of the BCS panels under combined bending and axial compression actions, are then investigated through validated numerical and simplified analytical approaches. Furthermore, a comparison is made between the axial compressive and combined compression and bending performances of the proposed BCS and conventional CLT panels.

Statement of Originality

This work has not previously been submitted for a degree or diploma in any university. To the best of my knowledge and belief, the thesis contains no material previously published or written by another person except where due reference is made in the thesis itself.

Signed: _____

Date: 16/03/2020

Siavash Darzi

Griffith University

Acknowledgement of Papers included in this Thesis

Section 9.1 of the Griffith University Code for the Responsible Conduct of Research ("Criteria for Authorship"), in accordance with Section 5 of the Australian Code for the Responsible Conduct of Research, states:

To be named as an author, a researcher must have made a substantial scholarly contribution to the creative or scholarly work that constitutes the research output, and be able to take public responsibility for at least that part of the work they contributed. Attribution of authorship depends to some extent on the discipline and publisher policies, but in all cases, authorship must be based on substantial contributions in a combination of one or more of:

- conception and design of the research project
- analysis and interpretation of research data
- drafting or making significant parts of the creative or scholarly work or critically revising it so as to contribute significantly to the final output.

Section 9.3 of the Griffith University Code ("Responsibilities of Researchers"), in accordance with Section 5 of the Australian Code, states:

Researchers are expected to:

- Offer authorship to all people, including research trainees, who meet the criteria for authorship listed above, but only those people.
- accept or decline offers of authorship promptly in writing.
- Include in the list of authors only those who have accepted authorship.
- Appoint one author to be the executive author to record authorship and manage correspondence about the work with the publisher and other interested parties.
- Acknowledge all those who have contributed to the research, facilities or materials but who do not qualify as authors, such as research assistants, technical staff, and advisors on cultural or community knowledge. Obtain written consent to name individuals.

Included in this thesis are papers in *Chapters 3, 4 and 5* which are co-authored with other researchers. My contribution to each co-authored paper is outlined at

the front of the relevant chapter. The bibliographic details and status for these papers including all authors, are:

Chapter 3:

Darzi, S, Karampour, H, Gilbert, BP & Bailleres, H 2018, 'Numerical study on the flexural capacity of ultra-light composite timber sandwich panels', *Composites Part B: Engineering*, vol. 155, pp. 212-24.https://doi.org/10.1016/j.compositesb.2018.08.022

Chapter 4:

Darzi, S, Karampour, H, Bailleres, H, Gilbert, BP, & L. McGavin. Experimental study on bending and shear behaviours of composite sandwich panels. *Construction and building materials* (Submitted 11th March 2020, under review).

Chapter 5:

Darzi, S, Karampour, H, Gilbert, BP, Bailleres, H, & Fernando, D. Load bearing sandwich timber walls with plywood faces and bamboo core, *Structures*, (Submitted 6th February 2020, under review).

(Signed) _____ Date: 16/03/2020

PhD Candidate: Siavash Darzi

(Countersigned) _____ Date: 16/03/2020

Principle Supervisor: Dr. Hassan Karampour

(Countersigned) _____ Date: 16/03/2020

Associate Supervisor: Associate Professor Benoit P. Gilbert

(Countersigned) _____ Date: 16/03/2020

External Supervisor: Dr. Henri Bailleres

List of Publications

Journal papers:

Darzi, S, Karampour, H, Gilbert, BP & Bailleres, H 2018, 'Numerical study on the flexural capacity of ultra-light composite timber sandwich panels', *Composites Part B: Engineering*, vol. 155, pp. 212-24.https://doi.org/10.1016/j.compositesb.2018.08.022

Darzi, S, Karampour, H, Bailleres, H, Gilbert, BP, & L. McGavin. Experimental study on bending and shear behaviours of composite sandwich panels. *Construction and building materials* (Submitted 11th March 2020, under review).

Darzi, S, Karampour, H, Gilbert, BP, Bailleres, H, & Fernando, D. Load bearing sandwich timber walls with plywood faces and bamboo core, *Structures*, (Submitted 6th February 2020, under review).

Conference papers:

Darzi, S, Karampour, H, Gilbert, BP & Bailleres, H 2018, 'Flexural behaviour of a novel bamboo-plywood sandwich composite panel', paper presented to 2018 World Conference on Timber Engineering (WCTE 2018), Seoul, Republic of Korea.

Darzi, S, Karampour, H, Gilbert, BP & Bailleres, H 2018, 'Efficiency of sandwich bamboo-plywood floor panels with various core configurations', paper presented to 25th Australasian Conference on Mechanics of Structures and Materials (ACMSM25), Brisbane, Australia, December 4 – 7, 2018.

Acknowledgements

Table of Content

List of Figures

List of Tables

List of Abbreviations

AAC	Autoclaved aerated concrete
BCS	Bamboo core sandwich panel
BGB	Bamboo glulam beam
CLT	Cross laminated timber
CDF	Cumulative distribution function
DIC	Digital image correlation
EPS	Expanded Polystyrene
EWP	Engineered wood product
FEA	Finite element analysis
FRP	Fibre reinforced polymer
GLT	Glue laminated timber
GFRP	Glass Fibre Reinforced Polymer
LBL	Laminated bamboo lumber
LSL	Laminated strand lumber
LVL	Laminated veneer lumber
MOE	Modulus of elasticity
OSB	Oriented strand board
PCS	Peeler core sandwich panel
PUR	Polyurethane
SCL	Structural composite lumber
SI	Strength index
SIP	Structural insulated panel

List of Symbols

The following symbols are used in this thesis:

a	Length
a_e	Effective length
A	Area
b	Width
b_c	Core width
c	Core height
C_c	Slenderness ratio
d	Distance between centrelines of opposite faces in a sandwich structure
d_a	Distance between the two centre axes of the top and bottom layers in CLT
D	Diameter
e	Bamboo wall-thickness
E	Modulus of elasticity
f_b	Bending strength
f_c	Compressive strength
E_T	Tangent modulus
G	Modulus of rigidity; shear modulus
h	Overall thickness/ depth of panel
h_i	Thickness of individual layer in CLT panel
I	Moment of inertia
k	Timoshenko shear coefficient

K_c	Slenderness factor
K_{zc}	Size factor
K_{rb}	Bending moment adjustment factor
M	Bending moment
M_r	Bending moment resistance
n	Number
N	Ratio of modulus of elasticity
P	Force
P_E	Euler buckling load
P_{EV}	Adjusted elastic buckling load
P_r	Compressive capacity
q	Force per unit length
Q	First moment of area
r	Inner radius
r_{eff}	Effective radius of gyration
R	Outer radius
R_{ij}	Yield ratios
S	Elastic section modulus
S_{eff}	Effective section modulus
t	Face thickness
u	Displacement in x-axis
U	Strain energy
$\boldsymbol{V}$	The potential energy
V	Shearing force
v	Displacement in y-axis

W	Weight
w	Displacement in z-axis
$\boldsymbol{w}$	Pressure
x, y, z	Rectangular coordinates, distance
γ	Shearing strain
δ	Deformation; displacement
ϵ	Normal strain
θ	Angle; slope
λ	Slenderness ratio
ν	Poisson's ratio
ρ	Radius of curvature
σ	Normal stress
τ	Shearing stress
Π	Total energy
Δ	Mid-span displacement

1 Introduction

1.1 General

The building industry has been subjected to continuous modification and improvement to meet the requirements of sustainable development, leading to a requirement for more durable, less labour and service intensive materials at a competitive price. The traditional approach of housing and building industry, producing conventional solutions which is exclusively built with the materials of the last century, steel and concrete. In Australia, 23% of the nation's Greenhouse Gas (GHG) emissions is caused indirectly by the residential and commercial building sectors as a result of construction materials, material inefficiencies, waste disposal and ongoing energy use (Green Building Council Australia 2011). However, due to the Australian Government's carbon pricing legislation, the building and industrial market continuously demands innovative and more energy-efficient alternatives to current practices. Engineered wood products (EWPs) are one of the most promising materials which meet the abovementioned requirements. The advantages of using EWPs include faster on-site construction times, lighter weight materials, use of a sustainable natural resource, improved insulation properties, carbon sequestration, lower embodied energy, and lower GHG emissions compared to typical concrete construction (Hindman & Bouldin 2014). The combination of materials in a composite construction system provide overall performance higher than the sum of their individual components, while minimize the use of resources. Composite concrete-based floor panel has become very common technologies in building industry. However, the use of non-renewable resources, the high demand of energy and the required curing time might impact its efficiency. Furthermore, sandwich panels provide an effective structural system with high stiffness and strength to weight ratios. By varying the material and thickness of core and skins, it is possible to obtain sandwich structures with different properties and performance to be utilised in building industry.

1.2 Hybrid/composite products in the building industry

The combination of materials in a composite construction system is a way to minimize the use of resources, and therefore reducing the environmental impact

of the building construction process. Composite systems commonly provide an overall performance higher than the sum of their individual components (Ceccotti 2002). There are a wide variety of composite systems which commonly includes the combination of timber with concrete, steel with concrete, steel with timber and timber with timber (Crocetti, Sartori & Tomasi 2014; Hassanieh, Valipour & Bradford 2016; Loss & Davison 2017; Spacone & El-Tawil 2004). Composite solutions are extensively used for the realization of floors or slabs in building construction. In these systems, the panel comprise of three components, which the upper and bottom element mainly resist compression and tension, respectively, and the connection provides a mechanism for the transfer of shear. Over the past decade, Timber-Concrete Composite (TCC) and Steel-Timber Composite (STC) floors (Figure 1.1 and Figure 1.2) have found extensive application because of lower cost of construction and maintenance compared with conventional reinforced concrete and steel (Hassanieh, Valipour & Bradford 2016; Khorsandnia, Valipour & Crews 2012). Compared to TCC floors, the STC floors have the advantage of being lightweight, while they can improve the speed of construction and accordingly reduce the cost of construction. Possible other inconveniences of hybrid composite concrete-based floors are the use of non-renewable resources, the required curing time which sometimes can complicate on-site construction, and the limited number of prefabricated solutions currently available.

Figure 1.1 Timber-Concrete Composite (TCC) floors system *(Wood Solutions design and build 2019).*

Figure 1.2 Steel-Timber Composite (STC) floor system (Loss & Davison 2017).

1.3   Engineered wood products in building industry

The commercial launch of the new generation of engineered wood product, such as Cross-laminated Timber (CLT), caused engineered timber products to recapture the market shares from the conventional construction materials (reinforced concrete and steel), particularly in the fields of residential and non-residential applications. The orthogonal, laminar structure of CLT panels increases the dimensional stability and allows its application in form of roof, floor, and wall elements, able to bear in-plane and out-of-plane loads. CLT combined with other engineered wood products such as I-beams, Laminated Veneer Lumber (LVL) and Glue-laminated Timber (GLT or glulam) and structural plywood, can be used as crucial elements in the construction of buildings made entirely from timber. Another advantage of CLT is that it can be prefabricated, reducing construction time and wastes. CLT is a lighter alternative to masonry and concrete systems with good thermal and sound insulation and good performance under fire because of a massive wood structure. CLT is also a product extremely well suited for mid-rise and high-rise buildings because of its versatility. Panel sizes vary by manufacturer; but with lengths up to 18 meters, widths of up to 2.4 meters and thicknesses up to 508 mm, almost any necessary shape can be found on the market today. Over the last few years, the use of CLT panels in building industry has increased in Europe, North America, Canada, and Australia. Hundreds of impressive buildings and other structures built around the world using CLT panels which show the many advantages of this product. The first multi-storey CLT building in Australia is the 10-storey Forte residential building in Melbourne. This building was built by Lend Lease and completed in December 2012. The building is 30% lighter than conventional concrete buildings. The construction time was also reduced by 30% and the carbon

3

footprint by 1,451 tons (Green & Taggart 2020). The recent multi-story CLT building in Australia is the 10-storey 25 King Street Office Building in Brisbane, shown in Figure 1.3. 25 King became the tallest and largest commercial mass wood building in the world when completed in spring 2019.

Figure 1.3 25 King Street Office Building in Brisbane, Australia (Green & Taggart 2020).

The CLT structure featuring orthogonally oriented adjacent layers, the CLT panels are prone to planar (rolling) shear under out-of-plane loading. The rolling shear constitutes a potential failure mechanism and contributes a noticeable amount to the overall deflection.

1.4 Structural sandwich panels in building industry

Sandwich structures are of interest and widely used because the concept is very suitable to the development of lightweight and efficient construction materials with exceptional stiffness. A sandwich panel normally consists of two thin layers of a stiff and strong material (face-sheets or skins) separated and bonded together by a lightweight and relatively thick material (core).

In modern engineering, sandwich structures are extensively implemented in the aerospace, marine, architectural and transportation industry, where low weight is a critical design factor. Depending on the specific structural applications, the requirements for the materials forming the sandwich structure are determined. The sandwich structure also draws a lot of interest in the building industry and is

now started to be used in civil engineering applications (Manalo, A et al. 2010). Sandwich panels could be significantly beneficial in flooring and wall applications as an alternative to traditional wood or concrete systems due to their lightweight and strength properties. The reduced dead weight of the floors contributes to lower overall load, and consequently smaller supporting members' requirement. Structural Insulated Panels (SIPs) are a common type of sandwich panel for building construction that combines a soft foam core as a layer of insulation with a lightweight structural skin. SIPs can be used for wall, roof and floor panels, where they are exposed to out-of-plane bending (Smith 2010). There is a variety of SIP skin and core materials based on its applications. As shown in Figure 1.4, the panel is typically made of plastic foam such as Extruded Polystyrene and Expanded Polystyrene (EPS) as well as Polyurethanes (PUR) foam, while the skins can be metal, fibre cement, cement, calcium silicate, gypsum and oriented strand board (OSB) (Mullens & Arif 2006; Panjehpour et al. 2013).

Figure 1.4 Structural Insulated Panel (SIP) made of polystyrene foam core and OSB skins (Panjehpour et al. 2013).

With its many advantages, structural application of sandwich panels in civil engineering has remained very limited. The main reason could be that most of the currently used core materials are not appropriate for structural application, as the core material is fabricated by low strength foam materials, and sensitive to failure by the application of compressive loads or shear failure of the core during the flexural loading (Dai & Hahn 2003; Manalo, AC et al. 2010). Therefore, numerous studies focus merely on the materials for its core and skins to improve its structural performance (Pardue 2011; Van Erp & Rogers 2008).

1.5   Research objectives

The research goals of this PhD project are: (1) to introduce novel composite timber sandwich panels made by gluing commercial plywood skins to either bamboo rings to produce Bamboo Core Sandwich (BCS) panels or to peeler core rings to produce Peeler Core Sandwich (PCS) panels, and (2) investigate appropriateness of the proposed panels for construction purposes such as floor diaphragms and load bearing walls.

The objectives of this study are summarised as below:

- To evaluate the theoretical flexural responses of the proposed panels with different aspect ratios in one-way and two-way bending configurations using a modified Ritz method and a validated FEA.
- To investigate the bending and shear performances of the panels using standard four-point bending and three-point shear tests, respectively and compare the results with commercial CLT panels with almost similar depth.
- To investigate the axial performances of the single and double core layer BCS panels under axial compressive load as well as combined bending and axial compression actions, through experimental, numerical and simplified analytical approaches.

1.6   Research methodology

The objectives of this research are achieved as follows:

1. Development of a modified Ritz method that can predict the flexural response of a sandwich panel with thick skins and thick-stiff core in one-way and two-way bending configurations.
2. Using the proposed Ritz formulation to evaluate the flexural responses of the proposed BCS and PCS panels with different aspect ratios under point load and uniformly distributed load.
3. Developing FEA, validated against Ritz and previous experimental work, to capture the ultimate capacity of the proposed panels.
4. Experimentally investigating the bending and shear performances of the proposed panels using standard four-point bending and three-point shear tests, respectively, and comparison with commercial CLT panel.
5. Experimental study of single and double core layer BCS panels under axial compressive load.

6. Numerical study of combined compression and bending performances of the proposed BCS panels, and conventional CLT panels.

1.7 Thesis outline

This thesis is structured as follows:

- Chapter 1 presents an introduction to the thesis and briefs the research objectives and methodologies.
- Chapter 2 reviews the literature relevant to this thesis. Mass timber products, particularly CLT and rolling shear, and available sandwich composite panels and associated problems in building industry are presented. In addition, the possibility of utilising bamboo as a structural element and studies on engineered bamboo products are discussed.
- Chapter 3 is based on the published journal paper. A modified Ritz method is developed and used to evaluate the flexural responses the proposed BCS and PCS panels in one-way and two-way bending configurations. A validated FEA is used to capture the ultimate capacity and failure modes of the panels. The results are then compared with commercial CLT panels with almost similar depths.
- Chapter 4 is based on the submitted journal paper. The proposed panels are manufactured and physically tested in standard bending (using four-point) and shear (using three-point) tests. Results are compared to the test results of conventional CLT panels with almost similar depths.
- Chapter 5 is based on the submitted journal paper. Single and double core layer BCS panels are manufactured and tested under axial compressive load. The capacity and failure modes of the BCS panels under combined bending and axial compression actions, are then investigated through validated numerical approaches. To provide comparison, the results are compared to conventional CLT panels.
- Chapter 6 summarises the thesis finding and provides the recommendations for future research.

2 Literature review

2.1 Mass timber products and mid-rise timber construction

With the advent of mass timber panels, the trend of mass timber construction is spreading throughout the world in recent years. Mass timber construction is a category of framing styles using heavy timber products including cross laminated timber (CLT), structural composite lumber (SCL) and glued-laminated timber (GLT) panels. The National Construction Code 2019 Volume One (NCC), Building Code of Australia, Class 2 to Class 9 Buildings, allows use of timber construction systems under the Deemed-to-Satisfy (DTS) Provisions for buildings up to 25 metres in effective height, known as mid-rise construction. Mass timber panels are engineered to have high strength and dimensional stability, which can be used as an alternative to concrete, masonry and steel in many building types and make wood skyscrapers possible. Mass timber panels intended for floor, wall and roof construction can be prefabricated with precise dimensions and openings in a factory (due to the outstanding machinability of wood), therefore allowing for a faster construction process and minimal construction waste.

Cross laminated timber (CLT), shown in Figure 2.1, is currently the most popular product. It is a prefabricated engineered wood product made of at least three orthogonal layers of graded sawn lumber or structural composite lumber (SCL) that are laminated by gluing with structural adhesive (*ANSI/APA PRG 320-2019 Standard for Performance-Rated Cross-Laminated Timber*). The edge surfaces of adjacent lumber in one layer can be bonded, known as edge bonding. CLT combined with other mass timber products have been successfully used in Europe, Canada and Australia to construct 8 to 14-story mid-rise structures (FWPA 2010; Goad & Snape 2015; Malo, Abrahamsen & Bjertnæs 2016; MGB Architecture and Design 2012). The orthogonally oriented adjacent layers in CLT panels results in excellent in-plane and out-of-plane strength, rigidity and stability, while reduces the degree of anisotropy in properties and the influence of natural variations (e.g. knots) (Sikora, McPolin & Harte 2016; Vessby et al. 2009). The CLT laminar composition increases the splitting resistance of timber and higher stiffness and strength in both direction, giving it a two way action capability analogous to reinforced concrete slab (Aicher, Hirsch & Christian 2016; FWPA 2010; Sikora, McPolin & Harte 2016).

Figure 2.1 Cross laminated timber (CLT) panel (MGB Architecture and Design 2012).

Besides lumber-based panels, structural composite lumber (SCL), including laminated veneer lumber (LVL), laminated strand lumber (LSL), oriented strand lumber (OSL), and parallel strand lumber (PSL), is an another important series of mass timber panels, which are created by layering dried and graded wood strands, flakes or veneers with moisture resistant adhesive into a block of material known as a billet. The billets are subsequently re-sawn into specified sizes. In SCL billets, the grain of each layer of veneers or flakes runs primarily in the same direction. A brief description of each product is as follows:

Laminated Veneer Lumber (LVL)

Laminated veneer lumber (LVL) is one of the most widely used of the structural composite lumber products (SCL) family. LVL is produced by bonding thin wood veneers together with moisture resistance adhesive to form a large billet (*ASTM D5456-19, Standard Specification for Evaluation of Structural Composite Lumber Products* 2019). The applications of LVL are hip and valley rafters, scaffold planking, headers and beams and the flange material for prefabricated wood I-joists.

Figure 2.2 Laminated veneer lumber (LVL) panel (MGB Architecture and Design 2012).

Laminated Strand Lumber (LSL)

Laminated Strand Lumber (LSL) is made from flaked wood strands that have a length to thickness ratio of approximately 150. Combined with an adhesive, the strands are oriented and formed into a large mat or billet and pressed (*ASTM D5456-19, Standard Specification for Evaluation of Structural Composite Lumber Products* 2019). LSL has a variety of applications from studs to millwork components.
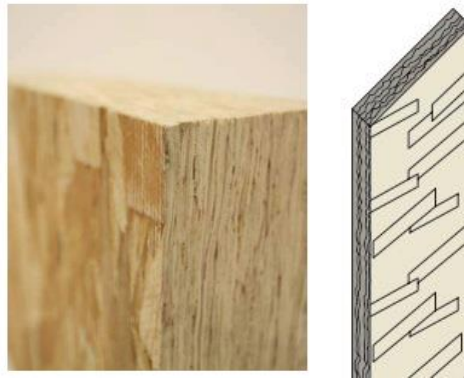
Figure 2.3 Laminated strand lumber (LSL) panel (MGB Architecture and Design 2012).

Oriented Strand Lumber (OSL)

Oriented Strand Lumber (OSL) is made from flaked wood strands that have a length to thickness ratio of approximately 75. Combined with an adhesive, the strands are oriented and formed into a large mat or billet and pressed (*ASTM D5456-19, Standard Specification for Evaluation of Structural Composite Lumber Products* 2019). OSL has a variety of applications from studs to millwork components.

Parallel Strand Lumber (PSL)

Parallel Strand Lumber (PSL) is made from veneers clipped into long strands laid in parallel formation and bonded together with an adhesive to form the section. The strands in PSL have a length to thickness ratio of approximately 300 (*ASTM D5456-19, Standard Specification for Evaluation of Structural Composite Lumber Products* 2019). Like LVL, it can be used for beam and headers where high bending strength is vital. Moreover, the PSL is widely used as load-bearing columns.

2.2 CLT and previous findings regarding rolling shear

Cross laminated timber (CLT) is currently experiencing increasing popularity for building construction, particularly for multi-storey residential and non-residential construction. The orthogonal orientation of adjacent layers in CLT panels results in excellent bi-directional strength, rigidity, and stability characteristics. However, this specific orientation causes CLT panels to be prone to rolling shear failure when it is subjected to out-of-plane bending. Rolling shear is described as inter-fibre cracking due to shear strains in the plane perpendicular to the longitudinal axis of wood fibres, the L axis shown in Figure 2.4. In the same figure, the axes R and T denote the radial and tangential directions of wood, respectively. Figure 2.5 shows a rolling shear failure in a 3-ply CLT panel. The crack path generally changes to delaminations when it reaches the interlaminar bonding area between two adjacent layers in CLT panel, as shown in Figure 2.5.
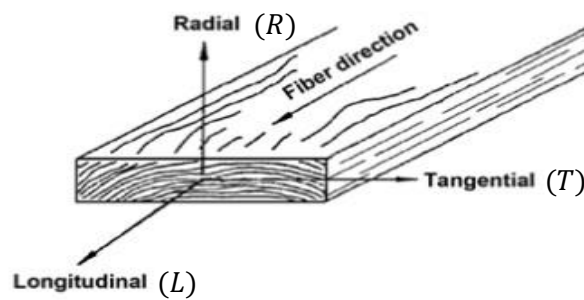
Figure 2.4 Principle axes of wood with respect to grain direction and growth rings.

Figure 2.5 Typical rolling shear failure in a CLT panel (Zhou 2013).

In the design of timber structures, with focus on CLT, rolling shear strength and modulus need to be taken into consideration, which depend on several aspects, such as wood species, sawing pattern, the span-to-depth ratio, the cross-sectional geometry and layup. Previous publications have addressed several aspects and influencing parameters of rolling shear experimentally and numerically.

Fellmoser and Blaß (2004) evaluated the rolling shear modulus in Norway spruce (*Picea abies*) boards by means of a bending vibration test and the influence of span-to-depth ratio on the rolling shear properties of a 3-ply CLT panel using shear analogy method. They found that the rolling shear modulus of 3-ply boards ranged from 40 MPa to 80 MPa. They observed that the influence of shear can be disregarded only for span-to-depth ratio higher than 30 for loading perpendicular to grain direction of outer skins.

Aicher, Hirsch and Christian (2016) investigated the influence of four different sawing patterns (flat-sawn, semi-quarter-sawn, quarter-sawn, and with pith) on the rolling shear modulus and strength of beech laminations using two-plate shear tests. The semi-quarter sawn lumber showed the highest rolling shear strength, while the lumber with pith showed the lowest rolling shear strength.

Yawalata and Lam (2011) investigated the influence of manufacturing process parameters on the rolling shear capacity of 3-ply spruce-pine-fir (SPF) and hemlock-fir CLT panels using centre-point bending test. The rolling shear strength of 3-ply SPF panels made under a pressure of 0.4 MPa and 0.1 MPa were 2.22 MPa and 1.85 MPa, respectively. Therefore, the higher manufacturing pressure has contributed to stronger panels and subsequently a higher shear strength. Furthermore, the SPF CLT panels had a higher rolling shear capacity than those made of hemlock-fir by (up to 13% under the same pressure), which clearly advised that wood species had an impact on the rolling shear strength.

Cao et al. (2019) investigated the effect of knots on the rolling shear strength of 3-ply southern yellow pine CLT panel. Experimental tests (centre-point bending tests and two-plate shear tests) were conducted on six CLT configurations consisting of different types of cross layer laminations based on knots conditions (No Knots, Sound Knots, and Decayed Knots) and pith conditions (Pith, No Pith). Shear analogy method was utilised to evaluate the rolling shear strength values

from the bending test results, which were compared against the results from the two-plate shear tests. The cross-layer laminations with either sound knots or decayed knots improved the rolling shear strength of CLT panel. In general, the rolling shear obtained from the shear analogy method was conservative.

Zhou et al. (2014) measured the rolling shear modulus and strength of the cross-layer in black spruce CLT panels using two test methods, variable span bending tests and two-plate shear test. They found that the results from the two-plate shear test could, in comparison to those from the variable span bending test, be used as input to accurately predict deflection of CLT beam specimen at common span-to-depth ratios, which is more practical and useful in CLT application.

Sikora, McPolin and Harte (2016) carried out an investigation to establish the effect of the thickness of Sitka spruce CLT panels on the bending stiffness and strength and the rolling shear. Bending and shear tests were conducted on 3-ply and 5-ply panels with loading in the out-of-plane and in-plane directions. The results indicated that both the bending strength and rolling shear decreased with panel thickness. Mean values for rolling shear strength ranged from 1.0 MPa to 2.0 MPa.

Overall, many studies have identified the rolling shear properties in engineered timber products (e.g. CLT panels) as critical design properties for out of plane bending applications. Many methods also have been proposed but each has its own advantages and drawbacks. To measure the rolling shear properties in CLT panels, some methods have been developed, such as a non-destructive evaluation method (Steiger, Gülzow & Gsell 2008). It should be noted that there is no standardized test method for measuring the rolling shear properties of full-size CLT panels. The compression shear testing method and varied-span bending method are the methods recommended in Europe (*BS EN 16351 : 2015 Timber Structures- Coss Laminated Timber- Requirements* 2015) and North America (*ASTM D2718-18, Standard Test Methods for Structural Panels in Planar Shear (Rolling Shear)* 2018). The compression shear test has been employed in many research studies to investigate the rolling shear properties of CLT panels (Ehrhart et al. 2015; Zhou et al. 2014). Apart from the experimental testing methods, theoretical models also have been studied in order to estimate the mechanical properties of CLT panels, Shear Analogy method (Kreuzinger, H. 1999), Composite Theory (*k*-method) (Bodig & Jayne 1982), and Mechanically

Jointed Beams Theory (γ-method) (*I.S. EN 1995-1-1: 2005, Eurocode 5: Design of timber structures - Part 1-1: General - Common rules and rules for buildings* 2005) are commonly used.

In Europe, the Mechanically Jointed Beams theory (γ- Method) is the most common analytical approach that has been adopted for CLT panels. This approach is available in Annex B of Eurocode 5 (EN 2004). Based on this theory, the Effective Bending Stiffness (*EI*$_{eff}$) and a Connection Efficiency Factor (γ_i) is used to account for the shear deformation of the perpendicular layer (cross layer). Based on this method, the stiffness properties of the mechanically jointed beams are defined using the *EI*$_{eff}$ that depends on the section properties and the factor γ. Factor γ depends on the slip characteristics of the fasteners (s/*K* ratio), With γ=0 representing no mechanical connection between the beams and γ=1 representing rigidly connected (glued) beams. In this method, it is assumed that longitudinal boards are carrying the load only, and the rolling shear stiffness (or deformability) of the perpendicular layers can be taken as stiffness (or deformation) which caused by "virtual fasteners" connecting the longitudinal layers. The ratio s/*K* for fasteners at each interface *i* is calculated as

$$\frac{s}{k_i} = \frac{\bar{h}_i}{G_R.b} \qquad (2.1)$$

G_R is the shear modulus perpendicular to the grain, h_i is the thickness of boards layers perpendicular to the action and *b* is the panel width. *S* is the spacing between mechanical fasteners and K_i is the slip modulus of mechanical fasteners. *S* and K_i are not physically present in glued CLT.

The Gamma Method is derived from simple bending theory and thus basic assumptions are valid. Shear deformations are neglected in longitudinal layers of the CLT (beams) and are considered only for the perpendicular layers (cross layers) by evaluating the rolling shear deformation. A closed (exact) solution for the differential equation only for simply supported panels with a sinusoidal load distribution can be provided in this approach. For uniformly distributed load or point load the differences of the exact solution are minimal, however can be used for engineering practices (Ceccotti, 2003). From simple bending theory and Gamma Method (theory of mechanically jointed beams), the maximum shear stresses can be obtained as:

14

$$\tau_i = \frac{V \sum_{j=i+1}^{n} \gamma_j E_j A_j a_j}{\left(EI_{eff}\right).b} \qquad (2.2)$$

where V is the maximum shear force, and b is the CLT panel width. Factor γ_j is the connection efficiency factor of longitudinal layer j, E_j is the modulus of elasticity of layer j along the beam axis, A_j is the cross section area of layer j, a_j is the distance from centroid of layer j to the neutral axis of the beam. The effective stiffness EI_{eff} of the panel is calculated by:

$$EI_{eff} = \sum_{i=1}^{n} \left(E_i I_i + \gamma_i E_i A_i a_i^2\right) \qquad (2.3)$$

where $0<\gamma\leq1$ ($\gamma=0$ for no connection and $\gamma=1$ for rigid connection). γ is typically taken as 0.85 to 0.99).

The second method is Composite Theory (k-method) to predict some design properties of CLT panels and have been applied by Fellmoser and Blaß (2004). This method is known in the plywood industry. The plies (veneers) of plywood panels stressed perpendicular to the grain are not considered in bending properties calculations. Compared to Gamma Method, this method does not account for shear deformation in individual layers and therefore this may be used for high span-to-depth ratios ($l/h>30$) only.

Shear Analogy method (Kreuzinger, H. 1999) has been developed in Europe that seems to be applicable for solid panels with cross layers such as CLT. Unlike k-method, the approach considers the shear deformation of the perpendicular layer (cross-layer) and not limited to a certain number of layers within a panel. Currently, this method is fairly accurate for CLT panels and has been used to determine the stiffness properties of CLT panels loaded perpendicular to the face, in PRG 320 and CSA O68 standards. In this method, a multilayer cross section is separated into two virtual beams: A and B. Beam A considers flexural strength of individual layers along their own neutral axes, while beam B considers the "Steiner" points part of the flexural strength, the flexible shear strength of the panel, as well as the flexibility of all connections. The two beams are coupled (with infinitely rigid web members), so equal deflections between beam A and beam B are obtained. Therefore, the shear stress in cross layer i is calculated by adding up the shear stresses τ_{Ai} and τ_{Bi} in beam A and B, respectively.

$$\tau_{Ai} = \frac{1.5V_A}{h_i.b} \cdot \frac{E_i I_i}{B_A}$$

$$\tau_{Bi} = \frac{V_B}{B_B.b} \cdot \sum_{j=i+1}^{n} E_j A_j a_j$$

(2.4)

V_A and V_B are the shear forces on beam A and B, E_i is the modulus of elasticity of layer i along the beam axis; A_i is the cross section area of layer i; a_i is the distance from centroid of layer i to the neutral axis of the beam. B_A and B_B are the bending stiffness (*EI*) of beam A and beam B, respectively, as

$$B_A = \sum_{i=1}^{n} E_i I_i$$

$$B_B = \sum_{i=1}^{n} E_i A_i a_i^2$$

(2.5)

2.3   Sandwich structures

2.3.1   Historical background

Throughout the 20th and 21st century, sandwich structures received increasing attention because of their excellent structural properties that pioneer the lightweight construction design. Sandwich panels were first extensively used in designing the famous Mosquito bomber aircraft in the early 20th century during World War II. Its fuselage was made of plywood-balsa-plywood to decrease the airplane weight while preserving stiffness and strength (Allen 1969). Later, in 1937, sandwich structures made of balsa wood core and cedar plywood face-sheets employed again in aerospace application in the De Havilland Albatross airplane (REIS 2005).

Some of the first theoretical works on sandwich construction were documented by the completion of World War II, in late 1940's. Theoretical analysis of the sandwich constructions started with several papers regarding strength and stability of sandwich beams, columns and plates during 1945 to 1955. The analysis was undertaken mostly by the Forest Product Laboratories of the United States Forest Service (March 1955). The research works consisted of both experimental, theoretical and also presented analytical solutions to various bending problems of beam and panel. The theory on sandwich plates which derives the differential equation for deflection of a sandwich panel first published by Reissner in 1945. Afterwards, Libove and Batford in 1945 considered the deflection and shear forces in orthotropic panels with thin face to derive

differential equations. The strain energy of a sandwich panel in terms of transverse and in-plane deflections was evaluated by Hoff in 1950. Mindlin in 1951 derived the equation of motion for an isotropic plate accounting for both transverse shear deflections and rotary inertia (Allen 1969; Vinson 1999). These research works then formed the basis of one of the most important texts on analysis and design of structural sandwich panels by Howard G.Allen in 1969.

2.3.2 Main principles of a sandwich structure

Typical sandwich composite structures are made of three main components, two face-sheets or skins and a core, as illustrated in Figure 2.6. The concept is similar to an I-shape beam in the sense that when subjected to bending, the flanges provide the resistance to the induced in-plane (as do the sandwich face-sheets or skins) compression and tension loads and the web carries shear loads (as does the structural sandwich core). Therefore, the main advantage of sandwich structures over other structural members (e.g. beam, plates or shells) is the combination of very high bending stiffness and strength with low weight (mass). As a result, a wide variety of different sandwich configurations and materials were investigated (Lakreb, Bezzazi & Pereira 2015; Panjehpour et al. 2013; Sohel & Liew 2011).

Figure 2.6 A schematic illustration of a standard sandwich panel.

In typical sandwich structures, the core material is not rigid and therefore, the shear displacement within the core is negligible in most cases. The shear displacement in the faces can be also insignificant. The effect of core shear rigidity in sandwich structure is shown in Figure 2.7. Figure 2.7 (a) clearly shows an ideal sandwich beam with a rigid core, while the two face-sheets or skins cooperate without sliding relative to each other. Figure 2.7 (b) shows a sandwich beam with a flexible or weak core, while the faces are no longer coupled together effectively, and each face works independently as plates in bending. Therefore,

application of a flexible core in shear contributes to a significant loss of the efficiency in sandwich structures.
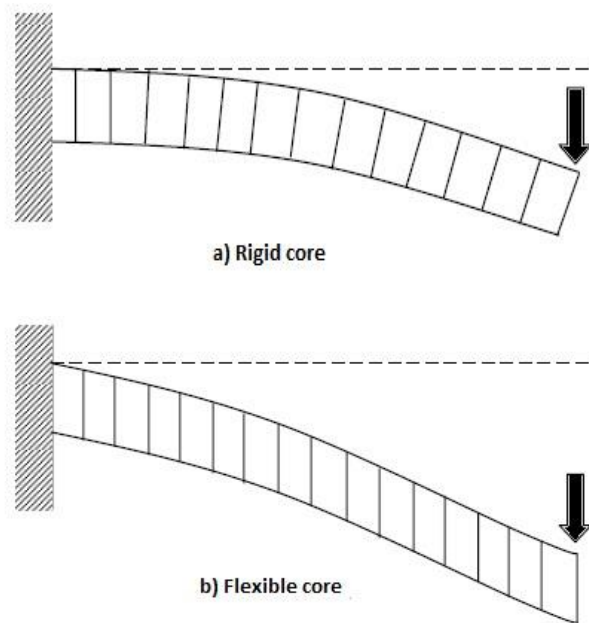
Figure 2.7 Core shear rigidity effect in a sandwich structure (REIS 2005).

The face-sheets in a typical sandwich structure carry the tensile and compressive stresses. Thus, the most common specifications to select the sandwich skins are high stiffness to achieve high bending rigidity, high tensile and compressive strength, impact resistance, environmental resistance, and surface finish. The most common materials used to build the face-sheets (or skins) of sandwich structures are composite materials, metals, wood and polymers (Dawood, Taylor & Rizkalla 2010; Liew & Sohel 2010; Sohel & Liew 2011).

The core must be rigid to resist the shear forces and to prevent sliding of the face-sheets relative to each other. The face-sheets behave as two independent beams or panels and the sandwich effect is lost If this condition is not fulfilled. Furthermore, the rigidity of the core maintains the faces nearly flat and prevent possibility of buckling in face-sheets under the influence of transverse loads. Typical requirements for core material can include low density, high stiffness and strength perpendicular to the sandwich skins, high shear modulus and strength, thermal and acoustic characteristics, thermal energy absorption and chemical stabilities for manufacturing. Many different materials and core morphologies have been employed in the core of sandwich structures. The most common core materials are balsa wood (Grenestedt & Bekisli 2003), polymers (Mamalis et al.

18

2008), and metals (aluminium) (Kabir, Vodenitcharova & Hoffman 2014; McCormack et al. 2001) and among core morphologies, homogeneous foam core, corrugated core, and honeycomb core have been utilised (Perotti 2011).

2.3.3 Sandwich panel and its application in building industry

Sandwich panels are effective structural system that takes advantage of materials with high strength-to-weight ratios for exterior thin face-sheets or skins, which are separated by a low-density core material. The concept of sandwich technology was initially used in construction sector in 1849s, but most of the developments have occurred in the aviation industry over the last century (Herrmann, Zahlen & Zuardy 2005). Sandwich panels are extensively used in automotive, aerospace, marine and industrial applications due to their high structural efficiency, ease of erection and thermal-insulation qualities. Recently, there has been a growing trend in the construction industry to use sandwich structural elements as floor and roof panels, pedestrian bridge decks and cladding walls (Sharaf, Shawkat & Fam 2010; Van Erp & Rogers 2008). A common practical sandwich panel in building industry consists of cellular polyurethane cores and glass fibre reinforced polymer (GFRP) skins (Steeves & Fleck 2004). However, this type of composite sandwich structures are sensitive to failure under out-of-plane loading due to core shear failure and also de-bonding of the skins from the core (Kim, J & Swanson 2001; Sharaf, Shawkat & Fam 2010; Triantafillou & Gibson 1987). The role of the core is critical, not only because it provides higher bending stiffness by separating the skins apart from each other, but also it transmits the shear between the face-sheets. Therefore, it is necessary to understand the shear behaviour of the core and the panel to maximize the performance of the sandwich construction and fully utilise its load bearing capacity. Many research studies have been published and used high-density core material to improve the shear carrying capacity of the sandwich structures.

In a study by Dai and Hahn (2003), the effect of core material on static failure of sandwich panels under flexure was investigated (three and four-point bending configurations). Two different core materials, balsa wood and PVC foam were used for the study. The face-sheets consisted of a quasi-isotropic E-glass non-woven fabric cured in Derakane 441-400 epoxy vinyl ester resin. Higher shear strength of foam core resulted in a higher load carrying capability. However, this benefit disappeared as the span becomes longer in the test plan.

19

Sharaf, Shawkat and Fam (2010) investigated the effect of core density on the flexural performance of a GFRP sandwich panel. The study showed that, by doubling the core density, strength and stiffness of the panels increased substantially, by 165% and 113%, respectively.

An Australian manufacturer, LOC Composites Pty Ltd has manufactured a new structural GFRP sandwich panel for civil engineering applications such as floors, pedestrian bridges and railway sleepers (Manalo, A et al. 2010; Van Erp & Rogers 2008). The sandwich panel is made of E-CR glass fibre skins and a modified phenolic solid core. The new GFRP sandwich panel is made of a higher core density to improve its structural behaviour.

The advancements of fabrication technology have allowed the development of FRP-reinforced polymeric foam cores to further improve the performance of composite sandwich panels. M. Reis and H. Rizkalla (2008) introduced a novel 3-D fibre reinforced polymer (FRP) panel to overcome typical core failure (e.g. delamination) in traditional sandwich panels made of GFRP laminates and foam core. The panels consist of GFRP skins with a foam core and through-thickness fibre insertions, as shown in Figure 2.8. The influence of different parameters, such as the fibre insertion density, skin thickness, panel thickness was evaluated on shear and flexure behaviour of the panels as well as tension and compression. They found that the fibre insertions increase the shear strength and stiffness of the panel and prevents delamination of the skins. In a subsequent study the one-way flexural behaviour of similar panels with seven different fibre insertion patterns, was evaluated by Patrick (2007).
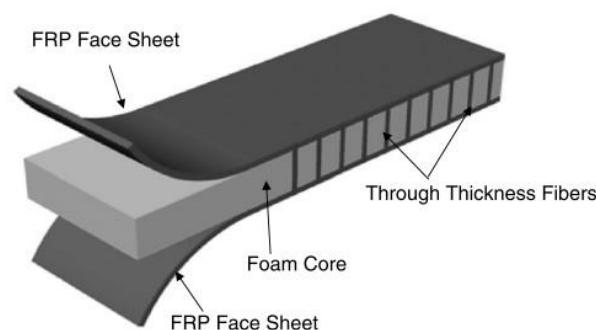
Figure 2.8 3-D FRP sandwich panel with through-thickness fibre insertions (M. Reis & H. Rizkalla 2008).

Kim, JH et al. (1999) investigated the one-way bending performance of GFRP sandwich panels with different polyurethane foam cores configurations. A plain foam core, a foam core with through thickness GFRP stitches and a foam core with continuous internal GFRP webs were the three different tested core configurations. They found that the presence of the stitches increased the one-way flexural strength of the GFRP sandwich panels by 50% compared to the specimens with plain foam cores. The ultimate strength of the panels with internal GFRP webs was about 10 times that of the panels with plain foam cores.

Mahfuz et al. (2004) used nanotechnology as an efficient technique to enhance the properties of polyurethane foam core material in a sandwich structure. Titanium dioxide (TiO_2) nanoparticles have been infused into the parent polymer of the core material when it was in the liquid stage. Their results showed that the flexural strength of Nano-phased core sandwich panels enhanced significantly by about 53% compared to sandwich panels with neat polycore.

Over the last two decades, a growing number of metallic sandwich panels with cellular cores have been studied by researchers. Traditionally, stochastic cores like aluminium alloy foam or micro-architecture lattice materials such as hexagonal honeycomb are used as core materials in metallic sandwich panels. However, the low strength of core under crushing (out of plane compression) is the typical failure of this type of sandwich panels (Bart-Smith, Hutchinson & Evans 2001; Nia & Sadeghi 2010). Daniel and Abot (2000) evaluated the behaviour of composite sandwich beams of unidirectional carbon/epoxy face sheets and aluminium honeycomb core under 4-point bending test. They found that premature shear failure of the composite sandwich near the points of load application can be prevented by filling the cells of the honeycomb core with epoxy resin. The same conclusion has been observed by Nia and Sadeghi (2010). In the study, the effects of foam filling of honeycomb panels on their plastic behaviour and mechanical properties were investigated by experimental tests. Their results indicated that the mean crushing strength and energy absorption capacity of the panel can increase up to 300%. Figure 2.9 shows an aluminium honeycomb core and a foam filled honeycomb core.
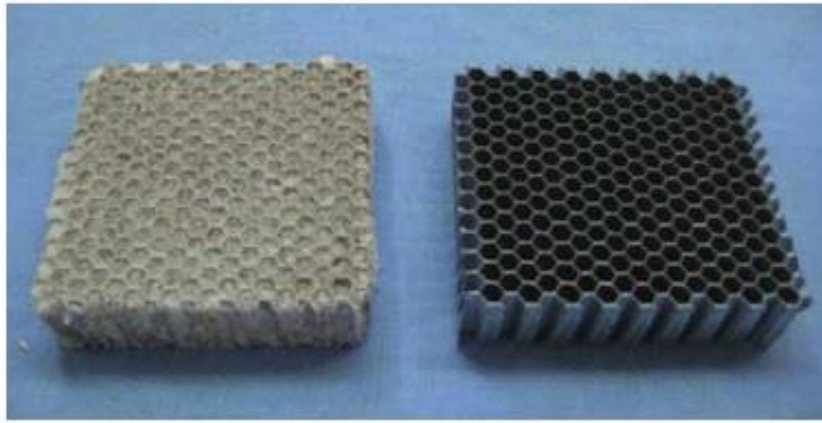
Figure 2.9 Honeycomb core (right) and foam filled honeycomb core (left) (Nia & Sadeghi 2010).

Xiong et al. (2011) designed a new type of light-weight sandwich panels with carbon fibre composite face sheets and hollow Al–Si alloy tubes as core material (Figure 2.10). The panels were tested under out-of-plane compression, in-plane compression as well as three-point bending until failure. Superior strength observed in Al-Si core sandwich panels under out-of-plane compression compared to common metallic and foam cores. The buckling of skins and de-bonding of hollow cores from the skins were observed under in-plane compression and three-point bending tests.

Figure 2.10 A sandwich panels with hollow Al-Si alloy tubes core (Xiong et al. 2011).

Mousa and Uddin (2009) investigated the structural behaviour of a hybrid structural panel consisting of fibre-reinforced polymer (FRP) skins and autoclaved aerated concrete (AAC) core under four-point bending test. AAC is an ultra-lightweight concrete with a distinct cellular structure, which has approximately 1/5 the weight of normal concrete with a compressive strength of 2 to 7 MPa. The hybrid panels were tested under four-point bending test to investigate their strength and ductility responses. The results demonstrated that

the FRP/AAC panel improved significantly in terms of strength (25-50%) and shear strength (300%) compared to the plain AAC.

Overall, low shear strength in core material (or brittle core materials) is contributed to sudden failure of the core. On the other hand, high shear strength of core material contributed to bond failure between core and face sheets (delamination). Both scenarios are catastrophic, therefore it is essential to completely understand the shear behaviour of core material and entire sandwich panel under service loads to exploit the load bearing capacity and improve the performance of a sandwich panel. These studies showed that the enhancement of the core material significantly improved the performance of the composite sandwich structures. However, the drawback was the weight and the production cost of these modified composite sandwich panels.

2.4 Bamboo as a structural element

There is a growing trend towards using bamboo for construction as part of the process of reducing the environmental impact and embodied energy of the built environment. Bamboo in its natural form is a cylindrical shoot, known as a culm and is part of the grass family *Gramineae* (*Poaceae*) (Janssen 1981). The culm is divided into sections by nodes that run transversely through the culm cross section, as shown in Figure 2.11. There are over 1200 species of bamboo worldwide, ranging from small diameter bamboo to large diameter woody bamboo. However, approximately 100 species are suitable for construction applications (Li, Xiaobo 2004; Mahdavi, Clouston & Arwade 2010). The most commonly used species for structural applications are *Guadia* (*Guadia angustifolis*) native to South America, and *Moso* (*Phyllostachys pubescens*) known as *Mao zhu* in China (Li, Y et al. 2012; Sinha, Way & Mlasko 2013).
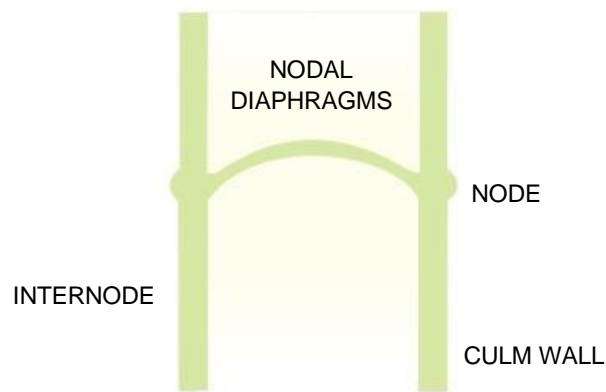
Figure 2.11 Bamboo parts.

Bamboo culms can normally reach 8 to15 m length, 50 to120 mm diameter with wall thickness of 5 to 10 mm within a year, after which the culm reaching the optimal structural properties within three to five years, depending on the species. Traditional bamboo construction has been used for many decades in low rise houses, construction platforms (scaffolding) and short span foot bridges, particularly in South East Asia, Latin America and East Africa (Chung & Yu 2002; Ramanathan 2008; Trujillo, Ramage & Chang 2013). In Australia, the application of bamboo is limited to architectural and decorative uses only.

2.4.1 Engineered bamboo composite products

The widespread use of bamboo is hampered due to the variation in geometric and mechanical properties, difficulty in making connections and joints for round sections, and lack of official design codes and standards. The design and testing standards exist for full culm bamboo (*ISO 22157:2019, Bamboo structures — Determination of physical and mechanical properties of bamboo culms — Test methods* 2019), but the standards themselves do not fully provide the foundation from which builders, engineers and architects can design with bamboo. To overcome these issues and obtain a sustainable and cost-effective alternative construction material, the development of engineered bamboo products is of interest, due to the standardisation of shape and the relatively low variability in material properties. Research studies vary from the use of full culm bamboo in construction and scaffolding (Ramanathan 2008) to engineered bamboo composite products, such as bamboo scrimber and laminated bamboo (Sharma et al. 2014). Bamboo scrimber is also referred to parallel strand bamboo. As shown in Figure 2.12a, the bamboo scrimber is manufactured from crushed fibre bundles saturated in resin, compressed and heated into a dense block. In

24

fabricating the laminated bamboo (Figure 2.12b), the bamboo culm is split, planed, processed (bleached or caramelised), laminated and pressed to form the board product.
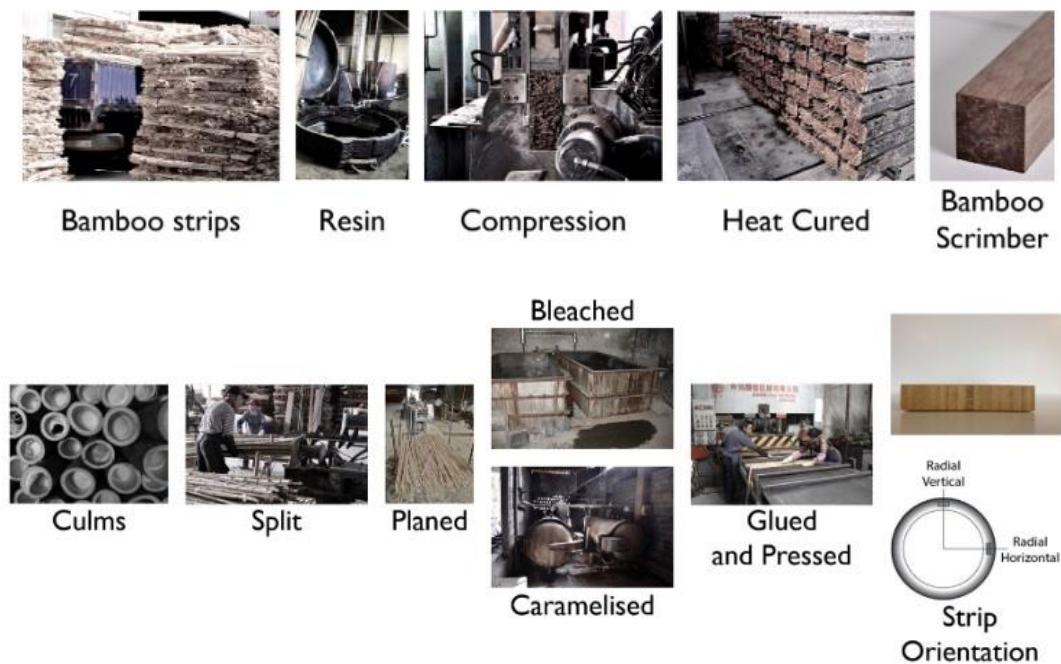
Figure 2.12 General manufacturing of (a) bamboo scrimber, and (b) laminated bamboo (Sharma et al. 2015).

Lee, Bai and Peralta (1996) assessed the feasibility of *Moso* bamboo (*Pyllostachys pubescens*) for manufacturing bamboo strand. The bamboo strand boards were formed using two phenol-formaldehyde resin content levels and two types of flake orientations (random and aligned) and compared to commercial strand boards in terms of physical and mechanical properties. The results showed that the resin content level and strand orientation have a significant effect on modulus of elasticity (MOE) and modulus of rupture (MOR). A higher MOE and MOR (from static bending test) in both the parallel and perpendicular directions were observed in the bamboo strand boards compared to the standard commercial OSB and wafer boards.

Nugroho and Ando (2001) studied the feasibility of using hot-pressed bamboo mat from *Moso* bamboo for manufacturing structural composite boards. The study showed that manufacturing of composite boards from *Moso* bamboo is technically feasible and its results from static bending tests indicated its superior strength properties (higher MOE and MOR) in comparison to commercial

products (like LVL, Glulam, OSB and etc.). Ahmad and Kamke (2011) also studied the viability of *Calcutta* bamboo (*Dendrocalamus strictus*) for manufacturing parallel strand lumber (PSL). They observed similar bending and compression mechanical characteristics to commercial structural composite lumber (SCL).

Mahdavi, Clouston and Arwade (2010) resolved the deficiencies of bamboo due to its natural shape by manufacturing composite lumber made from giant bamboo or laminated bamboo lumber (LBL). As shown in Figure 2.13, the manufacturing process is gluing together strands of bamboo in various forms (strands or mats taken from the culm) to form a composite rectangular structural member similar to lumber but with highly renewable characteristics. The results showed that bending strength and stiffness of LBL is comparable to laminated wood products like LVL.
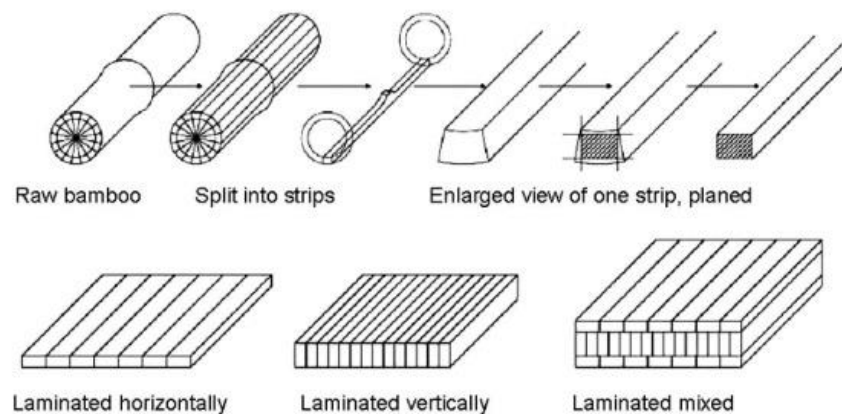
Figure 2.13 Manufacturing process of laminated bamboo lumber (LBL) using bamboo strips (Mahdavi, Clouston & Arwade 2010).

Sinha, Way and Mlasko (2013) investigated the structural performance of LBL and bamboo glulam beams (BGBs) to evaluate their potential application as structural elements. Both types of panels were tested for flexural, shear, tension, and compressive properties. The experimental results showed that, the LBL panels have a higher allowable and average strength values in tension and bending, while it possesses comparable stiffness values to a commonly used structural species of wood, such as Douglas fir.

In a study by Ghavami (2005), bamboo was used as a reinforcement of cement mortar to develop beams, columns and slabs, as shown in Figure 2.14. The

results indicated that bamboo can be considered as an appropriate substitution of steel. The durability of a steel reinforced concrete column and the first bamboo reinforced concrete beam which were tested in 1979 were also evaluated. The steel reinforced column was part of the tunnel structure of a metro in Rio and the bamboo reinforced beam was unprotected to open air in the university campus area. They observed that the treated bamboo segment of the beam reinforcement was still in satisfactory condition after fifteen years while the steel reinforcing bars of the column were rigorously corroded and must be replaced.

Figure 2.14 Rectangular concrete column reinforced with bamboo (right); and concrete slabs reinforce with bamboo (left) (Ghavami 2005).

Li, Y et al. (2012) examined the feasibility of a light-weight bamboo-steel composite slab floors made of cold-formed thin-walled steel channel and bamboo plywood sheathings. Three different types of connections were investigated (Figure 2.15) to assemble the composite slabs; including (a) simple adhesive connection, (b) self-tapping screw enhanced connection, and (c) stability improved connection with bamboo laths glued on the both sides of cold-formed steel channel. The results showed that the bamboo-steel floor slabs using the stability improved connection showed a significant improvement in stability, stiffness and bearing capacity compared with the other two connections and meet structural requirements of building floor slab.
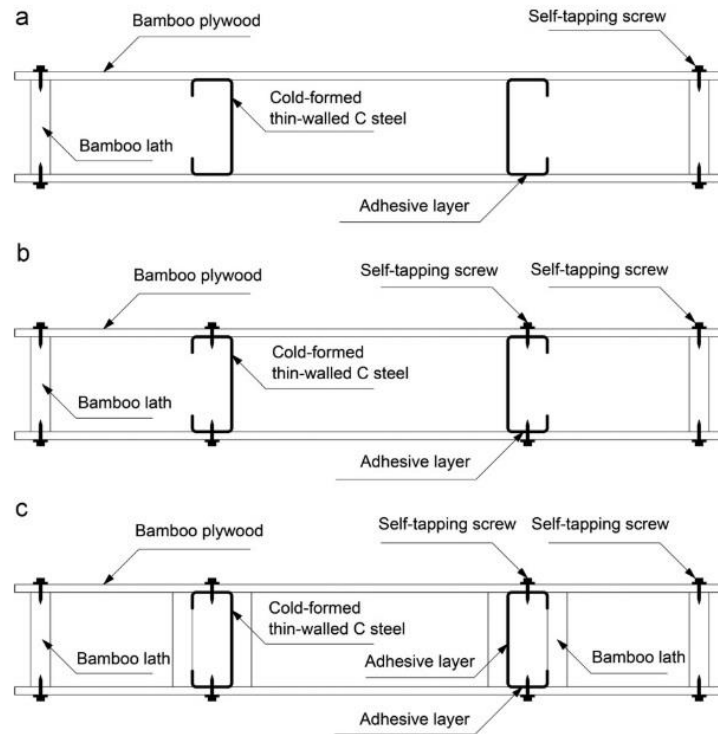
Figure 2.15 Cross-section of bamboo-steel composite slabs with three types of connections (Li, Y et al. 2012).

2.5 Summary

Mass timber products has gained popularity in the construction industry in the last decade. Existing mass timber buildings commonly use CLT floor diaphragms and load-bearing walls (Green & Taggart 2020). Due to the nature of the timber material and the manufacturing process, CLT panels are light-weight prefabricated load bearing elements. This in turn allows fast erection of light, economical and sustainable buildings. The specific orientation of CLT panels (orthogonally bonded layers of solid sawn lumbers) under out-of-plane loading shows significant rolling shear deformations because, in the radial-tangential plane, wood has a relatively low shear modulus. To address this issue, many studies have been performed, including the measurement of the planar shear properties, improvement of the planar shear properties and evaluation of the effects of CLT configuration and manufacturing parameters on the shear and bending properties of CLT (Aicher, Hirsch & Christian 2016; Cao et al. 2019; Yawalata & Lam 2011).

A smart combination of materials in composite construction is a way to minimize the use of resources, therefore reducing the environmental impact of the building

construction process. Sandwich panels have started to be utilized in the building industry. Structural Insulated Panels (SIPs) have had the most success penetrating the residential construction market (Mullens & Arif 2006). However, inner core of low transverse stiffness and strength (such as balsa wood and light weight foam core) makes the panels vulnerable to several different failure modes under bending actions, such as core shear failure and localized punching or flatwise crushing of the core (Dai & Hahn 2003; Manalo, AC et al. 2010). Therefore, a great deal of research has been conducted to enhance the core's mechanical performance, for example, by using high density PU foam core, hybrid core concept, stitched core, Z-pinning technique, or web core technique (Pardue 2011; Van Erp & Rogers 2008). However, the drawback was the weight and the production cost of these modified composite sandwich panels.

Following the push of sustainable building materials and environmentally conscious design, there is a need for a light-weight timber sandwich panel. The potential uses of sandwich panels in building industry, as a replacement for solid panels would greatly reduce the demand on timber resources. This study will investigate the feasibility of composite timber sandwich panels made by existing commercial wood products with affordable and sustainable local timber and wood waste, to manufacture sandwich panels for construction purposes. Light-weight sandwich panels are made using commercial plywood as skins, and two different core materials, bamboo, and peeler rings. Bamboo is used in the core of the proposed sandwich panel due to its local availability in Australia, outstanding stiffness-to-weight ratio, and its rapid harvest (3-4 years from the time of planting). The peeler core rings are source from the unused log core that remains after rotary peeling for veneer production, and they are normally considered as waste product and are readily available in hardwood plantations.

3 Numerical study on the flexural capacity of ultra-light composite timber sandwich panels

STATEMENT OF CONTRIBUTION TO CO-AUTHORED PUBLISHED PAPER

This chapter includes a co-authored paper. The bibliographic details of the co-authored paper, including all authors, are:

Darzi, S, Karampour, H, Gilbert, BP & Bailleres, H 2018, 'Numerical study on the flexural capacity of ultra-light composite timber sandwich panels', *Composites Part B: Engineering*, vol. 155, pp. 212-24.https://doi.org/10.1016/j.compositesb.2018.08.022

My contribution to the paper involved: literature review, analytical study, numerical modelling, run analyses, discussion of the results and writing and editing.

(Signed) _____ Date: 16/03/2020
PhD Candidate: **Siavash Darzi**

(Countersigned) _____ Date: 16/03/2020
Principle Supervisor/ Corresponding author of paper: **Dr. Hassan Karampour**

(Countersigned) _____ Date: 16/03/2020
Associate Supervisor: **Associate Professor Benoit P. Gilbert**

(Countersigned) _____ Date 16/03/2020
External Supervisor: **Dr. Henri Bailleres**

Numerical study on the flexural capacity of ultra-light composite timber sandwich panels

Abstract

The flexural stiffness and ultimate load capacity of novel ultralight composite sandwich panels, made of plywood faces and bamboo or peeling cores are investigated herein. Modified Ritz method and sandwich beam theory formulations for composite sandwich panels with thick faces and thick/stiff cores are developed and are used to find the bending stiffness of the panels in one-way and two-way bending. The ultimate capacity and failure modes of the panels are then predicted from nonlinear material and geometric finite element analyses (FEA). The numerical methods are validated against published experimental results of orthotropic composite sandwich panels. It is shown that at similar panel depths, the proposed composite timber panels can be as high as 15% stiffer and 40% lighter than the existing commercial cross-laminated timber (CLT) panels. Results of a parametric study on selected composite panels with different yield stresses in compression, show that panels with bamboo cores exhibit relatively more ductile behaviour compared to those with peeling cores. At the ultimate flexural capacity, the tensile face of the panels fails in tension parallel to the grain, while the compressive face almost reaches its yield capacity.

Keywords

Ultra-light panel, Composite timber panel, Bamboo core, Ritz method, Sandwich beam theory, Cross-laminated timber (CLT), Cellular structures

3.1 Introduction

In structural engineering applications, sandwich panels are typically fabricated by attaching two thin and stiff skins, to a lightweight, flexible and relatively thick core. Sandwich panels are extensively used in automotive, aerospace, marine and industrial applications due to their high strength-to-weight and stiffness-to-weight ratios. Recently, there has been a growing trend in the construction industry to use sandwich structural elements for floors and load bearing walls (Manalo, A et al. 2010). Common skin materials include thin metal sheets (Liew & Sohel 2010), fibre reinforced polymer (FRP) composites (Dawood, Taylor & Rizkalla 2010), and in some structural applications, reinforced concrete (Sohel & Liew 2011). Core materials include balsa wood (Grenestedt & Bekisli 2003), polymeric foams (Mamalis et al. 2008), Fibre Reinforced Polymer (FRP) cores (M. Reis & H. Rizkalla 2008), metallic foams (Kabir, Vodenitcharova & Hoffman 2014; McCormack et al. 2001), and honeycomb cells (Nia & Sadeghi 2010). With recent changes in legislations and the growing trend towards tall mass-timber buildings, engineered wood products (EWP) such as Cross-laminated Timber (CLT) have gained increased popularity in residential and commercial construction in the form of slabs and load bearing walls. A CLT panel Figure 3.1 (a), is comprised of an odd number of orthogonally bonded layers of solid sawn lumbers, which are bonded using adhesive, nails or wooden dowels (Brandner et al. 2016). CLT is a lighter alternative compared to concrete and composite concrete-steel slabs and walls. However, CLT is susceptible to rolling shear failure (Fellmoser & Blaß 2004), and the congestion of material in the vicinity of the neutral axis, reduces the efficiency of CLT panels in flexure. Unlike CLT, in a sandwich panel and with respect to bending characteristics, the material is efficiently distributed over the cross-section.

Most of the existing composite sandwich panels use low-strength material such as foam in the core component. In bending action, the role of the core is critical in transmitting the shear between the face in compression and the one in tension. Therefore, sandwich panels with soft cores are not optimal solution for structural members subject to bending actions such as slabs (Styles, Compston & Kalyanasundaram 2007). To overcome this issue, several researchers have used high-density core material to improve the load bearing capacity of the sandwich structures. Daniel and Abot (2000) filled the cells of a honeycomb core with epoxy

to prevent premature shear failure of the composite sandwich panels. CoDyre and Fam (2016) showed that doubling and tripling the foam core density in sandwich panels with GFRP skins led to increases in peak load by 170%, due to the enhanced composite action and reduced shear deformations. Mahfuz et al. (2004) improved the performance of composite sandwich panels under flexure by infusing titanium dioxide (TiO_2) nanoparticles into the parent polyethylene foam material to strengthen the core structure. Their results showed that a 53% increase in the flexural strength could be attained by infusing 3% loading of TiO_2 nanoparticles in the core. However, such advantages disappear as the floor spans become longer. Some researchers have proposed alternative forms for sandwich panels, by introducing FRP stitches through foam cores to improve the performance of the foam core (Dawood et al. 2010; Tuwair et al. 2015). The results show some improvements in the flexural response and the stitches prevent the de-bonding of the core from the faces.

The previously mentioned studies (Mahfuz et al. 2004; Tuwair et al. 2015) showed that the enhancement of the core material significantly improves the performance of the composite sandwich panels. The drawback, however, is that the weight and the production cost of these composite sandwiches are also significantly increased. To address these drawbacks, two novel lightweight sandwich panels, namely, (a) Bamboo Core Sandwich (BCS) panel, and (b) Peeling Core Sandwich (PCS) panel are proposed herein. The Bamboo Core Sandwich (BCS) panel is depicted in Figure 3.1 (b) and is comprised of vertically aligned hollow bamboo rings (core) and commercial plywood laminates (faces). The hollow bamboo rings are bonded to the face skins using a polyurethane structural adhesive. Bamboo is a light sustainable natural material, can be harvested in 3-4 years from the time of planting, is recyclable and has mechanical properties comparable to those of conventional building materials (Amada et al. 1997). The Peeling Core Sandwich (PCS) panel is shown in Figure 3.1 (c). Similar to the BCS panel, the faces of the PCS panel are made from commercial plywood laminates. The core is made up of peeling cores, which are the unused products left from the wood log peeled into veneers in a lathe machine. Depending on the specifications of the veneer log peeling lathe machine, the peeling cores may have diameters of 40-120 mm (Melo et al. 2014).

(a)
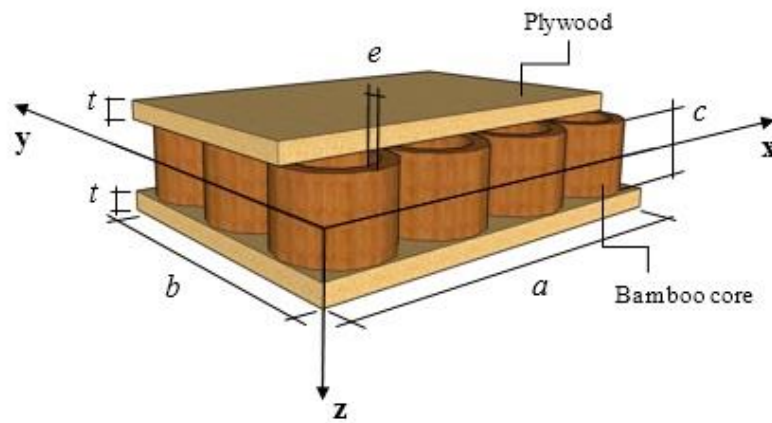
(b)
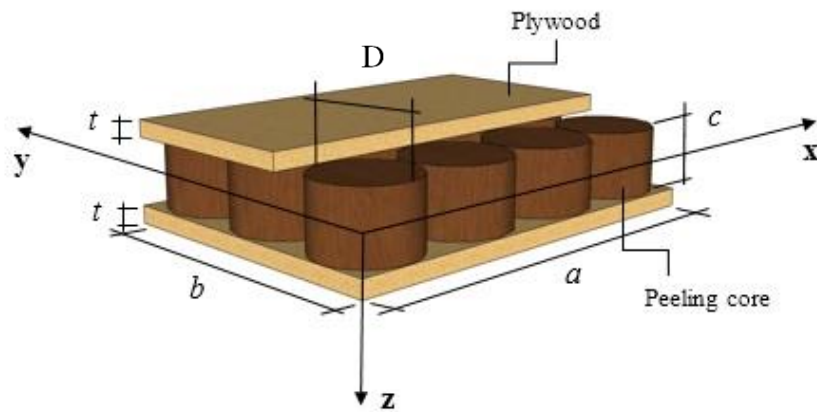
(c)

Figure 3.1 A schematic illustration of (a) existing commercial Cross-laminated Timber (CLT) panel, and (b) proposed Bamboo Core Sandwich (BCS) panel and, (c) Peeling Core Sandwich (PCS) panel.

In this paper, the flexural stiffness and ultimate strength of the proposed BCS and PCS panels under uniformly distributed transverse load are investigated. Using Ritz method (energy method), effects of the thickness and material properties of the plywood skins and height of the core, on the bending stiffness of the panels are first presented and discussed. The results are compared to the bending stiffness of commercially available CLT panels of almost similar depths. The ultimate flexural strength of the BCS and PCS panels is then calculated using a validated finite element analysis (FEA). The article is organised as follows. In Section 3.2, a Ritz formulation is developed that can capture the flexural stiffness of sandwich panels with thick cores, in one-way and two-way bending. The accuracy of the proposed Ritz-method is validated against published experimental results of a Glass Fibre Reinforced Polymer (GFRP) sandwich panel in two-way bending. The Ritz results are also compared to the theoretical predictions of sandwich beam theory (Timoshenko beam theory) in one-way bending. In Section 3.3, a parametric study on the flexural stiffness of BCS and PCS panels are presented using the Ritz method for panels in one-way and two-way bending. The flexural stiffness of the optimum BCS and PCS panels are compared against the CLT panels in this section. The manuscript is concluded with the discussion of the ultimate strength and failure modes of the BCS and PCS panels in one-way bending, using FEA in Section 3.4.

3.2   Methodology and validation

3.2.1   The Ritz method

The flexural behaviour of the BCS and PCS panels under uniformly distributed loads, with two-edge simply supported (one-way bending) and four-edge simply supported (two-way bending) configurations is investigated using the Ritz method. To do so, a new formulation for bending of sandwich orthotropic plates with thick core/thick face under transverse deflection is derived. In this method, the total strain energy of the system, which consists of the in-plane and shear strains of the core, membrane, shear and local bending strains of the faces, is calculated. Small deflection theory is adopted and therefore, it is assumed that the middle plane of the orthotropic plate does not stretch under transverse deflections. Due to the difference in stiffness of the core compared to the plywood faces, the strain energy terms incorporate the shearing strain of the core in

orthogonal directions and purely in-plane shearing strain of the faces. Unlike existing formulation for sandwich panels with soft cores, in derivation of the Ritz equations herein, the flexural rigidity of the cores of the BCS and PCS panels are not neglected. Also, to be able to extend the Ritz formulation to BCS and PCS panels with thick faces, the local bending stiffness of the faces are considered. By assuming an appropriate expression for the deflection of the orthotropic plate and considering the boundary conditions of the panels, the total energy of the system is obtained by adding the total strain energy of the deformed panel and the potential energy of the applied load. The deflected configuration that corresponds to the minimum total energy in the panel under assumed transverse load is obtained, and the corresponding mid-span deflection of the panel is calculated. The flexural stiffness of the BCS and PCS panel is obtained by finding the slope of the corresponding load-deflection curve. The problem formulation is discussed herein.

3.2.1.1 Displacements and Strains

Schematic view of the panels are shown in Figure 3.1 (b) and (c).The load is assumed to be applied on the top face and in the positive z direction. The displacement in the x, y and z directions are denoted with u, v and w respectively. A section of the deflected panel parallel with the xz plane, after undergoing a displacement in the z direction is shown in Figure 3.2.

During the subsequent displacement, if there were no shear strains, the line $abcde$, which is normal to the centre line of the undeformed panel, would rotate through an angle $\partial w/\partial x$ to the position $a'b'c'd'e'$ and would remain normal to the centre line of the sandwich panel. In the BCS and PCS panels, the cores are not soft and contribute to the flexural rigidity of the composite panel. Therefore, the line $abcde$ moves to a new position $a''b''c'd''e''$ during the subsequent displacement. Since the shear strains in the faces are assumed to be negligible, the lines $a''b''$ and $d''e''$ remain parallel with $a'b'c'd'e'$. The angle $\widehat{d'c'd}''$ is equal to the shear strain γ and $\widehat{d''c'z}$ is denoted with $\lambda\left(\partial w/\partial x\right)$. The quantity λ may take any value between +1 and $-t/c$ ($t<c$), where c is the core height and t is the face thickness. The value $\lambda = +1$ applies when $\gamma = 0$ and the panel behaves as composite beam.
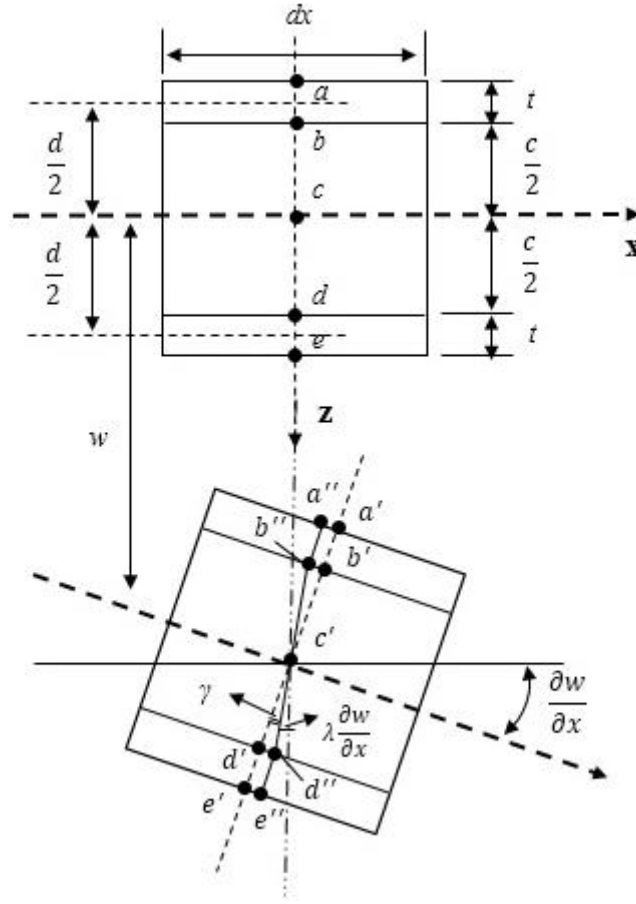
Figure 3.2 Deflected shape of a short section of the BCS/PCS panel in bending, used in the Ritz method formulation.

The other extreme, $\lambda = -t/c$ represents a sandwich panel with a core so flexible in shear that cannot provide any connection between the two faces (Allen 1969). For an orthotropic plate, a similar diagram may be drawn for the yz plane (not shown here) to obtain the displacement in y direction. In this case, μ would be a parameter such that a line in the core, which is originally vertical, rotates in the yz plane through an angle μ $(\partial w/\partial y)$.

The displacements u and v in x and y directions of any point within the deformed sandwich panel and with respect to the notations presented in Figure 3.2 can be obtained as follows:

Displacement field in the core

$$u_c = -z\lambda \frac{\partial w}{\partial x}, \quad -\frac{c}{2} \le z \le +\frac{c}{2} \tag{3.1a}$$

37

$$v_c = -z\mu\frac{\partial w}{\partial y}, \quad -\frac{c}{2} \le z \le +\frac{c}{2} \tag{3.1b}$$

Displacement field in the lower face

$$u_f = -\frac{c}{2}\lambda\frac{\partial w}{\partial x} - \left(z - \frac{c}{2}\right)\frac{\partial w}{\partial x} = -\left\{\frac{c}{2}(\lambda - 1) + z\right\}\frac{\partial w}{\partial x}, \quad \frac{c}{2} \le z \le \frac{h}{2} \tag{3.2a}$$

$$v_f = -\left\{\frac{c}{2}(\mu - 1) + z\right\}\frac{\partial w}{\partial y}, \quad \frac{c}{2} \le z \le \frac{h}{2} \tag{3.2b}$$

Displacement field in the mid-plane of the lower face

$$u_{fm} = -\frac{1}{2}(c\lambda + t)\frac{\partial w}{\partial x}, \quad z = \frac{c+t}{2} \tag{3.3a}$$

$$v_{fm} = -\frac{1}{2}(c\mu + t)\frac{\partial w}{\partial y}, \quad z = \frac{c+t}{2} \tag{3.3b}$$

where h is the overall depth of the panel as shown in Figure 3.2. The expressions for the strains are obtained by differentiation of the above displacements u and v within the corresponding displacement fields. The longitudinal strains $\in$ and shear strains γ in the core are

$$\in_x^c = \frac{\partial u}{\partial x} = -z\lambda\frac{\partial^2 w}{\partial x^2} \tag{3.4a}$$

$$\in_y^c = \frac{\partial v}{\partial y} = -z\mu\frac{\partial^2 w}{\partial y^2} \tag{3.4b}$$

$$\gamma_{zx}^c = \frac{\partial u}{\partial z} + \frac{\partial w}{\partial x} = (1 - \lambda)\frac{\partial w}{\partial x} \tag{3.4c}$$

$$\gamma_{yz}^c = \frac{\partial v}{\partial z} + \frac{\partial w}{\partial y} = (1 - \mu)\frac{\partial w}{\partial y} \tag{3.4d}$$

$$\gamma_{xy}^c = \frac{\partial u}{\partial y} + \frac{\partial v}{\partial x} = -z(\lambda + \mu)\frac{\partial^2 w}{\partial x\partial y} \tag{3.4e}$$

The strains in the faces consist of the longitudinal membrane strains $\in^{fm}$, shear membrane strains γ^{fm}, and local bending strains $\in^{fL}$. Membrane strains at the middle plane of the faces are obtained by differentiation of Eqs. (3.3a) and (3.3b)

$$\epsilon_x^{fm} = \frac{\partial u}{\partial x} = -\frac{1}{2}(c\lambda + t)\frac{\partial^2 w}{\partial x^2} \tag{3.5a}$$

$$\epsilon_y^{fm} = \frac{\partial v}{\partial y} = -\frac{1}{2}(c\mu + t)\frac{\partial^2 w}{\partial y^2} \tag{3.5b}$$

$$\gamma_{xy}^{fm} = \frac{\partial u}{\partial y} + \frac{\partial v}{\partial x} = -\frac{\partial^2 w}{\partial x \partial y}\left(\frac{c}{2}\lambda + \frac{c}{2}\mu + t\right) \tag{3.5c}$$

The x displacement of any point z in the lower face with respect to the middle plane of the lower face is

$$u_{fL} = -\left\{\frac{c}{2}(\lambda - 1) + z\right\}\frac{\partial w}{\partial x} + \frac{1}{2}(c\lambda + t)\frac{\partial w}{\partial x} = -\left(z - \frac{c}{2} - \frac{t}{2}\right)\frac{\partial w}{\partial x} \tag{3.6a}$$

$$v_{fL} = -\left\{\frac{c}{2}(\mu - 1) + z\right\}\frac{\partial w}{\partial y} + \frac{1}{2}(c\mu + t)\frac{\partial w}{\partial y} = -\left(z - \frac{c}{2} - \frac{t}{2}\right)\frac{\partial w}{\partial y} \tag{3.6b}$$

The corresponding local bending strains and shear strain in the lower face are

$$\epsilon_x^{fL} = -\left(z - \frac{c}{2} - \frac{t}{2}\right)\frac{\partial^2 w}{\partial x^2}, \quad \frac{c}{2} \leq z \leq \frac{h}{2} \tag{3.6c}$$

$$\epsilon_y^{fL} = -\left(z - \frac{c}{2} - \frac{t}{2}\right)\frac{\partial^2 w}{\partial y^2}, \quad \frac{c}{2} \leq z \leq \frac{h}{2} \tag{3.6d}$$

$$\gamma_{xy}^{fL} = \frac{\partial u}{\partial y} + \frac{\partial v}{\partial x} = -2\left(z - \frac{c}{2} - \frac{t}{2}\right)\frac{\partial^2 w}{\partial x \partial y} \tag{3.6e}$$

The total direct strain in the faces is calculated by adding the membrane and local bending strains. The total direct strain in the lower face in x direction $\in_x$ is the sum of the Eqs. (3.5a) and (3.6c), and in the y direction $\in_y$ is the sum of Eqs. (3.5b) and (3.6d).

3.2.1.2 Energy equation

The strain energy per unit volume of the faces U_f is calculated by adding the total strain energy and shear strain energy of the lower and upper faces

$$U_f = 2[\frac{1}{2g}\int_V \{E^f_x \in^2_x + E^f_y \in^2_y + 2E^f_x v^f_{yx} \in_x \in_y\}dV$$
$$+ \frac{1}{2}\int_V \{G^f_{zx}\gamma^2_{zx} + G^f_{xy}\gamma^2_{xy} + G^f_{yz}\gamma^2_{yz}\}dV]$$

(3.7)

where E_x, E_y are the elastic moduli, G_{xy}, G_{yz}, G_{xz} are the shear moduli and v_{xy}, v_{yx} are the Poisson's ratios of the faces. $\in_x$ and $\in_y$ are the total direct strains in the lower face in x and y directions and $g = (1 - v_{xy}v_{yx})$. The factor of two in Eq. (3.7) accounts for the strain energy of the upper face. It should be noted that, when the plywood faces are shallow in proportion to their spans, the shear strain energy in zx and yz planes can be neglected. Similarly, the strain energy per unit volume of the core U_c is obtained by adding the longitudinal and shear strain energies, obtained from the strain expressions defined in Eq. (3.4):

$$U_c = \frac{1}{2g}\int_V \left\{E^c_x\left(-z\lambda\frac{\partial^2 w}{\partial x^2}\right)^2 + E^c_y\left(-z\mu\frac{\partial^2 w}{\partial y^2}\right)^2 + 2E^c_x v^c_{yx}\left(-z\lambda\frac{\partial^2 w}{\partial x^2}\right)\left(-z\mu\frac{\partial^2 w}{\partial y^2}\right)\right\}dV$$
$$+ \frac{1}{2}\int_V \left\{G^c_{zx}\left((1-\lambda)\frac{\partial w}{\partial x}\right)^2 + G^c_{xy}\left(-z(\lambda+\mu)\frac{\partial^2 w}{\partial x\partial y}\right)^2 + G^c_{yz}\left((1-\mu)\frac{\partial w}{\partial y}\right)^2\right\}dV$$

(3.8)

Unlike previous studies with flexible core materials which neglect the core stiffness, Eq. (3.8) includes the in-plane stiffness of the core. The shear stiffness in the xy plane of the core is also considered in the present model. The strain energy due to direct stresses and strains in the z direction is neglected due to high stiffness of the core materials in z direction (low possibility of significant flattening or squashing) and small intensity of the transverse load.

The numerical integrations in Eqs. (3.7) and (3.8) are carried out over the volume of the face and core respectively. The numerical integration of Eq. (3.7) (in the faces) is straightforward, because the volume of the faces does not change in the xy plane. However, the in-plane (xy plane) cross-sectional areas of the bamboo and peeling cores vary across the panel. To simplify the numerical integration of Eq. (3.8), the factors K_B and K_P are introduced to define the ratio of the core

material to the total volume of the core, in the BCS and PCS panels, respectively. These factors are multiplied by the modulus of elasticity and shear modulus of the core in Eq. (3.8).

$$K_B = \left[\frac{\pi \left(R^2 - r^2 \right) \times c}{abc} \right] \times n \qquad (3.9a)$$

$$K_P = \left[\frac{\pi D^2 \times c}{4abc} \right] \times n \qquad (3.9b)$$

where R and r are the outer radius and inner radius of the hollow bamboo sections, respectively and D is the diameter of the peeling core. The total number of bamboo rings or peeling cylinders within the panel with length of a and width of b is equal to n.

3.2.1.3 Total potential energy

The change of potential energy associated with the deformation of the orthotropic sandwich plate under uniform transverse load q_{uni} is

$$V = -\int_0^a \int_0^b w q_{uni} dx dy = -q_{uni} \int_A w dA \qquad (3.10)$$

The load q_{uni} can be represented by a double Fourier series expansion

$$q_{uni} = \sum_{m=1}^{\infty} \sum_{n=1}^{\infty} \frac{16q}{\pi^2 mn} \sin\left(\frac{m\pi x}{a} \right) \sin\left(\frac{n\pi y}{b} \right) \qquad (3.11)$$

where a and b are the length and width of the panel shown in Figure 3.1. A point load can be regarded as a local pressure applied over a small rectangular area with length a' and width b', at the centre of the panel located at (ψ, η)), and can be shown in following double Fourier series format

$$q_{point} = \sum_{m=1}^{\infty} \sum_{n=1}^{\infty} \frac{16P}{\pi^2 mna'b'} \sin\left(\frac{m\pi\psi}{a} \right) \sin\left(\frac{n\pi\eta}{b} \right) \sin\left(\frac{m\pi a'}{2a} \right) \sin\left(\frac{n\pi b'}{2b} \right) \sin\left(\frac{m\pi x}{a} \right) \sin\left(\frac{n\pi y}{b} \right)$$

(3.12)

To thoroughly validate the method for the one-way and two-way bending deformations of the panels, two-edge simply supported, and four-edge simply supported boundary conditions are adopted. Knowing that deflection and bending

41

moments vanish at the simply supported edges, the following expressions for the deflected shapes are assumed for the two-way bending (four-edge simply supported)

$$w = \sum_{m=1}^{\infty} \sum_{n=1}^{\infty} a_{mn} \sin\left(\frac{m\pi x}{a}\right) \sin\left(\frac{n\pi y}{b}\right) \tag{3.13}$$

$$w = 0, \quad \frac{\partial^2 w}{\partial x^2} = 0 \quad \text{at} \quad x = 0 \quad \text{and} \quad x = a$$

$$w = 0, \quad \frac{\partial^2 w}{\partial y^2} = 0 \quad \text{at} \quad y = 0 \quad \text{and} \quad y = b \tag{3.13a}$$

and for the one-way bending (two-edge simply supported)

$$w = \sum_{m=1}^{\infty} a_m \sin\left(\frac{m\pi x}{a}\right) \tag{3.14}$$

$$w = 0, \quad \frac{\partial^2 w}{\partial x^2} = 0 \quad \text{at} \quad x = 0 \quad \text{and} \quad x = a \tag{3.14a}$$

where a_{mn} is the deflection amplitude at the middle of the panel ($x = a/2$, $y = b/2$). The total energy of system $\Pi = U_f + U_c + V$ and is equal to the summation of Eqs. (3.7), (3.8) and (3.10). Π is a function of a_{mn}, λ and μ. In the Ritz method, the stable deflected shape corresponds to the values of a_{mn}, λ and μ , which minimise the total energy Π. These values are calculated by solving the following system of equations in MATLAB.

$$\frac{\delta}{\delta \lambda}(\Pi) = 0$$

$$\frac{\delta}{\delta \mu}(\Pi) = 0 \tag{3.15}$$

$$\frac{\delta}{\delta a_{mn}}(\Pi) = 0$$

3.2.2 Sandwich beam theory

Narrow BCS and PCS panels act in one-way bending under transverse loads. Therefore, deflections of such panels can be approximated using Timoshenko beam theory (Timoshenko & Woinowsky-Krieger 1959). The model takes into account rotational bending and shear deformation effects. The total elastic

displacement of the mid-span of a simply supported narrow sandwich panel (Δ) is the sum of flexural (w_1) and shear (w_2) deformations:

$$\Delta = w_1 + w_2 = \frac{5a^4 q}{384(EI)_{eq}} + \frac{a^2 q\kappa}{8(AG)_{eq}} \tag{3.16}$$

where q is the uniformly distributed load, $(EI)_{eq}$ and $(AG)_{eq}$ are the equivalent flexural and shear rigidities, respectively, and κ is the Timoshenko shear coefficient. The flexural rigidity of the BCS or PCS narrow panels is the sum of the bending rigidities of the plywood faces and the bamboo/peeling cores

$$(EI)_{eq} = 2 \times E_f \frac{bt^3}{12} + 2 \times E_f bt \left(\frac{d}{2}\right)^2 + E_c \frac{(b_c)c^3}{12} \tag{3.17}$$

where E_f and E_c are the elastic modulus of the plywood faces and the core in the span direction, respectively. The width of the faces and the core are represented by b and b_c in Eq. (3.16), respectively. In the BCS panel at any given cross-section cut along the span (parallel to the yz plane in Figure 3.1 (b), b_c is almost equal to $2en_{yz}$, where e is the bamboo wall-thickness and n_{yz} is the number of bamboos across the width of the panel (Figure 3.1(b)). In the PCS panel, the width of the core (b_c) varies along the span at various x-coordinates. A cut-through single peeling core (parallel to the yz plane) of the PCS panel is depicted in Figure 3.3 (a).

(a)

(b)
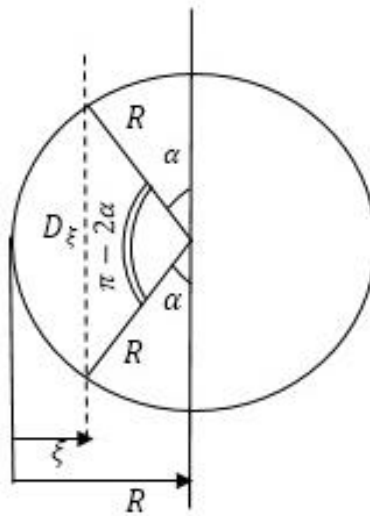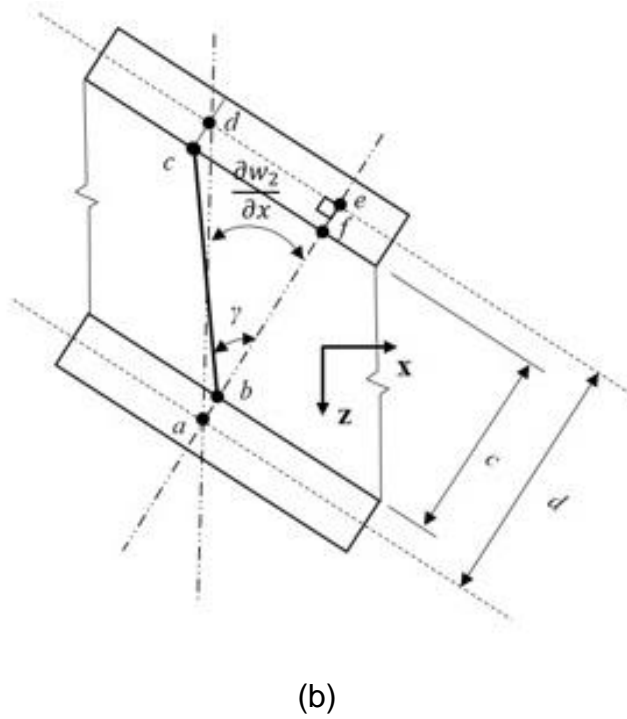
Figure 3.3 (a) Cross section of a single peeling core used to find the equivalent core width (b_c) and, (b) deflected shape of a short length of the BCS/PCS panel under transverse load used in the Beam Sandwich Theory formulation.

Since the third term in Eq. (3.17) corresponds to the flexural rigidity of the core, it is meaningful to find an equivalent core width b_c, based on the moment of inertia of the peeling core at the cut-section.

$$b_c = 2R\, n_{yz}\, \frac{\overline{I}_\xi}{I_\xi}$$

$$\overline{I}_\xi = \frac{1}{12}(2Rc^3) \tag{3.18}$$

$$I_\xi = \frac{1}{R}\int_0^R \frac{c^3}{12} D_\xi\, d\xi = \frac{1}{R}\int_0^R \frac{c^3}{12}\left(2R\sqrt{1-\left(1-\frac{\xi}{R}\right)^2}\right)d\xi$$

where D_ξ is the thickness of a peeling core (Figure 3.3(a)), cut at distance ξ away from an edge, and n_{yz} is the number of peeling cores with radius R, along the width of the PCS panel (Figure 3.1(c)). The deformation due to shear (w_2 in Eq. (3.16)), is calculated with respect to a tilted deformed section of the narrow panel shown in Figure 3.3 (b). The shear strain γ is assumed to be constant through the core height. Under a transverse load, the faces and the longitudinal centre-line of the narrow panel tilt, and the relation between the slope of the panel $\frac{\partial w_2}{\partial x}$

44

and the core shear strain γ is obtained from Figure 3.3 (b). As seen in the diagram $\gamma c = cf = de$. Hence

$$\frac{\partial w_2}{\partial x} = \gamma \times \frac{c}{d} = \frac{\tau}{G} \times \frac{c}{d} \qquad (3.19)$$

For a composite panel the shear stress can be expressed as (Allen 1969).

$$\tau = \frac{Q}{(EI)_{eq} b_c} \sum S_i.E_i \qquad (3.20)$$

where $(EI)_{eq}$ is the flexural rigidity of the entire section (Eq. (3.17)), S_i and E_i represent the first moment of area and modulus of elasticity of the face or the core, and Q is the shear force at the section. By substituting $(EI)_{eq}$ from Eq. (3.17) and γ from Eq. (3.19), into Eq. (3.20), the shear stress at any point within the core, at a distance z from the centre of the core is

$$\tau = \frac{Q}{(EI)_{eq}(b_c)} \left\{ E_f \frac{btd}{2} + \frac{E_c(b_c)}{2} \left(\frac{c^2}{4} - z^2 \right) \right\} \qquad (3.21)$$

The shear stress distribution in the core is assumed to be constant and equal to average of the shear stress at the bottom of the face ($z = c/2$) and shear stress at the centre of the core ($z = 0$). Thus, the shear rigidity of the core and corresponding Timoshenko shear coefficients for BCS and PCS panels are

$$(AG)_{eq} = (b_c d)G_c$$

$$\kappa = \frac{c}{(EI)_{eq}} \left(E_f \frac{btd}{2} + \frac{E_c(b_c)}{4} \left(\frac{c^2}{4} \right) \right) \qquad (3.22)$$

It should be noted that most of CLT floor slabs have dimensions of proportion $a/b > 2$ (Figure 3.1(a)), and are thus assumed to exhibit one-way bending. The same Timoshenko beam formulation (Eq. (3.16)) known as the shear analogy method (Kreuzinger, H 1995), is widely used in practice to calculate the deflection of the CLT panels. The flexural and shear rigidities of the CLT panel are

$$(EI)_{eff} = \sum_{i=1}^{n} E_i . b_i . \frac{h_i^3}{12} + \sum_{i=1}^{n} E_i . A_i . z_i^2$$

$$(AG)_{eff} = \frac{d_a^2}{\left[\left(\dfrac{h_1}{2.G_1.b} \right) + \left(\sum_{i=2}^{n-1} \dfrac{h_i}{G_i.b_i} \right) + \left(\dfrac{h_n}{2.G_n.b} \right) \right]} \qquad (3.23)$$

where E_i is the modulus of elasticity and b_i and h_i are the width and thickness of each individual layer, respectively. z_i is the distance between the centre axis of each individual layer and the neutral axis of the entire cross-section of the CLT panel (Figure 3.1 (a)). G_i and A_i are the shear modulus and the area of cross-section of each individual layer, d_a is the distance between the two centre axes of the top and bottom layers of the entire cross-section. h_n and G_n are the thickness and the shear modulus of the surface layer, respectively. The Timoshenko shear coefficient of CLT panel κ is equal to 1.2 (Karacabeyli & Gagnon 2019).

3.2.3 Validation of the Ritz and the Sandwich beam theory methods

3.2.3.1 One-way bending

The flexural responses of BCS and PCS narrow panels in one-way bending under uniformly distributed load, from the Ritz method (Section 3.2.1) and the sandwich beam theory (Section 3.2.2) are compared in Figure 3.4 (a). To do so, double layer BCS and PCS panels with length of 6 m and width of 1 m are considered. The panels consist of plywood ID 21-30-9 (described in Section 3.3.1) with a total thickness of 42 mm, and core depth of 200 mm. The outer radius of the bamboo and peeling cores (R) are 50 mm and the wall-thickness of bamboo (e) is 10 mm. The material properties of the core materials and plywood faces are represented in Table 3.1 and Table 3.2, respectively. As shown in Figure 3.4 (a), the results from the proposed Ritz method and the sandwich beam theory almost coincide.
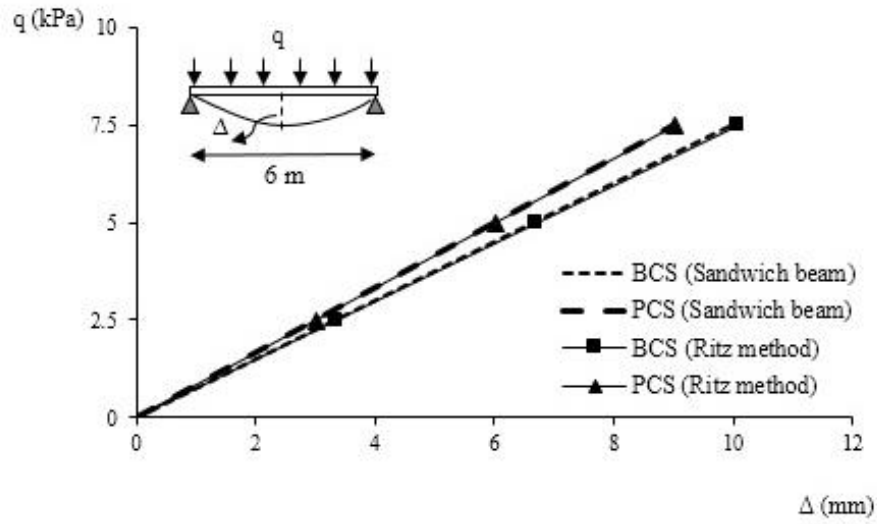
(a)
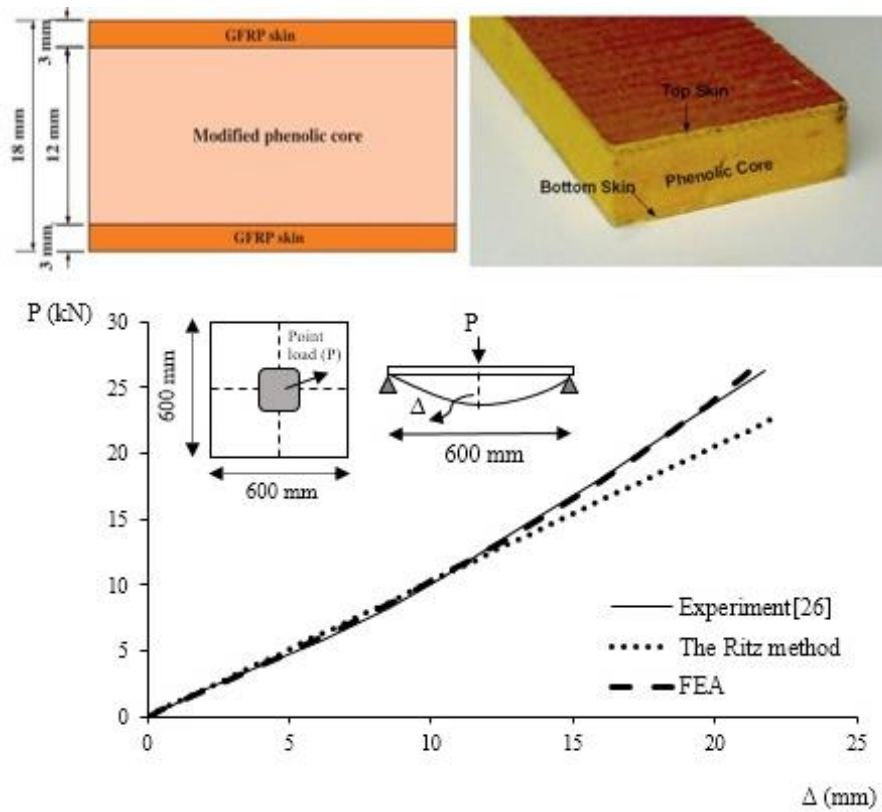
(b)

Figure 3.4 (a) Load versus mid-span deflection of BCS and PCS panels using the Ritz method and the sandwich beam theory, and (b) the GFRP sandwich panel and its cross section (top), and corresponding load-deflection response of the GFRP panel from experiment, the proposed Ritz method and current FEA (bottom).

Table 3.1 Material properties of bamboo, peeling cores and *Radiata Pine* used in the BCS and PCS panels.

Material	E_X (MPa)	E_Y (MPa)	E_Z (MPa)	G_{XY} (MPa)	G_{YZ} (MPa)	G_{XZ} (MPa)	u_{XY}	u_{YZ}	u_{XZ}	Density (kg/m³)
Bamboo core	10,500	1,260	1,260	630	630	630	0.3	0.3	0.3	740
Peeling core	10,500	1,260	1,260	630	630	630	0.3	0.3	0.3	440
Radiata ply	15,070	678	1,115	798	150	829	0.4	0.38	0.39	590
GFRP (faces)	11,750	9,650	9,650	2,465	2,173	2,173	0.3	0.3	0.3	-

Table 3.2 Material properties of the BCS and PCS faces calculated from the classical laminate theory (Nairn 2015).

Panel ID	MOE Longitudinal (MPa)	MOE Transverse (MPa)	Shear Modulus (MPa)	Poisson's ratio (in yx- plane)	Nominal thickness of individual plies through assembly (mm)
18-30-7 single layer	9,382	6,483	799	0.03	3.0/2.4/2.4/2.4/2.4/2.4/3.0
18-30-7 double layer	9,832	6,483	799	0.03	
21-30-9 single layer	11,037	4,827	799	0.06	3.0/1.5/3.0/1.5/3.0/1.5/3.0/1.5/3.0
21-30-9 double layer	11,037	4,827	799	0.06	
25-30-9 single layer	8,278	7,588	799	0.03	3.0/2.4/3.0/2.4/3.0/2.4/3.0/2.4/3.0
25-30-9 double layer	8,278	7,588	799	0.03	

3.2.3.2 Two-way bending

The Ritz method proposed in Section 3.2.1 is validated against experimental results of a square 600×600 mm Glass Fibre Reinforced Polymer (GFRP) orthotropic sandwich panel reported in (Awad et al. 2013). The sandwich panel used in the experimental study (Awad et al. 2013) is shown in Figure 3.4, and is made of glass fibre composite faces with wall thickness of 3 mm and a toughened phenol formaldehyde resin core with depth of 12 mm. The orthotropic material properties of the GFRP faces are represented in Table 3.1. The isotropic core has a modulus of elasticity 1,350 MPa and shear modulus of 746 MPa. In the experimental study, the panel was simply supported on four sides using steel screws that fixed the GFRP sandwich slab to the timber (two-way bending). A point load was applied via a 100×100 mm steel plate, positioned at the centre of the panel. The load-deflection responses of the GFRP slab from the experimental results and the proposed Ritz method are presented in Figure 3.4 (b). A reasonable correlation is observed between the Ritz method and the experimental results within the linear region. The difference between stiffness found from the experimental test and the Ritz method is less than 4%.

3.3 Flexural stiffness of the BCS and PCS panels in one-way and two-way bending

A parametric study is carried out in this section to investigate the influence of face thickness (t) and core height (c), on the flexural stiffness of the BCS and PCS panels in one-way (two-edge simply supported) and two-way (four-edge simply supported) bending. The flexural stiffness of the panels are obtained using the proposed Ritz method (Section 3.2.1), and are compared against those of CLT panels with almost identical depths, using the sandwich beam theory (shear analogy method), defined in Section 3.2.2.

3.3.1 The labelling scheme and the material properties of the panels

In the study that follows, three different structural plywood IDs are adopted for the faces of the panels, based on standard structural plywood construction in Australian/New Zealand standard (*AS/NZS 2269.0:2012 Plywood-Structural Part 0: Specifications* 2012). The selected plywood IDs are 18-30-7, 21-30-9 and 25-30-9. The numbering sequence in the ID gives, the nominal plywood thickness, the face veneer thickness multiplied by 10, and the number of plies in the assembly. For instance, Plywood ID 18-30-7 in Table 3.2 describes 18 mm thick

plywood, made of 3 mm thick veneers on the top and bottom plies, and total number of 7 plies. The nominal thickness of individual plies through the assembly is listed inTable 3.2. To increase the flexural stiffness of the panels, two plywoods of the same ID are glued together to construct the faces of the panels. Such panels are noted as double layer BCS/PCS panels herein. The double layer BCS/PCS panels have the same core depth as the single layer panels. For instance, to make a double layer BCS 18-30-7 panel, plywoods with nominal thickness of 18 mm, face veneer thickness of 3 mm, made of 7 plies are glued to the top and bottom faces of the single layer BCS 18-30-7 panel. Therefore, a double layer BCS 18-30-7 panel consists of plywood faces of 36 mm with 14 plies. It should be noted that in classical sandwich panel theory, panels with $d/t < 5.77$ are categorised as sandwich panels with thick faces and those with $5.77 < d/t < 100$ are considered thin face ($d = c + t$). All the single and double layer BCS/PCS panels used in this study have $5.77 < d/t < 14.89$, which suggest that the proposed BCS/PCS panels have relatively thick faces. The outer radius of the bamboo and peeling cores are 50 mm and the wall-thickness of bamboo is 10 mm in all the models. The material properties of the core materials and plywood plies in BCS and PCS panels are shown in Table 3.1. The x, y and z directions correspond to the longitudinal (parallel to fibres), tangential and radial direction, respectively. The plywood plies are assumed to be made of plantation pine (*Pinus Radiata*) and the material properties are taken from (*Wood Handbook: Wood as an Engineering Material* 2010b). The properties of bamboo are taken as the average values of *Moso* bamboo (*Phyllostachys pubescens*) reported in (Chung & Yu 2002). To find the mechanical properties of the plywood faces from orthotropic properties of each ply (*Radiata* plies), the *OSULaminates* tool, which is a *Java* application developed by *Oregon State University* for analysis of laminated plates (Nairn 2015) is utilised. *OSULaminates* uses classical laminate theory (Reddy 1987) to calculate the axial and bending rigidity of a laminated plate based on the properties of its individual layers. The material properties of the plywood laminate faces obtained by *OSULaminate*, comprised of *Radiata* plies with properties listed in Table 3.1, are presented in Table 3.2. For sake of comparison, two commercial CLT panels, *CL7/295* and *CL7/315* are selected from *XLam* CLT products (XLam 2016). The *CL7/295* and *CL7/315* panels consist of seven layers of sawn boards with a total thickness of 295 mm and 315 mm, respectively. The two outermost layers (1 and 7) and the middle layers (3 and 5)

shown in Figure 3.1 (a), are aligned in the span direction, and other layers are perpendicular to the span direction. The material properties of the CLT panel laminations are represented in Table 3.3 and are taken from *XLam* design guide (XLam 2016).

Table 3.3 Material properties of the CLT laminations and selected panels taken from *XLam* product sheet (XLam 2016).

	MOE Longitudinal (MPa)	MOE Transverse (MPa)	Shear Modulus (parallel to span) (MPa)	Shear Modulus (perpendicular to span) (MPa)
External laminations	8,000	360	440	80
Internal laminations	6,000	270	330	60
CL7/295	4,376	2,531	364	-
CL7/315	4,116	2,752	362	-

3.3.2 Flexural stiffness of the narrow panels (one-way bending)

Flexural responses of the BCS and PCS panels in one-way bending under a uniformly distributed load of 5 kPa are investigated using the Ritz method. The panels have lengths of 4, 6 and 7 meters (*a* in Figure 3.1), width of 1 meter (*b* in Figure 3.1), and are simply supported at either ends (at *x*=0 and *x=a* in Figure 3.1). To study the effect of face thickness and core depth on the flexural response of the BCS panels in one-way bending, different BCS 18-30-7 panels are examined. Results of the mid-span deflection (Δ) of the panels with spans of 4, 6 and 7 meters, and under a uniformly distributed load of 5 kPa are plotted against the core depth (*c*) in Figure 3.5. As shown in Figure 3.5, the mid-span deflections of the double layer panels are much lower than the single layer panels of the same core depth (c). The differences in the mid-span deflections are more noticeable in longer spans. In addition, it is evident from Figure 3.5 that the mid-span deflection of the double layer panels are less sensitive to the core depth (c), compared to the single layer panels.

51
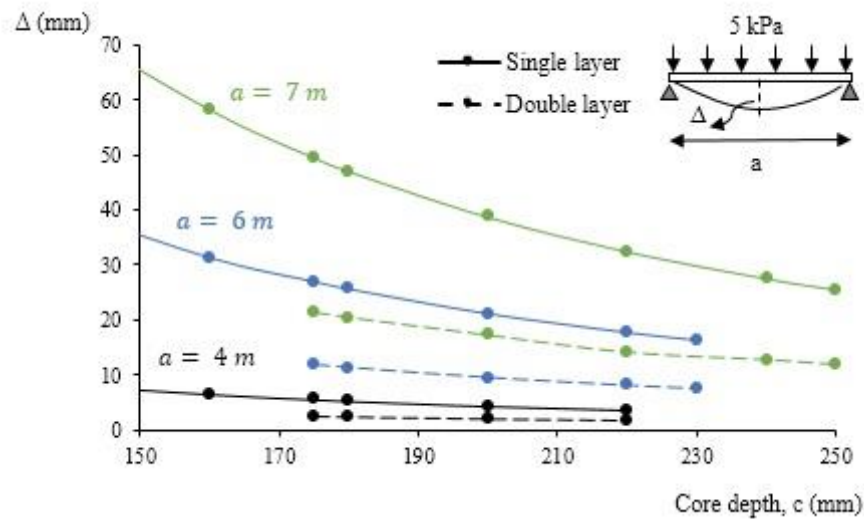
Figure 3.5 Mid-span deflection of single and double layer BCS 18-30-7 narrow panels in one-way bending.

Mid-span deflection versus the total depth (h) of the BCS panels with different face configurations, namely; BCS 18-30-7, BCS 21-30-9 and BCS 25-30-9 and under a uniformly distributed load of 5 kPa are presented in Figure 3.6. The data points shown in black and red correspond to the single layer and double layer BCS panels, respectively. The target deflections for the BCS panels are shown with the dashed lines in each curve, and correspond to the deflection of *CL7/295* in the 4 and 6 m panels, and to the deflection of *CL7/315* in the 7 m panel under 5 kPa uniformly distributed load. To reach the target deflection, total depth of the single layer BCS panel ($h = 2t + c$) is enlarged by increasing the core height (c). As shown in Figure 3.6 (a), (b) and (c) by increasing the core height, the deflection of the single layer BCS panel is reduced. However, deflections of the single layer BCS panels only get smaller than the CLT panel, when the depth of the BCS panel exceeds the depth of the target CLT panel. Optimal results are obtained in double layer BCS panels (red data points in Figure 3.6).
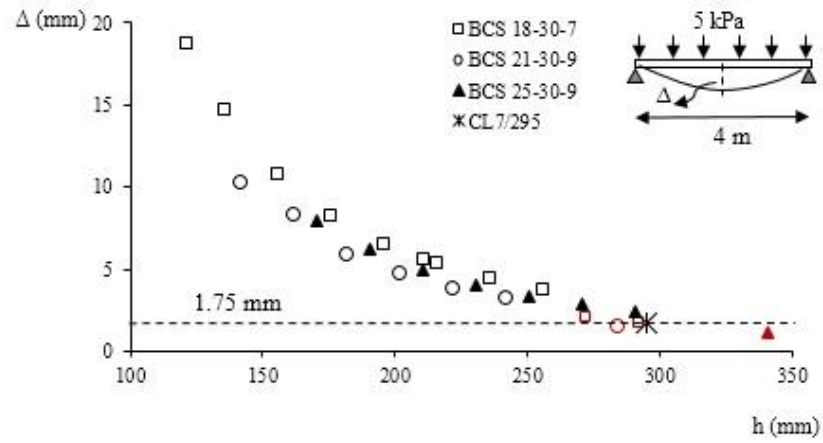
(a)
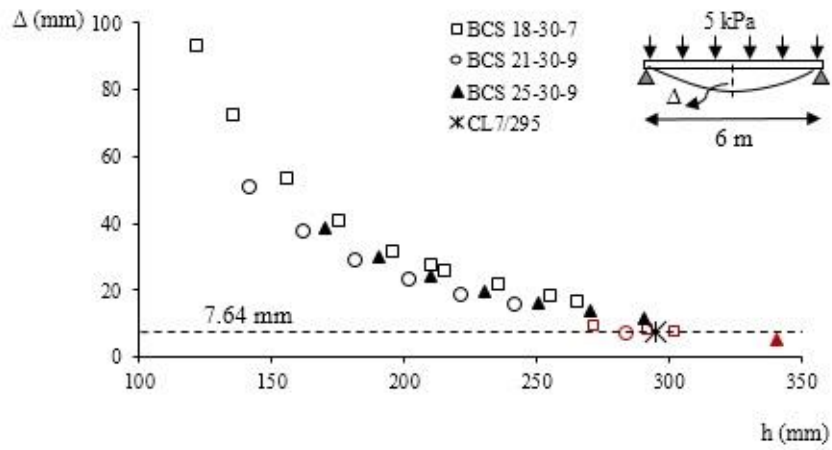
(b)
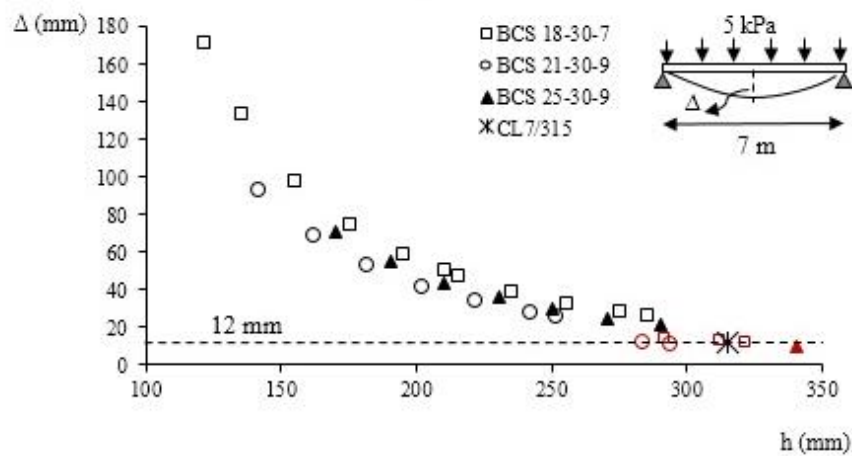
(c)

Figure 3.6 Maximum deflection of BCS and CLT panels in one-way bending, (a) 4 m span, (b) 6 m span and, (c) 7 m span.

53
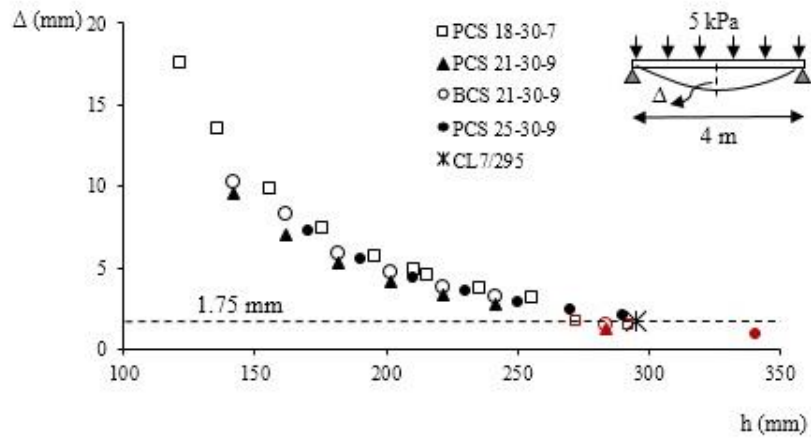
(a)
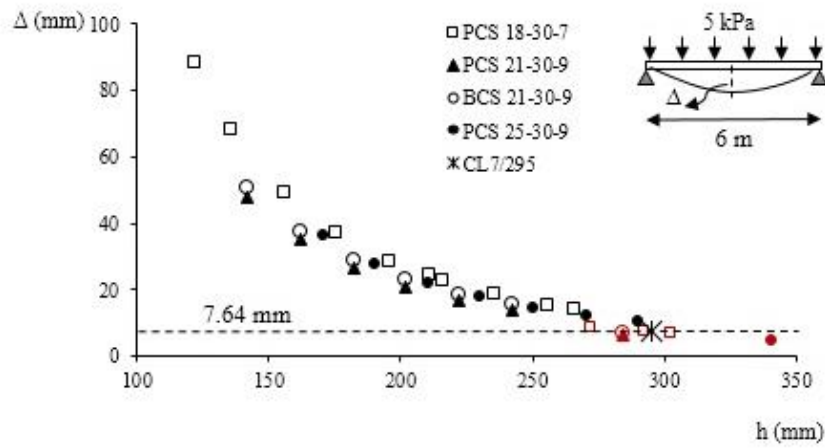
(b)
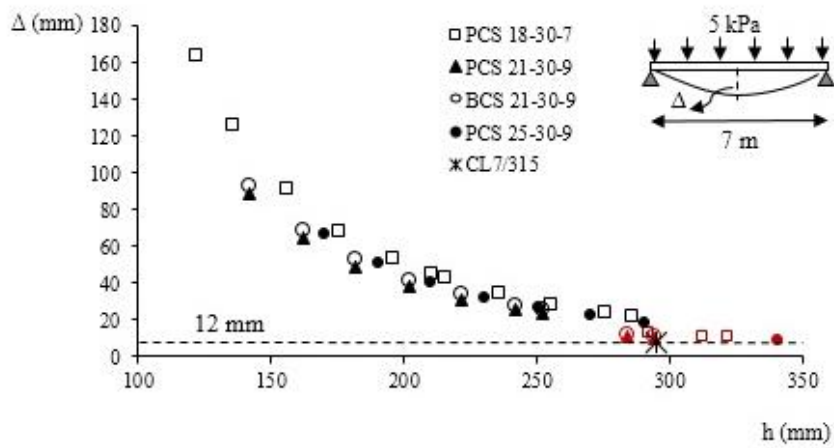
(c)

Figure 3.7 Maximum deflection of BCS, PCS and CLT panels in one-way bending, (a) 4 m span, (b) 6 m span and, (c) 7 m span.

The minimum deflections correspond to the double layer BCS 21-30-9 panels. At almost similar deflections, the depth (h) of the BCS 21-30-9 panel is 4% lower than the CLT panel (*CL7/295*) in 4 and 6 m spans, and 7% lower smaller than the depth of the CLT panel (*CL7/315*) in the 7 m span. This ideal result is associated with the higher MOE of the faces of the double layer BCS 21-30-9 panel in the longitudinal direction, as represented in Table 3.2. In Figure 3.7 (a) to (c), mid-span deflections of the BCS 21-30-9 panels are compared against PCS panels of similar specifications and are benchmarked against their commercial CLT competitors. Regardless of the span lengths, the PCS 21-30-9 panel exhibits smallest deflections. At similar panel depth of h =284 mm, the deflection of the PCS 21-30-9 panels are 16%, 10% and 8% lower than the BCS 21-30-9 panels, in 4, 6 and 7 m spans, respectively.

Shear to flexure deformation ratios (w_2/w_1) of BCS 21-30-9, PCS 21-30-9 and CL7/295 panels in one-way bending and under a uniform distributed load of 5 kPa are shown in Figure 3.8. Contribution of shear and flexure in total deformation of the panels in one-way bending are calculated using the beam sandwich theory (Section 3.2.2).
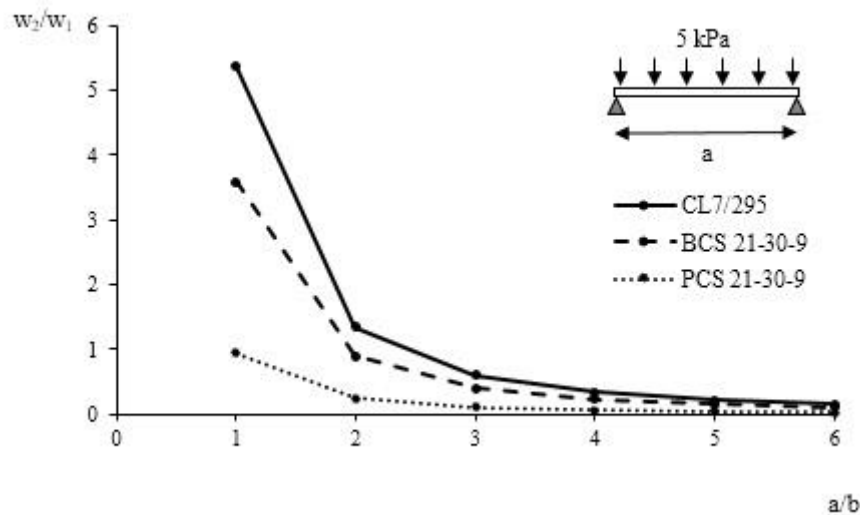
Figure 3.8 The contribution of shear (w_2) and flexure (w_1) components, in the total deflection of the BCS, PCS and CLT panels in one-way bending.

As shown in Figure 3.8, at small aspect ratios ($a/b<2$), there is significant shear contribution. This is more evident in the CLT and BCS panels. At larger aspect ratios ($a/b>5$), the shear contributions almost vanish. In the PCS panel, the w_2/w_1 is consistently smaller than one, and becomes negligible at $a/b>3$. The

Timoshenko beam coefficients of the BCS and PCS panels are 0.817 and 0.815, respectively, and are much smaller than the coefficient 1.2 of the CLT panels. Using the Ritz method, in one-way bending, the shear angle factor λ (see Section 3.2.1), are found to be between 0.77-0.95 in the BCS panels, and between 0.92-0.98 in the PCS panels. It can be construed that due to the high stiffness of the peeling cores, the shear strain γ of the PCS cores, are almost equal to zero and thus, the panels behave similar to a composite panel.

3.3.3 Flexural stiffness of the wide panels (two-way bending)

Two-way flexural behaviour of the proposed sandwich panels under a 5 kPa uniformly distributed load is investigated, by modelling 6×8 m panels with three different face configurations (similar to narrows panels), by means of the Ritz method. Mid-span deflections of the BCS and CLT panels (deflection at the centre of the panel) are plotted against the corresponding panel depths in Figure 3.9 (a). Similar to the one-way bending response, the double layer BCS 21-30-9 panel yields the optimum results. At the target deflection (7.64 mm), the depth of the double-layer BCS 21-30-9 panel is 4% smaller than the *CL7/295* panel.

Mid-span deflections of the BCS panels in two-way bending are compared against the PCS panels in Figure 3.9 (b). Single layer PCS 21-30-9 and PCS 25-30-9 panels show smaller deflections compared to the single-layer BCS 21-30-9 panel. However, the optimum results in two-way bending is obtained by using double layer PCS 18-30-7 panel. At the target deflection (7.64 mm), panel depth of the double layer PCS 18-30-7 is h=272 mm, compared to h=295 mm in the *CL7/295* panel. In two-way bending, the BCS panels have shear angle factors λ and μ between 0.86-0.97 and 0.90-0.98, respectively. The λ and μ factors in the PCS panels, under two-way bending range between 0.96 and 0.99.
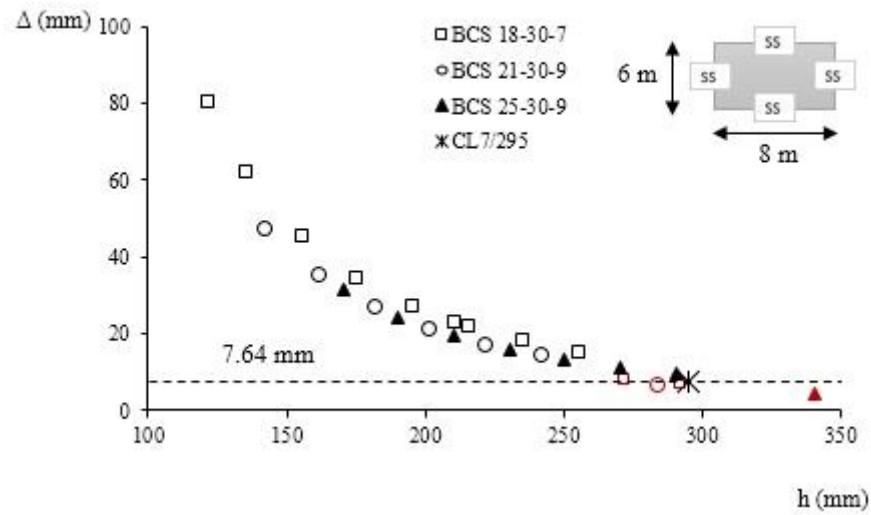
(a)
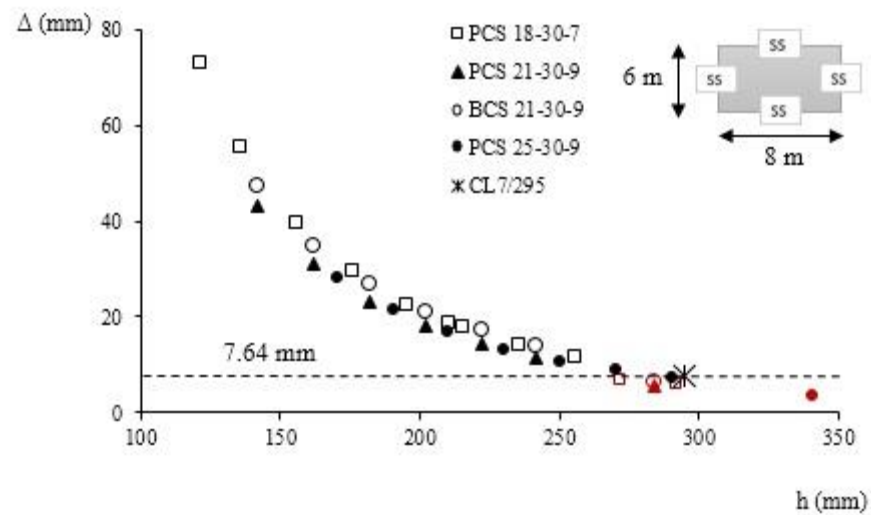
(b)

Figure 3.9 Maximum deflection of BCS, PCS and CLT panels in two-way bending.

3.3.4 Efficiency of the BCS and PCS panels in comparison with the CLT panels

Geometric properties of the BCS and PCS panels, commercial CLT panels and their corresponding deflections, weight and stiffness ratios are represented in Table 3.4. The deflections of the CLT panels are calculated based on the sandwich beam theory (shear analogy method) and are compared with the deflections of selected BCS/PCS panels obtained from the Ritz method. Due to

their optimal flexural behaviour, double layer BCS 21-30-9, double layer PCS 18-30-9 and double layer PCS 21-30-9 panels are selected. The stiffness of the panel (K) in Table 3.4 is calculated by inversing the mid-span deflection of the panel under the uniformly distributed load.

As represented in Table 3.4, in one-way bending (*a/b*>2), the BCS panel has stiffness between 6-17% higher than the CLT panel. The ratio between the stiffness of the CLT and the BCS panels, varies with the corresponding change in the aspect ratio (*a/b*). This is due to the fact that, in smaller aspect ratios, the contribution of the shear deformation (w_2 in Figure 3.8) is more significant in CLT, which makes it less efficient compared to the BCS panel. As the aspect ratio (*a/b*) becomes larger, the shear contribution is decreased and the difference between stiffness of CLT and BCS panels becomes less significant. The stiffness of the PCS panels are larger than the CLT panels at all aspect ratios in one-way bending. A 25% increase in stiffness is obtained in PCS 21-30-9 with aspect ratio of 6, compared to the CLT. In two-way bending (6×8 m panel), the stiffness of the BCS and PCS panels are about 20% and 30% larger than the CLT. The panel depth of PCS 18-30-7 is 4% lower than BCS 21-30-9 panel, and 8% lower than the CLT panel.

The selected BCS and PCS panels represented in Table 3.4, weigh about 40% and 20% less than the CLT panel, respectively. The BCS panels are in average 23% lighter than the PCS panels. In the BCS panels, the weight of the core is 85% of the weight of the faces. On the other hand, in the PCS panels, the core weighs almost twice the faces. This suggests that the BCS panels are the favourable sandwich products in terms of the material used in the core compared to the PCS panels.

Table 3.4 Properties of the BCS, PCS and CLT panels and corresponding weight and stiffness ratios.

Dimensions		CLT		BCS			PCS			Ratios			
a (m)	b (m)	h_{CLT} (mm)	W_{CLT} (kg/m^2)	h_{BCS} (mm)	C_{BCS} (mm)	Double layer	h_{PCS} (mm)	C_{PCS} (mm)	Double layer	$W_{(BCS)}/W_{(CLT)}$	$K_{(BCS)}/K_{(CLT)}$	$W_{(PCS)}/W_{(CLT)}$	$K_{(PCS)}/K_{(CLT)}$
4.0	1.0	295	151	284	200	21-30-9	272	200	18-30-7	0.61	1.17	0.79	1.01
6.0	1.0	295	151	284	200	21-30-9	284	200	21-30-9	0.61	1.13	0.79	1.25
7.0	1.0	315	161.2	294	210	21-30-9	284	200	21-30-9	0.58	1.06	0.74	1.07
6.0	8.0	295	151	284	200	21-30-9	272	200	18-30-7	0.61	1.20	0.79	1.29

3.4 Ultimate strength of the BCS and PCS panels

3.4.1 Finite Element model and validation

The ultimate flexural capacity of the BCS and PCS panels are studied using the commercial finite element analysis (FEA) software, ANSYS 17.0 (*ANSYS 17.0 Mechanical User's Guide*). The FE model is validated against the experimental results of the 600 × 600 mm Glass Fibre Reinforce Polymer (GFRP) sandwich panel, reported in (Awad et al. 2013) and discussed in Section 3.2.3. Orthotropic-elastic and isotropic elastic material properties are adopted for the GFRP faces and the modified phenolic core, respectively in the FEA. These are meshed with eight-node solid elements. The core and GFRP faces are bonded using no slippage contact definition in the FEA. The orthotropic material properties of the GFRP faces are represented in Table 3.1 and the isotropic core properties are reported in Section 3.2.3. Due to symmetry, only a quarter of the panel is modelled and simply supported boundary conditions are imposed on the edges. Uniform pressure is gradually applied over a 100 × 100 × 1 mm steel plate ($E = 200$ GPa) at the centre of the panel, similar to the loading procedure in the test (Awad et al. 2013). The FEA result using nonlinear geometric analysis is shown in Figure 3.10 (b), and is in a good agreement with the experimental results.

Using the validated FEA, double layer BCS 21-30-9 and PCS 21-30-9 panels, with dimensions of 6 × 1 m are modelled. The height of the bamboo and peeling cores are 200 mm and the total panel depth is 284 mm. The wall-thickness of the bamboo cores are 10 mm and the radius of the bamboo and peeling cores are 50 mm. Eight-node solid 186 elements (*ANSYS 17.0 Mechanical User's Guide*), with three degrees of freedom at each node are utilised to model the plywood veneers and the bamboo/ peeling cores. A schematic view of a short length of the FE mesh of the BCS and PCS panels are shown in Figure 3.10 (a). Perfect bond contact definitions are adopted to model the contact between the plywood veneers, and between the cores and the faces. To account for the possible contact between the faces of the bamboo or peeling cores, bonded contact is defined between the core faces. Based on results from a convergence study, the faces and the cores are discretised with element length of 20 mm. Plywood veneers have one element along the veneer thickness, and the bamboo and the peeling cores are discretised with two and eight elements along the thickness,

respectively (Figure 3.10 (a)). Using symmetry, only a quarter of the panel (3×0.5 m) is modelled in the FEA, and simply supported and symmetry conditions are imposed on the edges.
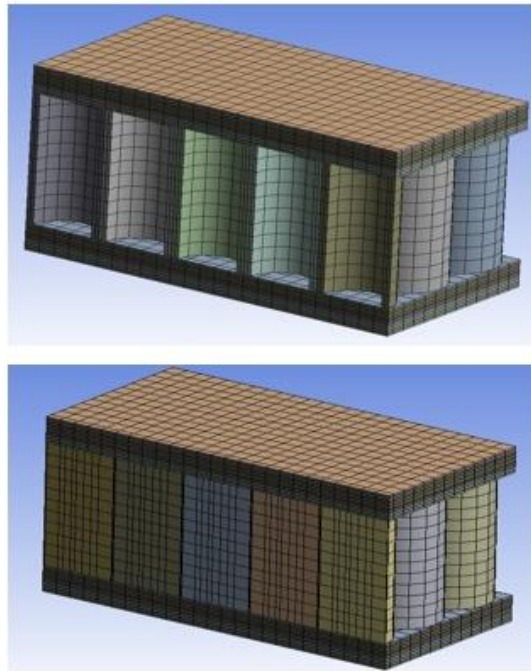
(a)
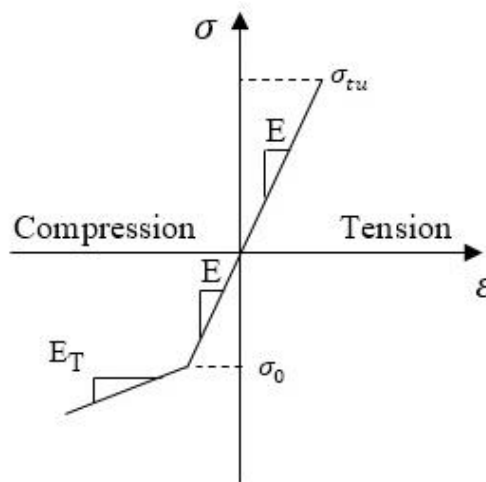
(b)

Figure 3.10 A schematic illustration of (a) the FEA mesh of short section of BCS (top) and PCS (bottom) panels, (b) the adopted stress-strain relationship in the faces of the BCS/PCS panels.

3.4.2 Material properties and failure criteria

The elastic material properties of bamboo, peeling core and *Radiata* ply veneers used in the FEA, are similar to those adopted in the Ritz method and are represented in Table 3.1. The x, y and z directions correspond to the longitudinal (parallel to the fibres), tangential and radial directions, respectively. The material properties are assigned to the PCS and BCS panels in the FEA, using a *Cartesian* coordinate system and to the cores via a *cylindrical* coordinate system. The bamboo/peeling cores are deemed to remain in the elastic region and thus, orthotropic elastic material definition is assumed in the cores. Material properties of the core are assumed to be identical in radial and tangential directions (transverse isotropic behaviour), as represented in Table 3.1.

In tension, the behaviour of timber is rather brittle (Raftery & Harte 2013) and the capacity in the direction perpendicular-to-grain ($\perp$) is much lower than in the direction parallel-to-grain ($\parallel$). The maximum normal stress criterion, which is an acceptable failure criterion for anisotropic brittle materials (Xu, Taazount, et al. 2009), is adopted for the failure of *Radiata* in tension (the face in tension). The timber is assumed to fail in tension when any one of the stresses in the principal material directions exceeds the material strength in that direction. This assumes that failure is independently controlled by each stress type and it is not a function of interaction between stresses. A schematic view of the material definition in tension is shown in Figure 3.10 (b). The timber tensile strength values are adopted in the FEA: $\sigma_{tu}^{\parallel} = 27$ MPa, and $\sigma_{tu}^{\perp} = 0.5$ MPa (Valipour & Crews 2011; Xu, Bouchaïr, et al. 2009). It should be noted that the variability of wood is high and the determination of values can influence the results of simulation.

In compression, timber exhibits relatively ductile behaviour (Raftery & Harte 2013) which can be represented with elastic-plastic material constitutive laws. To account for plastic behaviour of *Radiata* veneers (faces) in compression, the Hill yield criterion (Hill 1998) is used. Hill criterion (Hill 1998) is an extended formulation of the Von-Mises yield criterion, which accounts for the anisotropy of the material. The elastic-plastic stress-strain relationship of timber in compression used in the FEA is shown in Figure 3.10 (b). The stress potential in the Hill criterion is expressed as

$$\sigma_e = \sqrt{F_{33}\left(\sigma_x - \sigma_y\right)^2 + F_{11}\left(\sigma_y - \sigma_z\right)^2 + F_{22}\left(\sigma_z - \sigma_x\right)^2 + 2N_{12}\tau_{xy}^2 + 2N_{23}\tau_{yz}^2 + 2N_{31}\tau_{xz}^2}$$

(3.24)

where $F_{ii}(i = 1,2,3)$ and $N_{ij}(i \neq j = 1,2,3)$ are constants obtained from the material tests conducted in different orientations

$$F_{ij} = \left[\frac{\left(\sigma_0\right)^2}{2}\right]\left[\frac{1}{\left(\sigma_{jj}^y\right)^2} + \frac{1}{\left(\sigma_{kk}^y\right)^2} - \frac{1}{\left(\sigma_{ii}^y\right)^2}\right] = \frac{1}{2}\left[\frac{1}{R_{jj}^2} + \frac{1}{R_{kk}^2} - \frac{1}{R_{ii}^2}\right]\begin{Bmatrix} i = 1,2,3 \\ j = 2,3,1 \\ k = 3,2,1 \end{Bmatrix}$$
(3.25a)

$$N_{ij} = \frac{3}{2}\left[\frac{\left(\tau_0\right)^2}{\sigma_{ij}^y}\right] = \frac{3}{2}\left[\frac{1}{R_{ij}^2}\right] \quad (i \neq j = 1,2,3)$$
(3.25b)

where σ_{ii}^y and σ_{ij}^y correspond to the normal and shear yield stresses, and subscripts 1, 2 and 3, are associated with the longitudinal, tangential and radial directions, respectively. R_{ij} are the yield ratios which relate the yield level for stress components σ_{ij}^y, to the reference yield stress σ_0 of the material. The yield ratios are defined as follows:

$$R_{ij} = \begin{cases} \dfrac{\sigma_{ij}^y}{\sigma_0}, & \text{if } i = j \\[3mm] \dfrac{\sigma_{ij}^y}{\tau_0}, & \text{if } i \neq j \end{cases}$$
(3.26a)

$$\tau_0 = \frac{\sigma_0}{\sqrt{3}}$$
(3.26b)

In the current study, $R_{11} = 1, R_{22} = 0.25, R_{33} = 0.26, R_{12} = R_{13} = 0.9, R_{23} = 0.66$ and the reference yield stress $\sigma_0 = 18$, 21 and 30 MPa with tangent modulus of $E_T = 345$ MPa are adopted (Alam 2004).

3.4.3 FEA results

The load vs. mid-span deflection responses of the 6 × 1 m, double layer BCS and PCS panels are shown in Figure 3.11, and the stress ratios at failure and corresponding failure modes are represented in Table 3.5. The solid lines in Figure 3.11, correspond to the Ritz method results based on linear orthotropic

63

material properties, and small deflection theory. The dashed lines are associated with the FEA results with different reference yield stress (σ_0). The FEA curves are stopped when the failure is reached. All the investigated panels experienced failure in tension parallel to the grain. As shown in Figure 3.11, the slopes of the load-deflection responses from the Ritz method and the FEA match perfectly for deflections up to 6 mm (Δ/L =0.001). Beyond this point, the nonlinear geometric behaviour is observed in the FEA results. The contribution of the nonlinear material behaviour corresponding to the faces in compression, is only observed at very large deflections. At similar reference yield stress σ_0 =18 MPa, the material nonlinearity commences at deflections beyond 40 mm in BCS (Δ/L =0.007) and, 35 mm in the PCS panels (Δ/L =0.006), respectively. As the σ_0 value is decreased, the plateau region of the load-deflection curve prior to the ultimate load is extended. This is more evident in the BCS response, and suggests relatively more ductile behaviour in the BCS panels compared to the PCS panels.

Table 3.5 Modes of failure for BCS (21-30-9) and PCS (21-30-9) panels under one-way bending.

Panel ID (Double layer)	σ_0 (MPa)	q_u (kPa)	$\sigma^{\parallel}/\sigma_{tu}^{\parallel}$	$\sigma^{\perp}/\sigma_{tu}^{\perp}$	σ_e/σ_0	Failure mode
BCS 21-30-9	30	38.09	1.0	0.96	0.87	Tension (Parallel)
BCS 21-30-9	21	37.49	1.0	0.96	1.01	Tension (Parallel)
BCS 21-30-9	18	34.48	1.0	0.96	1.05	Tension (Parallel)
PCS 21-30-9	30	48.24	1.0	0.94	0.87	Tension (Parallel)
PCS 21-30-9	21	47.57	1.0	0.96	1.04	Tension (Parallel)
PCS 21-30-9	18	38.39	1.0	0.98	1.07	Tension (Parallel)
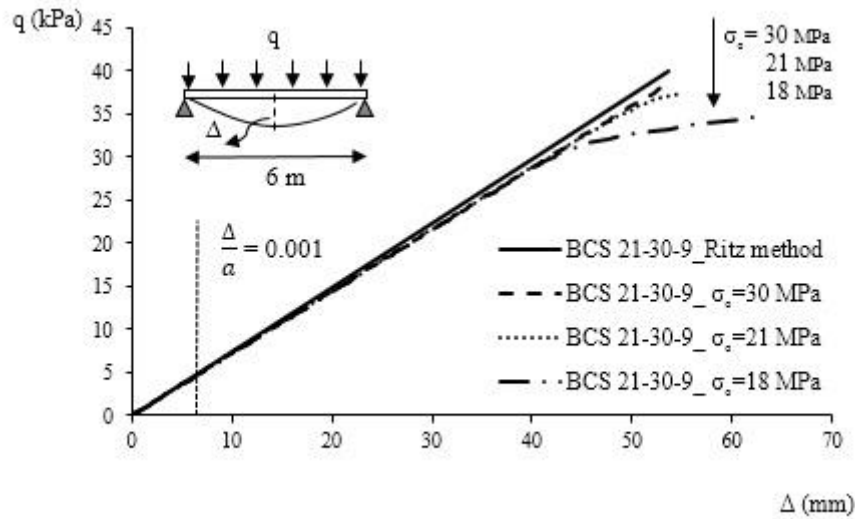
(a)
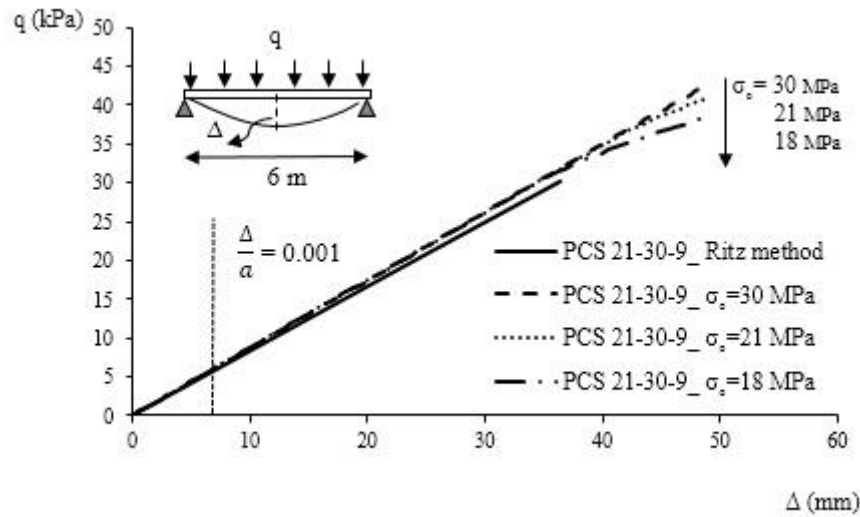
(b)

Figure 3.11 The load vs. mid span deflection response of 6×1 m, (a) double layer BCS 21-30-9 and, (b) double layer PCS panels, showing the Ritz prediction, and FEA for different reference compressive yield stresses ($\sigma_\circ$).

The ultimate capacities (q_u) of the panels obtained from the FEA are represented in Table 3.5. The largest capacity is q_u =48.24 kPa, corresponds to the PCS panel with σ_0 =30 MPa, and is 27% larger than the capacity of the BCS panel with the same reference yield stress (σ_0). However, the PCS 21-30-9 panel is 30 % heavier than BCS 21-30-9 panel according to the weight ratios of Table 3.4 with $a = 6$ m and $b = 1$ m. As the σ_0 value is decreased, the ultimate capacity of

the panel decreases. This drop in the ultimate capacity is more evident in the PCS panel. As represented in Table 3.5, at the failure point ($\sigma^{\text{II}}/\sigma_{tu}^{\text{II}} = 1.0$), the panels almost reach the ultimate capacity in tension perpendicular to the grain. The largest capacities are observed in panels with the highest $\sigma_0 = 30$ MPa. In these panels the face in tension fails due to the normal stress in direction parallel to the grain exceeding the capacity, σ_{tu}^{II}, while the face in compression has not reached the yield point.

3.5 Conclusions

The flexural stiffness and ultimate load capacity of novel ultralight composite sandwich panels, namely; (a) Bamboo Core Sandwich (BCS) panel, and (b) Peeling Core Sandwich (PCS) panel were investigated. A modified Ritz method was developed herein, which unlike previous formulations of sandwich orthotropic plates, accounts for the local bending stiffness of the faces (thick face) and the flexural rigidity of the cores (thick-stiff core) of the BCS and PCS panels. Results of the Ritz method were compared against predictions of a sandwich beam theory (Timoshenko beam) and were validated against published experimental results. Using the validated Ritz method, bending stiffness of the BCS and PCS panels were compared with CLT panels of almost similar depths. Ultimate capacities of the panels were obtained from FEA, which accounts for nonlinear geometric and material effects.

It was understood that in one-way bending, the studied PCS panels of different lengths are in average 10% stiffer than the BCS panels. The Timoshenko beam coefficients of the BCS and PCS panels were found to be 0.817 and 0.815, respectively, which are much smaller than the coefficient 1.2 for the CLT panels. Using the validated FEA, the ultimate capacity of the 6×1 m PCS panel was found to be 27% larger than the capacity of the BCS panel. These numbers should be interpreted with regards to the 30% larger weight of the PCS compared to its counterpart BCS panel. The stiffness of BCS and PCS panels can get as high as 17% and 25% of the stiffness of the CLT panels with similar panel depths, respectively. In two-way bending (6×8 m panel), the stiffness of the BCS and PCS panels are 20% and 39% larger than the CLT at almost similar panel depth. The mentioned BCS and PCS panels are almost 40% and 21% lighter than their competitive CLT panel (*CL*7/295). The FEA results showed that in all the studied

BCS/PCS panels, failure occurred in tension parallel to the grain. Further experimental studies are planned to manufacture and test the BCS and PCS panels and to obtain the ultimate capacity and optimised geometric configuration of the cores within the panel.

4 Experimental study on bending and shear behaviours of composite timber sandwich panels

STATEMENT OF CONTRIBUTION TO CO-AUTHORED PUBLISHED PAPER

This chapter includes a co-authored paper. The bibliographic details of the co-authored paper, including all authors, are:

Darzi, S, Karampour, H, Bailleres, H, Gilbert, BP, & L. McGavin. Experimental study on bending and shear behaviours of composite sandwich panels. *Construction and building materials* (Submitted 11th March 2020, under review).

My contribution to the paper involved: literature review, test setup, conduct experiments, evaluation of experimental results, discussion of the results, writing and editing.

(Signed) _____ Date: 16/03/2020

PhD Candidate: **Siavash Darzi**

(Countersigned) _____ Date: 16/03/2020

Principle Supervisor/ Corresponding author of paper: **Dr. Hassan Karampour**

(Countersigned) _____ Date: 16/03/2020

Associate Supervisor: **Associate Professor Benoit P. Gilbert**

(Countersigned) _____ Date 16/03/2020

External Supervisor: **Dr. Henri Bailleres**

Experimental study on bending and shear behaviours of composite timber sandwich panels

Abstract:

Composite sandwich panels were manufactured by gluing plywood skins to either bamboo rings to produce Bamboo Core Sandwich (BCS) panels or to peeler core rings to produce Peeler Core Sandwich (PCS) panels. Single and double core layer panels were made. The optimum adhesive spread rate was identified through conducting shear bond tests. The manufactured panels were physically tested in standard bending (using four-point) and shear (using three-point) tests. Results were compared to the test results of conventional Cross-laminated Timber (CLT) panels with almost similar depth. Under bending action, both the BCS and PCS panels showed tensile failure in the plywood, while the plywood in compression exceeded its plastic limit at the ultimate load. In shear, BCS panels failed due to the loss of shear interface contact between bamboo core rings and the plywood skins, whereas PCS panels showed local indentation/ bond failure between the peeler core rings and the plywood skins. No significant improvements were observed in the double-layer panels compared to single-layer panels in bending. However, in shear, double-layer panels showed more consistent capacities. One PCS panel with thicker plywood skins and less peeler core rings (PCS-TH) was manufactured, and was shown to achieve 0.77 times the bending stiffness-to-weight ratio of the commercial CLT panel. Reduced weight, lower material costs, ease of manufacturing and usage of sustainable/waste products, make the proposed sandwich panels a potential alternative for CLT in terms of structural performance. Moreover, the proposed peeler core sandwich panels displayed better ductile performances in bending and shear compared to CLT suggesting it could be a preferred product choice in some building applications.

4.1 Introduction

Sandwich panel structures with high stiffness-to-weight and strength-to-weight ratios, are preferred to conventional systems in the aerospace, automobile and ship industries. However, structural applications of sandwich panels in civil engineering remains very limited due to the usage of core materials with low mechanical properties (Awad et al. 2012). Typically, a sandwich panel is fabricated by attaching two thin and stiff skins to a light-weight thick core. Common skin materials are steel (Zhang et al. 2018), fibre reinforced composites (Manalo, AC et al. 2010)and less frequently reinforced concrete (Jensen et al. 2020). Typical core materials include balsa wood (Dawood, Ballew & Seiter 2011), polymeric and metallic foams (Mamalis et al. 2008; Reyes 2008), fibre reinforced polymer (FRP) (Fam & Sharaf 2010) and metallic alloys (Crupi, Epasto & Guglielmino 2012). By combining different skins and core materials with varying geometries, an optimum design can be produced for a specific application.

With the recent global trend towards mid-rise to high-rise timber buildings, more attention is given to lightweight, cost-effective and sustainable wood products. Existing mass timber buildings commonly use Cross-Laminated Timber (CLT) floor diaphragms and load-bearing walls (Reynolds, Casagrande & Tomasi 2016). A CLT panel is comprised of an odd number of orthogonally bonded layers of solid sawn lumbers, which are bonded using adhesive, nails or wooden dowels (Karacabeyli & Gagnon 2019). The orthogonal orientation of layers in CLT results in excellent in-plane and out-of-plane strength, rigidity, and stability characteristics. However, this specific orientation under out-of-plane loading shows significant planar (rolling) shear deformations because, in the radial-tangential (RT) plane, wood has a relatively low shear modulus. To address this issue, many studies have been performed, including the measurement of the planar shear properties (Zhou et al. 2014), improvement of the planar shear properties (Wang, Zhiqiang et al. 2017) and evaluation of the effects of CLT configuration and manufacturing parameters on the shear properties of CLT (Aicher, Hirsch & Christian 2016; Sikora, McPolin & Harte 2016).

A smart combination of materials in composite construction is a way to minimize the use of resources, therefore reducing the environmental impact of the building construction process. Existing composite systems used in slab and load-bearing walls typically use a combination of steel/concrete (Spacone & El-Tawil 2004),

timber/concrete (Gutkowski et al. 2008; Khorsandnia, Valipour & Crews 2012), timber/timber (Giongo, Piazza & Tomasi 2012), steel/timber (Chiniforush et al. 2018) or other less common mixes of materials. Over the past decade, Timber/Concrete Composite (TCC) and Steel/Timber Composite (STC) floors have found extensive applications (Gutkowski et al. 2008), mainly because of the lower cost of construction and maintenance compared with conventional reinforced concrete and steel systems. The possible inconveniences of TCC floors are the required curing time, inherent self-weight and limited number of prefabricated solutions (Crocetti, Sartori & Tomasi 2015). Therefore, timber composites and steel/timber composite systems, in which concrete is replaced by engineered wood products such as CLT or Laminated Veneer Lumber (LVL) have attracted more attention (Loss & Davison 2017). More recently, bamboo has been the focus of engineering research due to its high stiffness-to-weight ratio and fast growth. The inherent variability in the geometric and mechanical properties, and the lack of standardisation lead to prohibitive use of bamboo for mainstream construction (Gatóo et al. 2014). However, engineering wood products such as Laminated Bamboo Lumber (LBL) can be manufactured by gluing together bamboo material in various forms (e.g., strands or mats) to form rectangular boards similar to lumbers (Li, H-t et al. 2016; Li, Xin et al. 2020; Sharma et al. 2015).

Most structural sandwich panels have inner core of low transverse stiffness and strength (such as balsa wood and light weight foam core), which makes the panels vulnerable to a number of different failure modes under bending actions. These include buckling or wrinkling instability, delamination of the skins from the core, core shear failure and localized punching or flatwise crushing of the core (Kabir, Vodenitcharova & Hoffman 2014; Mostafa, Shankar & Morozov 2013). Since the failure mode is heavily dependent on the core material and configuration, a great deal of research has been conducted to enhance the core's mechanical performance, for example, by using high density PU foam core, hybrid core concept, stitched core, Z-pinning technique or web core technique (George et al. 2014; Sharaf, Shawkat & Fam 2010; Song et al. 2015). Regardless, in comparison to the conventional sandwich composites, these processes appear technically complex to manufacture.

The current study aims to investigate appropriateness of composite timber sandwich panels made by combining existing commercial wood products with affordable and sustainable local timber and wood waste, to manufacture sandwich panels for construction purposes. To do so, sandwich panels are made using commercial plywood as skins, and bamboo or peeler core rings. Bamboo is used in the core of the proposed sandwich panel due to its local availability in Australia, outstanding stiffness-to-weight ratio, and its rapid harvest (3-4 years from the time of planting). The peeler core rings are sourced from the unused log core that remains after rotary peeling for veneer production (McGavin et al. 2019). This Bamboo Core Sandwich (BCS) panel and the Peeler Core Sandwich (PCS) panel (Figure 4.1) concept has been previously examined for their theoretical flexural performances, using numerical methods (Darzi et al. 2018a, 2018b). The current paper aims to investigate the bending and shear performances of the novel sandwich panels, experimentally, and to compare the results with those of CLT panels with almost similar depth. To do so, four-point bending and three-point shear tests are conducted on the sandwich panels and the CLT panels. The experimental results are interpreted using analytical equations.

4.2   Panels and manufacturing

4.2.1   The panels

Two types of panels, Bamboo Core Sandwich (BCS) and Peeler Core Sandwich (PCS) panels, each in single-layer and double-layer core configurations as shown in Figure 4.1, were manufactured. In single-layer panels (BCS-S and PCS-S), a single layer core of 70 mm was sandwiched between two 7.2 mm thick structural plywood skins. In double-layer panels (BCS-D and PCS-D), a core of two layers of 32 mm thick separated by a thin layer of plywood (4 mm thick), was sandwiched between two 7.2 mm thick plywood skins. The structural plywood laminates were commercially available and were manufactured to Australia/New Zealand Standard (*AS 1720.1:2010 Timber structures Part 1: Design methods* 2010) from softwood veneers of plantation pine (*Pinus radiata*). The selected plywood IDs were 7-24-3 (Stress grade F8) and 4-14-3 (Stress grade F8) (*AS 1720.1:2010 Timber structures Part 1: Design methods* 2010). The numbering sequence in the ID gives the nominal plywood thickness, the outer (or face) veneer thickness multiplied by 10, and the number of plies in the assembly. For example, plywood ID 7-24-3, describes a 7 mm thick plywood, with 2.4 mm thick outer veneers, and

a total number of 3 veneer layers. To investigate the effect of skin thickness on the sandwich performance, single-layer PCS panels with thicker plywood skins were manufactured, labelled as PCS-TH (Figure 4.1). In this panel, two plywood skins 21 mm thick (ID 21-24-9 Stress grade F14) were separated by a single layer peeler core of 42 mm thickness. In order to reduce the total weight of the PCS-TH panel, a 50 mm gap between individual peeler cores was considered in perpendicular to the span direction (*b*) along the panel (Figure 4.1). To provide comparison, a commercially available CLT panel, CL3/75 was selected and purchased from XLam CLT products (XLam 2016). The CL3/75 has three layers of solid sawn boards with a layup of 20/35/20. The two outermost layers (20 mm) are aligned along the major axis, and the middle layer (35 mm) are perpendicular to the major axis, as shown in Figure 4.1.
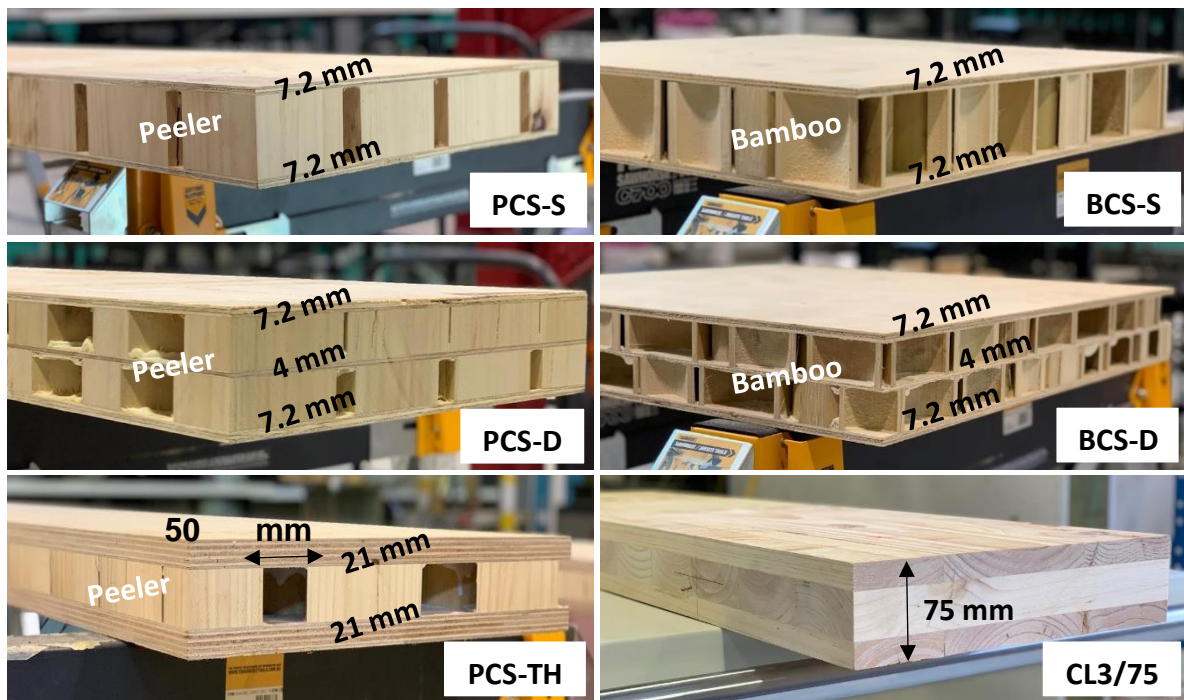
Figure 4.1 Manufactured BCS, PCS and PCS-TH panels and commercially available CLT products.

4.2.2 Manufacturing

Fabrication process of the BCS and PCS panels is illustrated in Figure 4.2. The structural plywood laminates were delivered in sheets of 2,400 mm × 1,200 mm. To fabricate the panels, peeler cores and mature Moso bamboo (*Phyllostachys Pubescens*) culms were cut into rings with nominal heights of 70 mm and 32 mm

73

in the single and double-layer panels, respectively, and 42 mm in the PCS-TH panel. Bamboo rings were obtained from the bottom, middle and top part of node-less bamboo culms. The bamboo rings had an average diameter of 100 ± 20 mm and a wall thickness of 10 ± 2 mm. The peeler cores used had an average diameter of 133 mm. The bamboo and peeler core rings were stored in a conditioning chamber until an equilibrium moisture content of between 8% and 12% was achieved for manufacturing stage. To manufacture the BCS panels, a timber frame with dimensions slightly smaller than the aspired panel dimensions was made, (Figure 4.2 (c)). The timber frame was filled with the bamboo rings, adjusting the arrangement such that to keep the bamboo rings packed as closely as possible. The timber frame was not required for manufacturing the PCS panels due to less dimension variations in peeler cores. The adhesive used for the bonding of the plywood skins and core layers was one-component PUR pre-polymer (*Jowapur 686.70*) with a spreading rate of 180 g/m^2 and 540 g/m^2 for the BCS and PCS panels, respectively. A higher spread rate was applied for manufacturing the PCS panels due to increased contact surface area and higher expected absorption of glue by peeler core fibres in its major direction. Prior to adhesive application, the plywood surface was moistened with a light water spray. Then, the peeler core rings or the timber frame packed with bamboo rings were placed on top of the plywood skin, which was cold pressed at a pressure of 0.8 MPa, for a period of 120 min (Figure 4.2 (d)). Prior to manufacturing the second side of the panels, the first side was passed through the belt sander to make the core heights (either bamboo or peeler) even, as shown in Figure 4.2 (e). After manufacture, the BCS and PCS panels were kept in the open air under ambient conditions for 24 hours.

In total, eight sandwich panels with length of (a=2,400 mm), width of (b=1,200 mm) and nominal depths of (h=85 mm) were manufactured. These include: two BCS-S, one BCS-D, three PCS-S, one PCS-D and one PCS-TH panel. The panels were cut in the format shown in Figure 4.3. From each manufactured panel (with dimensions of 2,400 mm × 1,200 mm × 85 mm), one test sample for four-point bending test (with dimensions of 2,300 mm × 450 mm ×85 mm) and two test samples for three-point shear test (with dimensions of 600 mm × 450 mm × 85 mm) were cut. No shear test was conducted for PCS-TH panels. However, two samples from the PCS-TH panel were tested in four-point bending. The

panels were labelled as shown in Figure 4.3. For instance, the panel labelled PCS-S-V#1-2 indicates the single-layer PCS panel under three-point test and is sample number 2, cut from panel number 1.

It should be noted that, in manufacturing the first PCS panel (PCS-S#1), sanding prior to the manufacturing of the second side of the panel was missed. Moreover, one BCS-D and one BCS-S panel were manufactured almost 2.5 years before the other panels. These two older panels are distinguished from other panels with an asterisk (*) sign. In manufacturing of all sandwich panels commercial plywood with Stress grade F8 (*AS 1720.1:2010 Timber structures Part 1: Design methods* 2010) was used, except in PCS-TH panel, a higher grade (Stress grade F14) (*AS 1720.1:2010 Timber structures Part 1: Design methods* 2010) was utilised.

Figure 4.2 Fabrication process of the BCS and PCS panels showing; (a) panel components: peeler, bamboo culm and commercial plywood laminates, (b) bamboo and peeler core cuts, (c) bamboo and peeler core arrangement on plywood laminates, (d) placement of the panel on cold press, and (e) passing through the belt sander prior to manufacturing the second side.
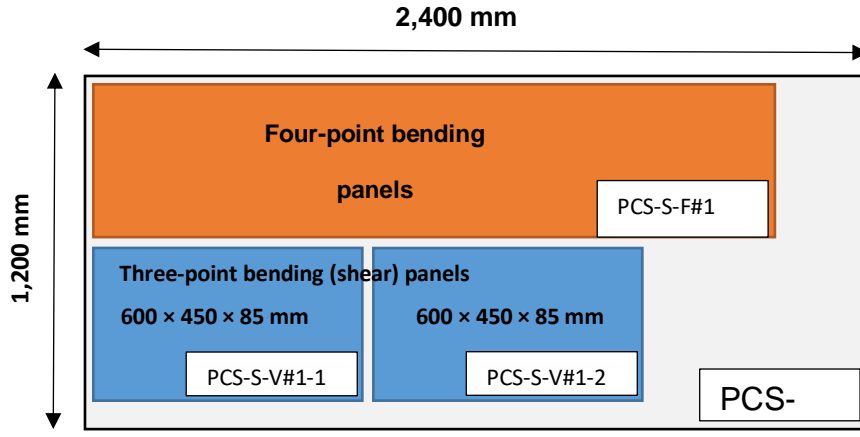
Figure 4.3 Cutting plan of the manufactured sandwich panels.

4.3 Materials and test procedures

4.3.1 Tensile tests

From each plywood skin of the BCS-S* and BCS-D* panels, a total of five coupon (dog bone) samples were cut using a CNC machine. The coupon samples had nominal widths of 6.5 mm and gauge lengths of 64 mm, and were tested according to the recommendations of ASTM D3500-14 (*ASTM D3500 - 14, Standard Test Methods for Structural Panels in Tension* 2014). The ends of the samples were clamped in the jaws of a 100 kN capacity Instron testing machine as shown in Figure 4.4 (a). The load was applied on the plywood coupons at a constant speed rate of 0.5 mm/min to reach failure in 3-5 min. The tensile strength $\sigma_{tu}^{\parallel}$ (strength in the fibre direction of plywood) of each coupon was calculated as

$$\sigma_{tu}^{\parallel} = \frac{T_{\max}}{b_t \times t_{par.}} \tag{4.1}$$

where T_{max} is the maximum recorded force, and b_t and $t_{par.}$, are the measured width and thickness of plies (only parallel to the direction of loading), respectively. Moreover, the ultimate strain at failure of each test $\varepsilon_{tu}^{\parallel}$ was also recorded. The material properties of plywood laminates obtained from the tensile tests are represented in Table 4.1. To find the mechanical properties of the plywood veneers from properties of plywood laminates listed in Table 4.1, a classical laminate theory tool (OSULaminates tool developed by Oregon State University) was utilised (Nairn 2015). To do so, the average value E_L of *P .radiata* was taken from (*Wood Handbook: Wood as an Engineering Material* 2010a), and the other properties were approximated based on their corresponding ratios to E_L. The

mechanical properties of the plywood veneers of the BCS-S* and BCS-D* plywood skins are listed in Table 4.2.

4.3.2 Non-destructive vibration test

The dynamic longitudinal and the shear moduli of elasticity of the peeler cores were measured using a non-destructive resonance method (Brancheriau & Baillères 2002). To do so, the peeler cores in their original dimensions were simply supported on rubber bands and impacted with a hammer (Figure 4.4b). The sample natural frequency was recorded using a microphone and analysed using the BING (Beam Identification by Non-destructive Grading) software (CIRAD 2012). The test method could not be extended to bamboo culms, due to its intrinsic irregular geometry. The material properties of peeler cores were calculated from the non-destructive vibration test method are represented in Table 4.3. The material properties of CLT panels were taken from the supplier's catalogue (XLam 2016), and are denoted in Table 4.4.
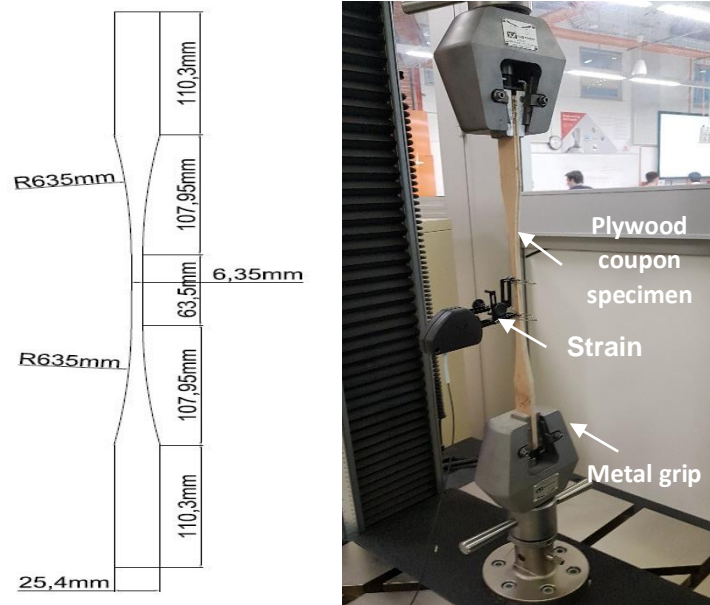
(a)
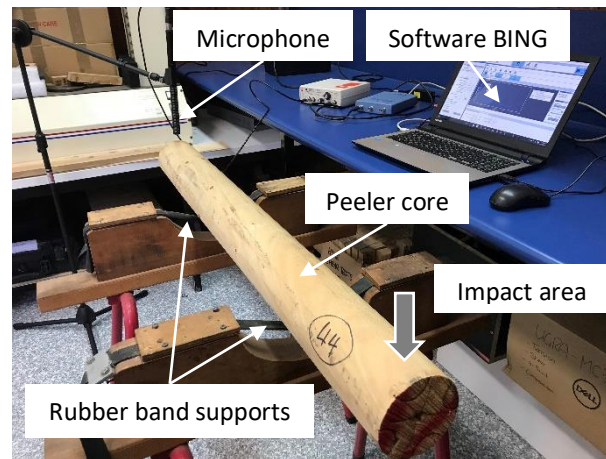
(b)

Figure 4.4 Material testing procedures: (a) tensile coupon test, and (b) non-destructive vibration test (BING) (Brancheriau & Baillères 2002; CIRAD 2012).

Table 4.1 Tensile test results of the plywood skins (numbers in brackets indicates the number of tests on which the average and coefficient of variation (COV) are calculated.

sample	E_L (MPa)	COV (%)	$\sigma_{tu}^{\parallel}$ (MPa)	COV (%)	$\epsilon_{tu}^{\parallel}$(×10⁻⁶)	COV (%)
P. radiata plywood (BCS-S*)	7,781 (5)	17.1	40.8 (5)	22.5	5,100 (5)	16.5
P. radiata plywood (BCS-D*)	10,216 (5)	11.0	69.0 (5)	4.0	6,800 (5)	12.1

Note: Subscripts *L* is associated with the longitudinal direction. Superscripts * indicates old panels.

Table 4.2 Material properties of the *P. radiata* veneers obtained from classical laminate theory (Nairn 2015).

sample	E_L (MPa)	E_T (MPa)	E_R (MPa)	G_{LT} (MPa)	G_{TR} (MPa)	G_{LR} (MPa)	V_{LT}	V_{TR}	V_{LR}	$\sigma_{tu}^{\parallel}$ (MPa)	$\epsilon_{tu}^{\parallel}$(×10⁻⁶)	$\sigma_{cu}^{\parallel}$ (MPa)	$\sigma_{cy}^{\parallel}$ (MPa)	$\epsilon_{cy}^{\parallel}$(×10⁻⁶)	Layer's thickness (mm) and lay up
P. radiata veneer (BCS-S*)	11,380	500	1,001	922	125	1,092	0.31	0.30	0.34		5,211			2,761	2.4 / 2.4 / 2.4
										59.3		41.9	31.4		
P. radiata veneer (BCS-D*)	14,941	657	1,315	1,210	164	1,434	0.31	0.30	0.34		3,969			2,103	2.4 / 2.4 / 2.4

Note: Subscripts *L*, *T* and *R* are associated with the longitudinal, tangential and radial directions, respectively.

Table 4.3 Bamboo properties taken from (Chung & Yu 2002), and peeler core properties obtained from the non-destructive vibration test method.

sample	D (mm)	E_L (MPa)	COV (%)	G_{LR} (MPa)	COV (%)
Peeler core (PCS-S #1)	125.9 (44)	10,462 (44)	12.7	944 (44)	20.5
Peeler core (PCS-S #2 and #3)	141.4 (16)	9,585 (16)	18.5	1,281 (16)	61.8
Bamboo core [46]	100.0 (-)	10,500 (-)	-	630 (-)	-

Table 4.4 Material properties of the CLT laminations taken from XLam product sheet (XLam 2016).

	MOE (parallel to span) (MPa)	MOE (perpendicular to span) (MPa)	Shear Modulus (parallel to span) (MPa)	Shear Modulus (perpendicular to span) (MPa)	Compression strength σ_{cu}" (parallel to span) (MPa)	Tensile strength σ_{tu}" (parallel to span) (MPa)
External laminations	8,000	267	500	50	41.9	59.3
Internal laminations	6,000	200	375	37.5	-	-

4.3.3 Moisture content

To determine the moisture content at the time of testing, samples were cut from the plywood skins and core materials (bamboo and peeler), and were weighed immediately after the three-point shear tests. The oven-dry methodology in the Australian and New Zealand standard AS/NZS 1080.1 (*AS/NZS 1080.1:2012 Timber-Methods of test, Method 1: Moisture content* 2012) was followed. The samples were dried in a ventilated drying oven at a temperature of 103±2°C between 24 to 36 hours, to the point where the weight of sample remained unchanged. The moisture content (MC) was determined by comparing the initial weight of the samples, to the weight after drying in the oven (the oven dry mass). MCs are expressed as a percentage of the oven-dry mass in Table 4.5.

Table 4.5 Moisture content (MC) of the panels measured following the three-point tests.

Samples	Core MC (%)	AVE (COV)	Skin MC (%)	AVE (COV)
BCS-S-V #1	8.38	11.67 (39.8%)	9.23	9.67 (6.5%)
BCS-S-V #2	14.96		10.12	
BCS-S-V* #1	9.26	9.20 (0.9%)	10.76	10.66 (1.3%)
BCS-S-V* #2	9.14		10.57	
BCS-D-V* #1	-	-	10.09	10.10 (0.1%)
BCS-D-V* #2	-		10.10	
PCS-S-V #1-1	10.18	10.38 (2.7%)	9.83	9.57 (3.9%)
PCS-S-V #1-2	10.58		9.30	
PCS-S-V #2-1	9.75	9.85 (1.4%)	9.81	9.78 (0.3%)
PCS-S-V #2-2	9.95		9.76	
PCS-S-V #3-1	10.23	12.81 (28.4%)	9.23	9.31 (1.2%)
PCS-S-V #3-2	15.38		9.39	
PCS-D-V #1	9.04	9.48 (6.5%)	9.01	8.64 (6.1%)
PCS-D-V #2	9.91		8.26	
PCS-TH-F #1	9.37	9.61 (3.5%)	9.68	9.54 (2.0%)
PCS-TH-F #2	9.84		9.41	
CL3/75-V #1	10.41	11.59 (8.9%)		
CL3/75-V #2	12.04			

4.3.4 Shear bond tests

Adhesive spread rate study was conducted to evaluate the shear strength between bamboo and plywood. To accomplish this, adhesive shear block test was performed in adhesive spread rates of 180, 360 and 540 g/m^2 in BCS-S panels. For each adhesive spread rate, four BCS-S panels with dimensions of 300 mm × 300 mm × 85 mm were manufactured. The panel dimensions were selected such that three whole bamboo rings could fit inside the panel in each direction (Figure 4.5). Two timber planks were glued to the top and bottom surfaces of the panel. Using a 100 kN Instron machine, a lateral displacement was imposed on the top plank, while the bottom plank was fixed in the machine's jaw. The shear bond strength was calculated by dividing the ultimate load by the total wall-thickness area of the nine bamboo rings. Results are given in Table 4.6. No shear bond test was conducted for the PCS panels, since the contact surface area in the PCS panels were much larger than the BCS panels and thus less susceptible to shear interface failure.
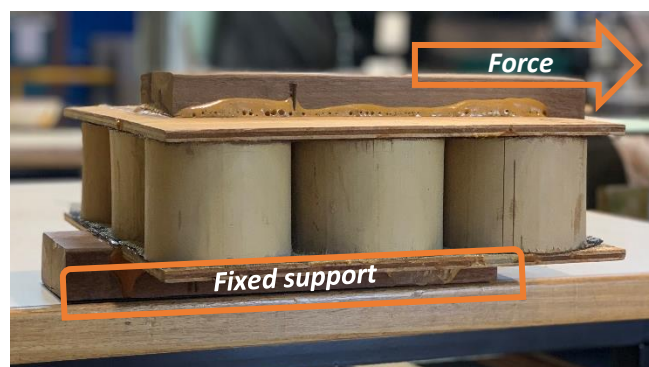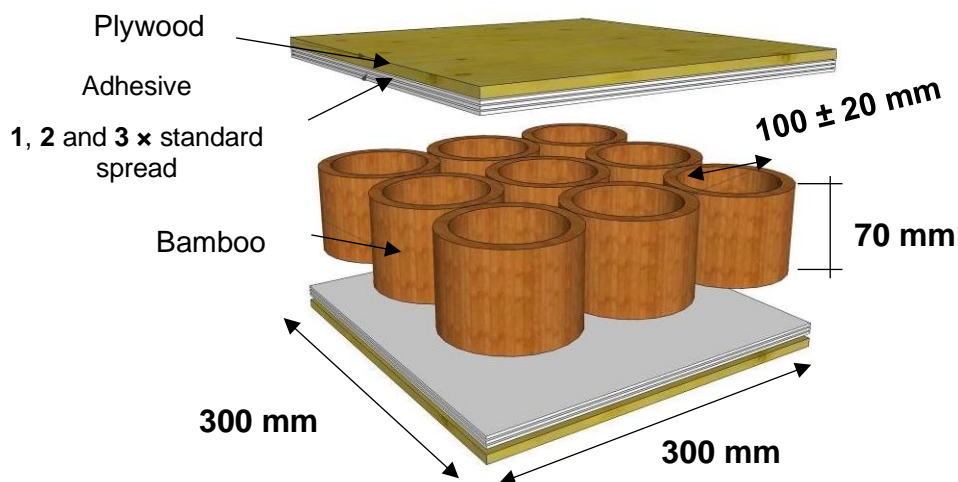
Figure 4.5 Shear bond tests of a BCS-S panel.

Table 4.6 Summary of adhesive shear block tests in BCS-S panels.

Specimen	Spread rate of adhesive (g/m^2)	Bamboo wall-thickness area (mm^2)	Failure load (kN)	Shear strength (MPa)
BCS 1-1		19,330	25.4	1.31
BCS 1-2	180	23,458	26.7	1.14
BCS 1-3		24,174	17.8	0.74
BCS 1-4		19,695	15.8	0.80
AVE (COV)		21,664 (11%)	21.4 (25%)	0.99 (27%)
BCS 2-1		18,715	22.4	1.20
BCS 2-2	360	23,421	27.1	1.16
BCS 2-3		21,365	26.6	1.25
BCS 2-4		17,697	19.3	1.09
AVE (COV)		20,299 (13%)	23.8 (16%)	1.17 (5%)
BCS 3-1		24,913	27.7	1.11
BCS 3-2	540	20,963	25.0	1.19
BCS 3-3		26,089	31.7	1.21
BCS 3-4		20,113	25.4	1.26
AVE (COV)		23,019 (13%)	27.4 (11%)	1.19 (5%)

4.3.5 Four-point bending tests

4.3.5.1 Test set-up

Four-point bending tests were carried out according to the recommendations of BS EN 16351:2015 (*BS EN 16351 : 2015 Timber Structures- Coss Laminated Timber- Requirements* 2015) to measure the bending strength and stiffness of the panels. The standard (*BS EN 16351 : 2015 Timber Structures- Coss Laminated Timber- Requirements* 2015) dictates a minimum span between 24h to 30h, where h is the panel depth. The test set-up is shown in Figure 4.6. Tested panels had dimensions of a=2,300 mm and b=450 mm, and h= 85 mm. The actual centre-to-centre span of the panels was 2215 mm, with a span-to-depth ratio of 26. The distance between the supports and the nearest end of the panels was equal to half of the depth of the panels, which was 42.5 mm. The panels were simply supported during the tests, and the point loads were applied across the

whole width of the panels by using an assembly of spreader beam and steel solid tubes with diameter of 50 mm.
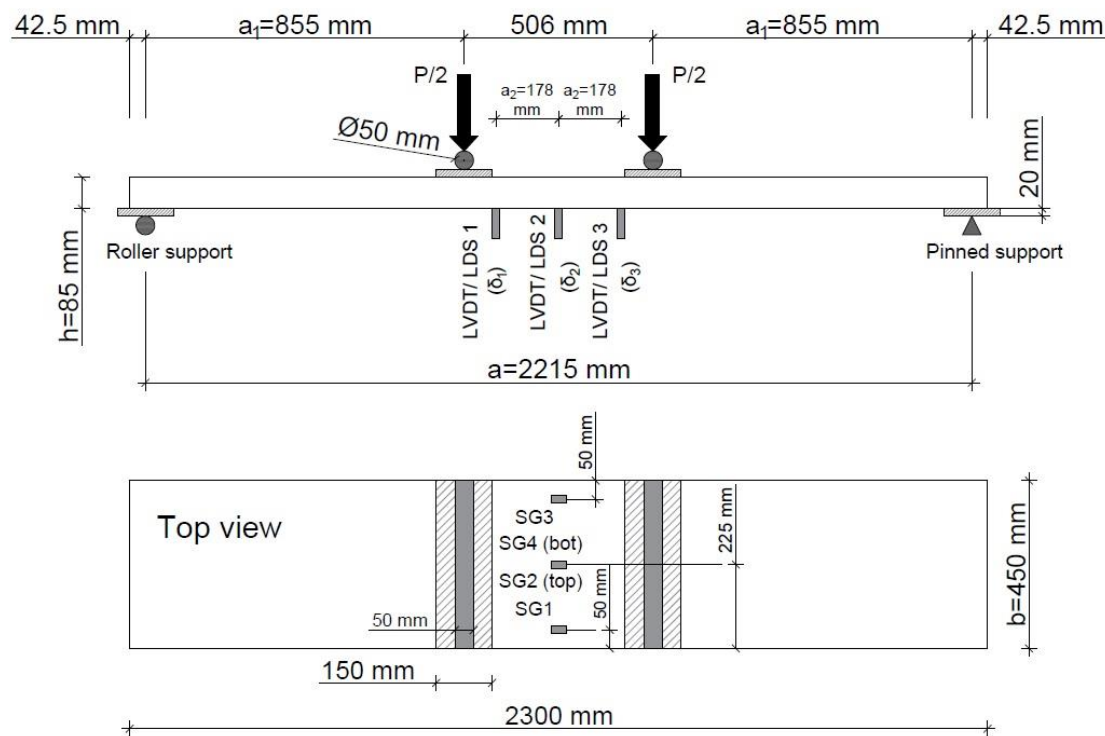
(a)
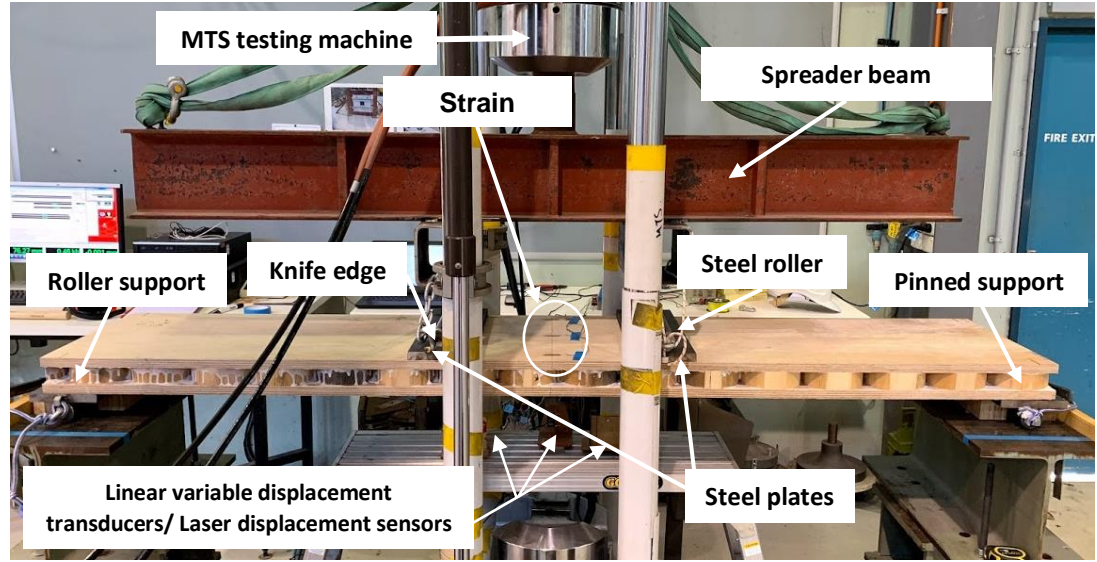
(b)

Figure 4.6 Four-point bending test set-up, (a) a schematic illustration, and (b) the experimental rig.

The distance between the two loading points was six times the depth of the panels (6*h*). Steel plates with width of 150 mm and length of 450 mm were positioned under the loading points and the supports to prevent localised failures. The panels were tested in a 500 kN capacity MTS universal testing machine, with the load being applied to the steel solid tubes. A constant displacement loading rate of 10 mm/min was applied, so that the maximum load was reached within 5-6 min. To measure the deflection during loading, three Linear Variable Displacement Transducers (LVDTs) were used (see Figure 4.6). LVDT 2 was located at the mid-span, while (LVDTs 1&3) were located 4.2 times (*h*) apart, and closer to the point loads. The distance between LVDT 1 and LVDT 3 was slightly less than the recommend distance of five times the panel depth (5*h*) in the BS EN 16351 (*BS EN 16351 : 2015 Timber Structures- Coss Laminated Timber-Requirements* 2015). Strains in both top and bottom surfaces of the panels were monitored using four 30 mm long strain gauges (SGs), installed along the panel direction. As shown in Figure 4.6 (a), SGs 1-3 were attached to the top surface (compression side), while SG4 was installed on the bottom surface (tension side) at mid-span right under SG2. The applied load, displacement and strains were recorded and synchronised using a digital data acquisition (DAQ) system.

4.3.5.2 Evaluations

The moment in the mid-section of the sample (*M*) is

$$M = \frac{(P + P_W)a_1}{2} \tag{4.2}$$

where *P* is the load applied by the MTS, a_1 is the distance between the loading head and the nearest support, given in Figure 4.6 (a), and P_w= 0.33 kN is the weight of the steel plates and the rollers. The relative defection (*δ*) of the panel is calculated from the displacements $δ_1$, $δ_2$ and $δ_3$ recorded by the LVDT number 1, 2 and 3, respectively

$$\delta = \delta_2 - \frac{\delta_1 + \delta_3}{2} \tag{4.3}$$

Curvature (*k*) of the panel under four-point bending is calculated from the LVDT readings as

$$k = \frac{2\delta}{(a_2)^2} \tag{4.4}$$

where a_2 (given in Figure 4.6 (a)) is the distance between LVDT 2 and LVDTs 1 or 3.

To acquire the flexural stiffness (EI) of the panels, two methods were adopted: (1) the strain method, and (2) the deflection method. In the strain method, $(EI)_{SG}$ was obtained from the strain-curvature relationship using the strain gauge readings (SG1, SG2 and SG3) on the top surface (compression side) over the width of the panels

$$(EI)_{SG} = \left(\frac{\Delta M}{\Delta \varepsilon}\right)\left(\frac{h}{2}\right) \tag{4.5}$$

where h is the total depth of the panel, and $\Delta M / \Delta \varepsilon$ is the slope of the linear part of the moment-strain curve (M-ϵ), and calculated between an applied load of 1 kN and 2 kN. In the deflection method, $(EI)_\delta$ was calculated from the LVDT readings, under the point loads (LVDTs 1 and 3)

$$(EI)_{\delta 1/3} = \frac{a_1\left(3ax - 3x^2 - a_1^2\right)}{12}\left(\frac{\Delta P}{\Delta \delta}\right) \tag{4.6}$$

and at the mid-span (LVDT 2)

$$EI_{\delta 2} = \frac{a_1\left(3a^2 - 4a_1^2\right)}{48}\left(\frac{\Delta P}{\Delta \delta}\right) \tag{4.7}$$

where a and a_1 are shown in Figure 4.6 (a), and x= 930 mm is the distance from the supports to LVDT 1 and LVDT 3. The load-displacement slope ($\Delta P / \Delta \delta$) is taken from the linear part of the load-deflection curve and corresponds to (1 kN<P<2 kN).

The former expressions (Eqs. 4.6, 4.7) are based on Bernoulli beam deflection theory, and neglect the shear effects. A more suitable deflection theory is the Timoshenko shear deformation theory (Timoshenko & Woinowsky-Krieger 1959), and accounts for shear effects in bending. In a Timoshenko beam and in a four-point bending test, the mid-span deflection (δ_2) is the sum of flexural (w_1) and shear (w_2) deformations:

$$\delta_2 = (w_1) + (w_2) = \frac{23Pa^3}{1296(EI)} + \frac{Pa}{6k(GA)} \tag{4.8}$$

where *GA* is the shear stiffness, and *κ* is the Timoshenko shear coefficient. Using an analytical approach, current authors calculated *κ* of 0.817 and 0.815 for the BCS and PCS panels, respectively (Darzi et al. 2018b). Recommended *κ* for a CLT panel (with rectangular cross-section) is 1.2 (Karacabeyli & Gagnon 2019). The Timoshenko expression (Eq. 4.8) will be used later to estimate *GA*, and find the contribution of shear deflection (w_2) to flexural deformation (w_1) for each panel.

4.3.6 Three-point tests (shear)

4.3.6.1 Test set-up

The three-point (short span bending) tests were conducted in accordance with the US ANSI/APA PRG 320 standard (APA—The Engineered Wood Association 2018). Panels with dimensions of *a*=600 mm, *b*=450 mm and *h*= 85 mm were tested using a 100 kN Instron testing machine. The test setup and the boundary conditions are shown in Figure 4.7. The tests were performed in a displacement control method and reached failure in about 3-4 min. The panels were simply supported, with a distance between supports of 500 mm. The load was applied at the mid-span using a steel solid tube placed on a 20 mm thick steel solid plate. Two Laser Displacement Sensors (LDS) placed at both sides of the panel recorded the mid-span vertical displacements of the neutral axis (Δ_1 and Δ_2). One 30 mm, strain gauges (SGs) was installed at the bottom surface (tension side) of the panel, and was used to measure strains in the longitudinal direction. A 10 mm tri-axial strain gauge rosette, was attached to the core of the sandwich panel, on the neutral axis, and at a distance 150 mm from one edge of the panel (see Figure 4.7 (a)). The strain gauge rosette was used to measure the shear strain.
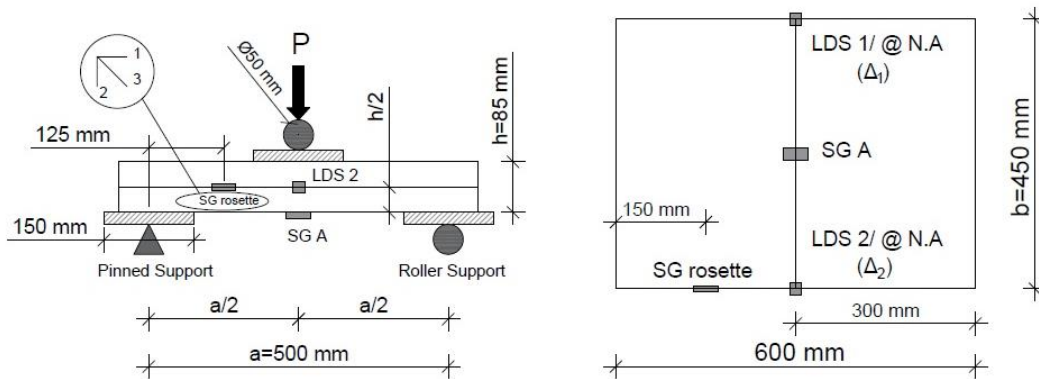
(a)
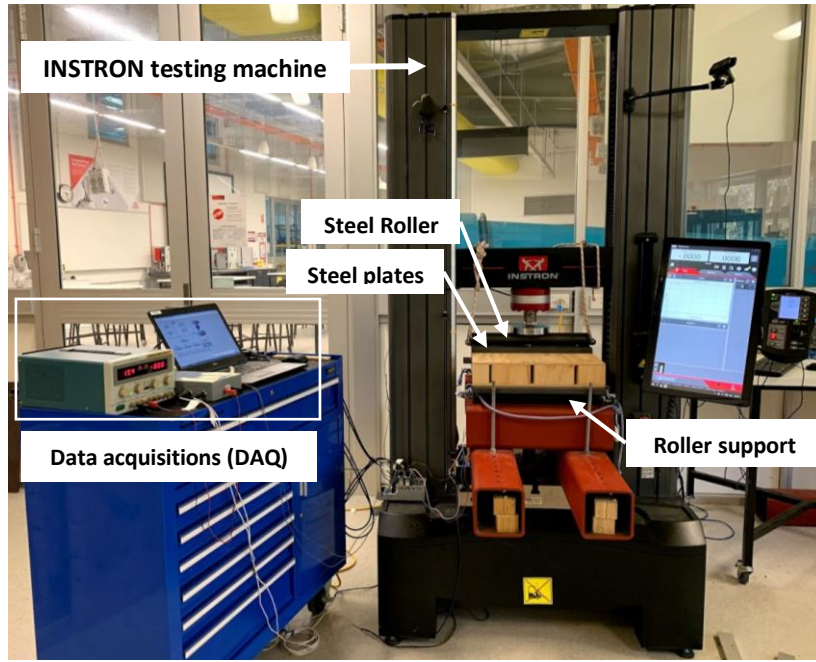
(b)

Figure 4.7 Three-point tests, (a) schematic illustration, and (b) the experimental rig.

4.3.6.2 Evaluations

The shear stress of the sandwich panels, was calculated using a section transformation analogy

$$\tau = \frac{PQ_{trans.}}{2I_{trans.}b} \tag{4.9}$$

where $P/2$ is the shear force, $Q_{trans.}$ is the first moment of area of transformed section at the point of interest, and b is the width of the panel at the cut. Denoting the ratio E_{skin}/E_{core} of the two moduli of elasticity by N, the moment of inertia of the total transformed section ($I_{trans.}$) can be expressed as

$$I_{trans.} = \frac{b_c c^3}{12} + 2\left(\frac{1}{12}bNt^3 + (bNt)(\frac{c}{2}+\frac{t}{2})^2\right), \quad N = \frac{E_{skin}}{E_{core}} \tag{4.10}$$

where E_{skin} is the modulus of elasticity of the plywood skin in the parallel-to-grain direction, E_{core} is the modulus of elasticity of core in the radial direction, and t and c are the plywood thickness and core height in the manufactured sandwich panels, respectively. In a BCS panel, at any given cross-section cut along the span, the width of the bamboo core (b_c) is almost equal to $2en_b$, where e is the

89

nominal bamboo wall-thickness and n_b is the number of bamboo rings across the width of the panel. In a PCS panel, an equivalent core width is based on the moment of inertia of the peeler core at the cut-section

$$b_c = 2R \, n \frac{I_\xi}{\bar{I}_\xi} \; , \; \bar{I}_\xi = \frac{1}{12}(2Rc^3) \; , \; I_\xi = \frac{1}{R}\int_0^R \frac{c^3}{12}D_\xi d\xi = \frac{1}{R}\int_0^R \frac{c^3}{12}\left(2R\sqrt{1-\left(1-\frac{\xi}{R}\right)^2}\right)d\xi$$

(4.11)

where D_ξ is the thickness of a peeler core, cut at distance ξ away from an edge, and n is the number of peeler cores with radius R, along the width of the PCS panel. In a CLT panel, the shear strength (Karacabeyli & Gagnon 2019) can be calculated from

$$\tau = \frac{1.5V}{c.A}$$

(4.12)

where A is the total cross-sectional area of the CLT panel and coefficient c is a reduction factor

$$c = \frac{I_{eff}}{I_{total}}$$

(4.13)

where I_{total} and I_{eff} are the total and effective moment of inertia for the major strength axis, respectively. I_{eff} is the effective moment of inertia of the panel accounting only for the layers with laminations oriented parallel to major strength axis

$$I_{eff} = \sum_{i=1}^{n} b_i.\frac{h_i^3}{12} + \sum_{i=1}^{n} A_i.z_i^2$$

(4.14)

where b_i, h_i and A_i are the width, thickness and cross-sectional area of each individual layer, respectively. The distance between the centroid of each layer and the centroid of the total cross-section of the CLT panel is z_i.

4.4 Results and discussion

4.4.1 Material properties

The average modulus of elasticity (E_L), ultimate tensile stress in the fibre direction ($\sigma_{tu}^{\prime\prime}$) and ultimate tensile strain in the fibre direction ($\epsilon_{tu}^{\prime\prime}$) of the plywood skins obtained from coupon tests are represented in Table 4.1. The mechanical properties of the individual *P. radiata* veneers (that make the plywood) were

calculated from the properties of plywood listed in Table 4.1. The mechanical properties of the *P. radiata* veneers of the BCS-S* and BCS-D* plywood skins are listed in Table 4.2. The ratios between longitudinal moduli of elasticity and mechanical properties in other directions, and the Poisson ratios (v) are taken from (*Wood Handbook: Wood as an Engineering Material* 2010b).

Table 4.3 presents the average values for measured diameter (D), and modulus of elasticity parallel to the grain (E_L) and shear modulus perpendicular to the grain (G_{LR}) of peeler core from the NDT vibration method (Brancheriau & Baillères 2002). The properties of bamboo core were taken as the average values of *Moso* bamboo (*Phyllostachys Pubescens*) reported in (Chung & Yu 2002).

The material properties of the CLT (CL3/75) panel laminations are represented in Table 4.4, and are taken from *XLam* design guide (XLam 2016). European CLT panels are mainly manufactured with softwood spruce-pine-fir (SPF) lumber, therefore similar strength values as species *P. radiata* are assumed for laminates parallel to the major strength axis of the CLT panel. Moisture contents at the time of the three-point tests of the panels are reported in Table 4.5. Maximum and minimum MCs vary between 8.64% and 12.81%.

4.4.2 Shear bond strength

The ultimate loads at failure of the shear bond tests are represented in Table 4.6. The shear strength at the bond is found by dividing the ultimate load by the bamboo wall-thickness area. It can be seen that doubling or tripling the glue spread rate, does not translate into a significant increase in the bond strength of the BCS panel. Hence, in the manufacturing of the BCS panels, spread rate of 180 g/m^2 was adopted. At this spread rate, the average shear strength at the bamboo-plywood contact is 0.99 MPa.

4.4.3 Bending tests

The four-point bending test results are presented in Figure 4.8 to Figure 4.10 and represented in Table 4.7 and Table 4.8. The bending results are discussed in terms of capacity, ductility and stiffness, for each panel type.

4.4.3.1 Capacity and failure mode

The load versus mid-span displacement behaviour (P-δ_2) of the panels under four-point bending tests are shown in Figure 4.8 (a). The corresponding failure modes at the ultimate loads are shown in Figure 4.10 and reported in Table 4.7.

The ultimate moment capacity of the BCS-S-F panel is 27.3% higher than BCS-S-F* panel (the panel that was made 2.5 years earlier). The BCS-S-F panel failed due to the rupture in the bottom skin, a tensile failure within the pure bending zone (see Figure 4.10 (a)). Whereas, a premature failure outside the pure bending zone was observed in the BCS-S-F* panel. This is probably due to the biological degradation and loss of interface bond caused by *Dinoderus Minutus* (bamboo borer), that was visible in the bamboo core rings (Saikia et al. 2015).

Using double-layer BCS-D*, the ultimate capacity of the panel in bending increased by 33.9% compared to the similar (*) single-layer panel. No improvement in stiffness can be observed with a double core layers, considering the slope of the linear part of the (P-δ_2) curve. At larger moments, a nonlinear behaviour was observed in the response of the single-layer BCS panels. The softening nonlinearity prior to reaching the ultimate is more pronounced in the bending response of the double-layer BCS panel. This softening nonlinearity could be attributed to the higher contact surface area between the plywood skins and bamboo core, and eventuates in a total flexural rupture of the panel in the bending zone (Figure 4.10 (a)).

Amongst the peeler core panels, the highest ultimate moment capacity of 20.78 kN.m corresponds to the PCS-S-F#1 panel, which is 31.6% and 26.4% higher than PCS-S-F #2 and PCS-S-F #3 panels, respectively. In the manufacturing of the PCS-S-F#1 panel, no sanding process was performed. Apparently, the shear interface bond of peeler core panels without sanding is stronger than those with sanding. The superior interface strength resulted in higher bending capacity of the PCS-S-F#1 panel, compared to other peeler core panels. This is evident in the failure modes of Figure 4.10 (b). In terms of elastic stiffness (slopes of linear parts of the curves in Figure 4.8 (a)) comparable values are observed between PCS-S-F #1 and PCS-S-F #3 panels, while a reduced slope (up to 30%) is seen in the PCS-S-F #2 panel. In all PCS-S-F panels, plywood failed in the tension face and within the pure bending region. As shown with arrows in Figure 4.10 (b), plywood cracks led to separation of plywood veneers within the plywood laminates. No face/core debonding (interface delamination) was observed as the bottom plywood veneers were still attached to the peeler cores after the failure. Unlike BCS-D-F* (double-layer) panel, no improvement in ultimate capacity and elastic stiffness was observed in the double-layer PCS panel (PCS-D-F). Similar

failure mode to the single-layer PCS panel was observed in the PCS-D-F panel, as shown in Figure 4.10 (b).

The PCS-TH-F panels showed much higher capacity and stiffness compared to the BCS and PCS panels. Moreover, load-deflection responses of the PCS-TH-F panels (#1 and #2) were consistent as shown in Figure 4.8 (a). The improvement in the capacity is attributed to the augmented moment of inertia due to the thicker skins as well as application of higher grade timber in the plywoods. The consistency is because of the lower bending strains at the skin/core interface, and thus reduced chances of skin/core debonding. The load-drop observed in PCS-TH-F#1 at around 24.12 kN is due to the initiation and development of a crack in a peeler core ring at one side of the panel. Prior to reaching the ultimate moments, both PCS-TH-F panels depicted nonlinear response (Figure 4.8 (a)). At this stage interlaminar or delamination failure between the plywood plies was observed which propagated within the top and bottom plywood skins. Local buckling (buckling drive delamination) in the top plywood skin led to the separation of the plies in the top plywood skin in pure bending region, as shown in Figure 4.10 (c). This type of failure mode (local buckling) was previously reported in sandwich panels where the skin is subjected to compressive load and out-of-plane shear or localised impact loads (Martakos 2016). In responses of both PCS-TH-F panels, the first drop in the load-deflection curve (Figure 4.8 (a)) corresponds to the local buckling of the compressive skin. After this point, delamination between plywood veneers in the top and bottom skins is initiated and is quickly increased until rupture of the tensile skin occurs.
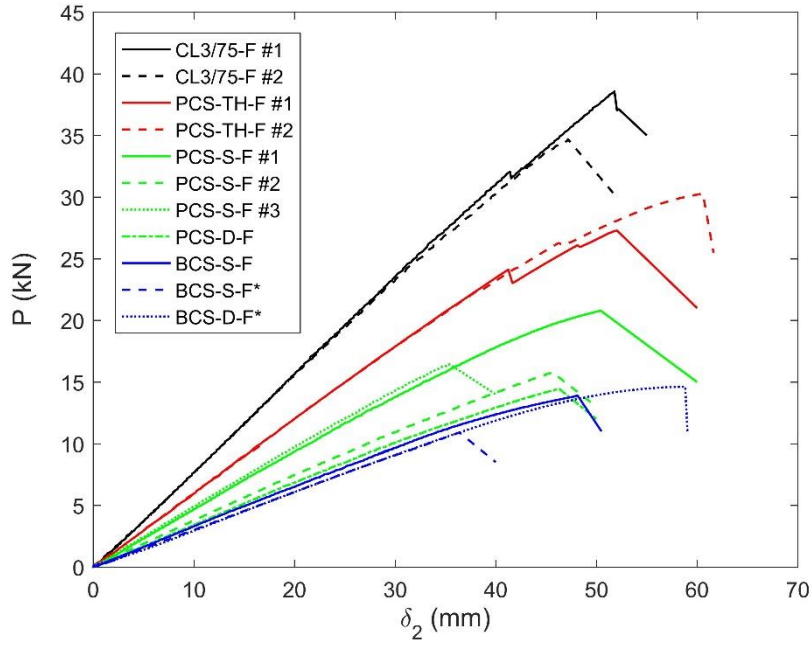
(a)
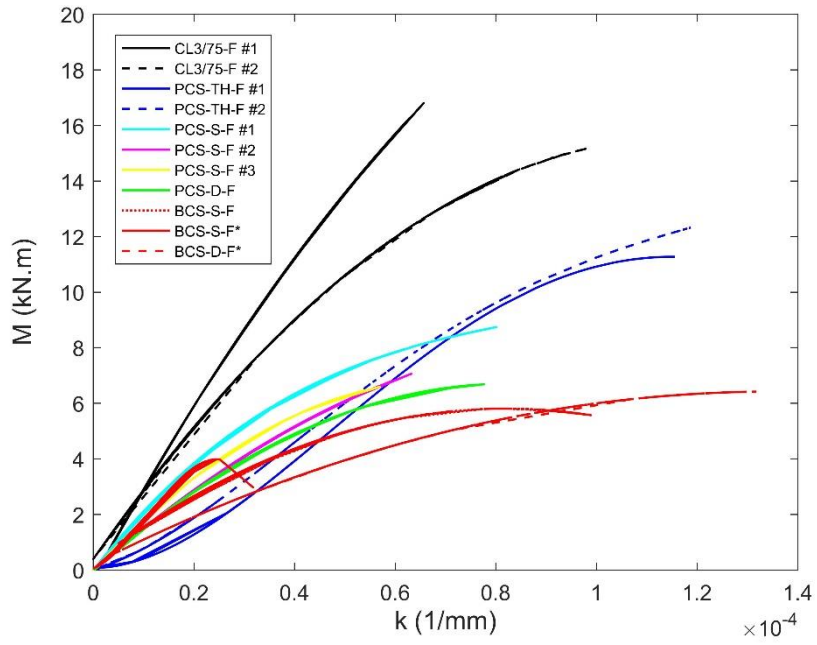
(b)

Figure 4.8 Four-point bending test results, (a) load vs. mid-span displacement (raw data), and (b) moment-curvature (M-k) response using polynomial curve fitting of raw data from Eq. 4.4.
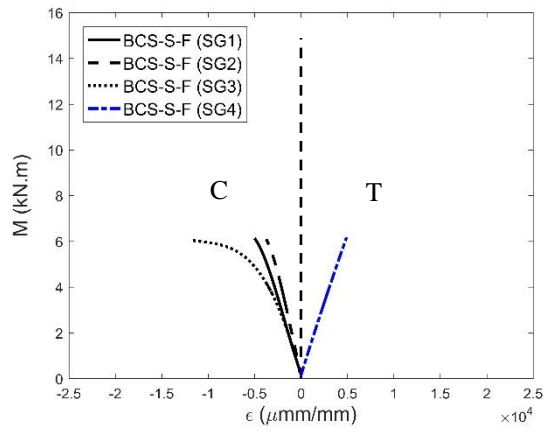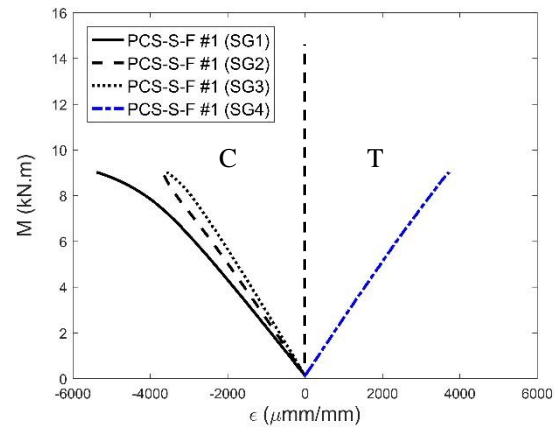
(a)   (d)
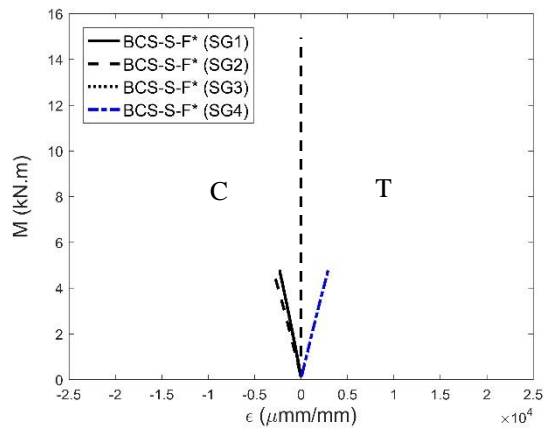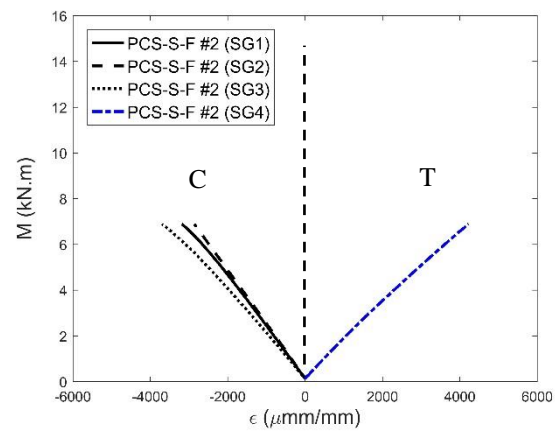
(b)   (e)
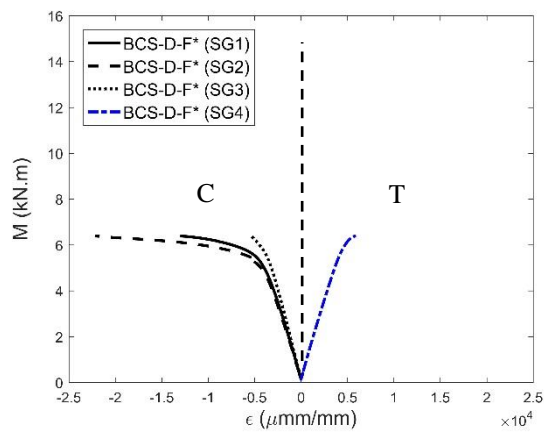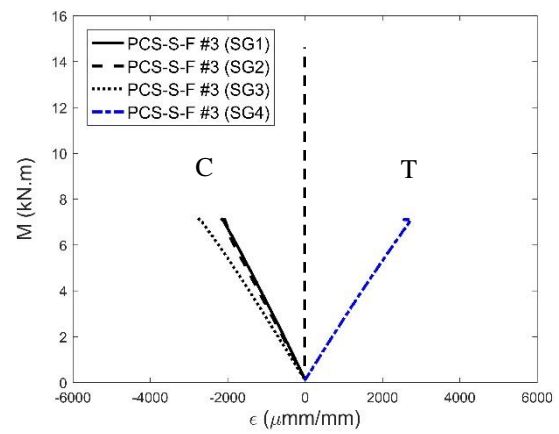
(c)   (f)
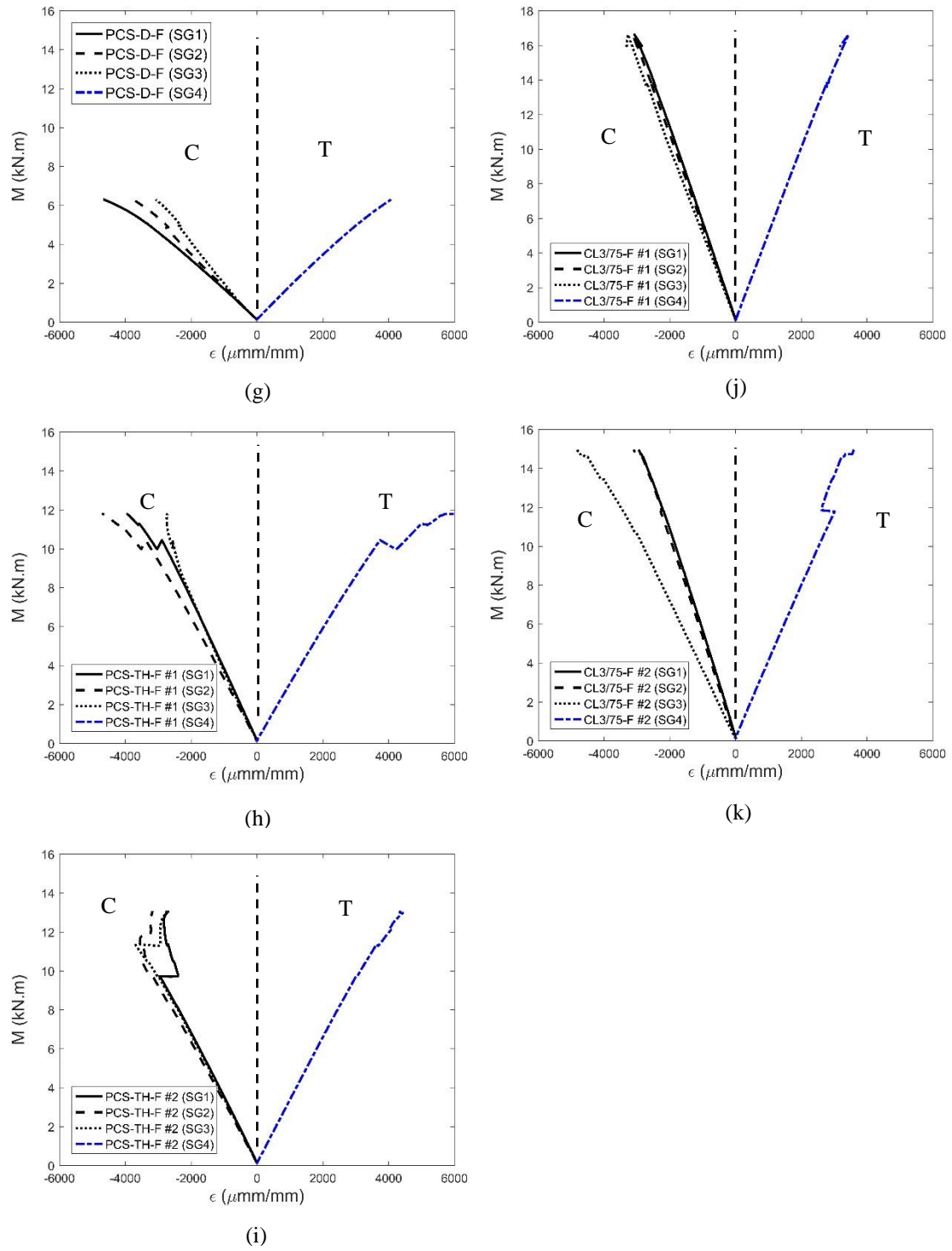
Figure 4.9 Four-point bending test results, showing Moment vs. longitudinal strains: (a)-(c) single and double-layer BCS, (d)-(g) single and double-layer PCS, (h)-(i) PCS-TH, and (j)-(k) CLT panels.

(a)

(b)

(c)

97
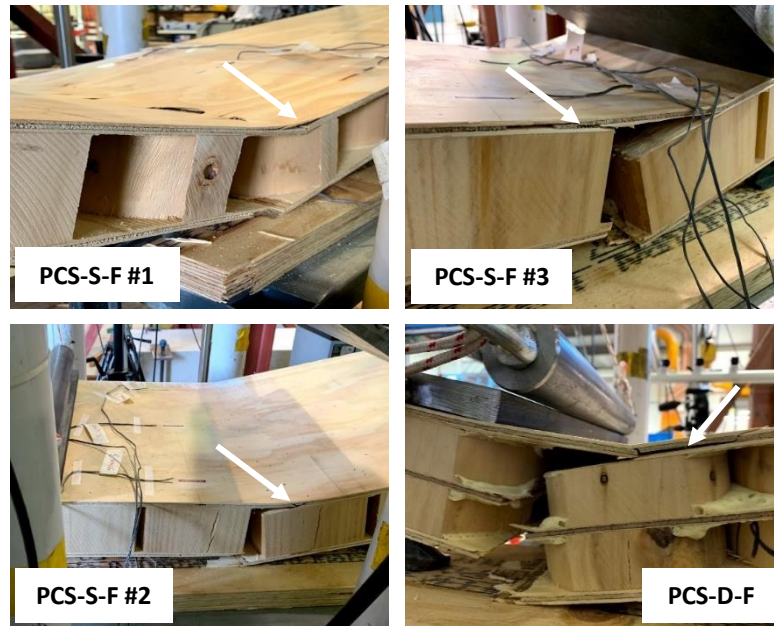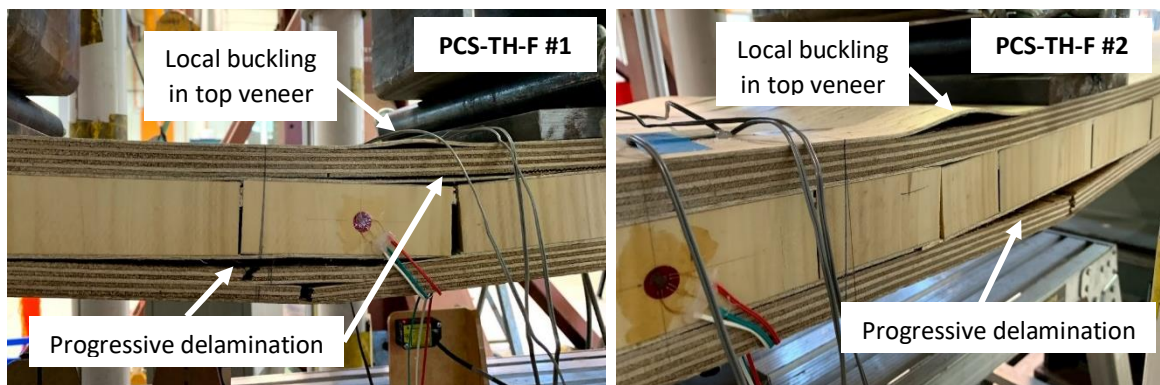
(d)

Figure 4.10 Four-point bending test results, showing failure modes of: (a) BCS, (b) PCS, (c) PCS-TH, and (d) CLT panels.

Table 4.7 Four-point bending test results.

Sample	P_{ult} (kN)	M_{ult} (kN.m)	$\epsilon_{cu}/\epsilon_{cy}$	$\epsilon_{tu(exp)}/\epsilon_{tu}$	Failure mode	Location of failure
BCS-S-F	13.90	6.08	4.28	0.94	Skin failure	
BCS-S-F*	10.92	4.80	1.09	0.56	Biological attack (mold)	
BCS-D-F*	14.62	6.39	10.56	1.49	Skin failure	
PCS-S-F#1	20.78	9.02	1.95	0.71	Skin failure	
PCS-S-F#2	15.79	6.89	1.34	0.81	Skin failure	
PCS-S-F#3	16.44	7.16	1.00	0.49	Skin failure	
PCS-D-F	14.44	6.31	1.69	0.78	Skin failure	
PCS-TH-F#1	27.28	11.79	2.24	1.65	Interlaminar and tensile skin failure	
PCS-TH-F#2	30.29	13.08	1.30	1.10	Interlaminar and tensile skin failure	
CL3/75-F#1	38.59	16.63	0.83	0.46	Rolling shear	
CL3/75-F#2	34.70	14.97	1.23	0.49	Rolling shear followed by tensile failure	

4.4.3.2 Ductility

Moment curvature responses of the panels are shown in Figure 4.8 (b). Since the raw data (Eq. 4.4) had too much noise, smoother curves obtained from polynomial curve fitting are plotted. The ultimate curvature of the BCS-D-F* panel is 1.32×10^{-4} mm^{-1}, and is 5.28 and 1.35 times the ultimate curvatures of the BCS-S-F* and BCS-S-F panels, respectively. Similar to BCS panels, in the PCS panels, the double-layer panel shows greater curvatures at similar moments, compared to the single-layer panels. The more ductile behaviour observed in double-layer BCS and PCS panels compared to single-layer panels can be attributed to higher contact area between core and plywood skins. A more ductile behaviour can be seen from the PCS-TH panels compared to single and double-layer BCS and PCS panels, as shown in Figure 4.8 (b). The ultimate curvature of the PCS-TH-F #1 and PCS-TH-F #2 panels are 1.16×10^{-4} mm^{-1} and 1.19×10^{-4} mm^{-1}, respectively.

Figure 4.9 shows the moment versus longitudinal strains of the top (compression) and bottom (tension) surfaces of the tested panels. The three SGs (SG 1, 2 and 3) show the longitudinal compressive strain distributions over the width of the panel, and SG 4 shows the tensile strain at the mid-span. The compressive strains are denoted with (C), while the tensile strains are shown with (T). Ratios of the ultimate compressive strain to compressive yield strain of *P. radiata* $\left(\varepsilon_{cu}/\varepsilon_{cy} \right)$, and ultimate recorded tensile strain to maximum tensile strain of *P. radiata* $\left(\varepsilon_{tu}^{\exp}/\varepsilon_{tu} \right)$ in each panel are reported in Table 4.7. As shown in Figure 4.9 (a) to Figure 4.9 (c), BCS-S-F panel failed at a tensile strain of 4,908 micro-strain which is 94% of the maximum tensile strain of *Radiata*. The compressive skin showed plasticity at M=2 kN.m. At the ultimate load, the compressive strain SG3 is equal to 11,830 micro-strain, and is 4.28 times larger than the assumed yield strain in *P. radiata* (Table 4.7). In the BCS-S-F* panel, the compressive strain at ultimate is 1.09 times the yield strain, whereas the ultimate tensile strain is 0.56 times the predicted tensile strain limit (premature failure). As shown in Figure 4.9 (c), the BCS-D-F* panel showed a more ductile behaviour compared to BCS-S-F panel in both tension and compression sides. A slight decrease in stiffness on the tension side was observed at about 4 kN.m, whereas plasticity occurred on the compression side. Both ultimate recorded compressive and tensile strains in

BCS-D-F* panel were significantly higher than the compressive yield strain (2,103 micro-strain) and maximum tensile strain (3969 micro-strain) of the *P. radiata*, as reported in Table 4.7.

Figure 4.9 (d) to (g) show the moment-strain curves in PCS-S-F#1, PCS-S-F#2, PCS-S-F#3 panels and PCS-D-F panel, respectively. At higher moment capacity, lower strains of both tension and compression skins are observed in single-layer PCS panels compared to single-layer BCS panels. This is attributed to higher moment of inertia due to higher peeler core width (b_c) within the PCS panels. Similar to single-layer BCS panels, the strains recorded on tension side are almost linear, except in PCS-S-F#2 panel where a slight reduction in stiffness was observed. From Table 4.7, it is obvious that the ultimate recorded tensile strains (SG4) for single-layer PCS panels did not reach the maximum tensile strain (5,211 micro-strain). However, the recorded compressive strains exceeded the compressive yield strain (2,761 micro-strain). Overall, compared to single-layer panels (in both BCS and PCS panels), the plywood skins of double-layer panels are more stressed.

Figure 4.9 (h) to (i) show the measured longitudinal strains in PCS-TH-F #1 and PCS-TH-F #2 panels, respectively. Linear trends in tensile and compressive strains up to the failure are observed. The compressive strains along the width of the compressive face (SG 1, SG 2 and SG 3) are more consistent, particularly in PCS-TH-F#2 panel, compared to BCS and PCS panels. As shown in Figure 4.9 (h), both tensile and compressive strains increased linearly up to M=10.44 kN.m in the PCS-TH-F#1 panel. At this point, a slight load-drop and consequent decrease in stiffness were accompanied with an increase in strains on tension and compression sides. This is due to the cracking of peeler core rings at one side of the panel, where SG1 and SG2 were located. Nonlinearity in the compression and tension strains were then observed indicating the development of failure in the plywood skins. From Table 4.7, it can be construed that the strain values on compression and tension sides exceed the compressive yield strain (2,103 micro-strain) and the maximum tensile strain (3,969 micro-strain) of *P. radiata* by 124% and 65%, respectively. In PCS-TH-F#2 panel, at M=9.72 kN.m the panel emitted a snapping sound. This was due to the occurrence of interlaminar failure (local buckling) in the top plywood skin, as shown in Figure 4.10 (c), and was accompanied by a localised nonlinearity in readings of SG1,

while other measured strains remained linear as shown in Figure 4.9 (i). From Table 4.7, the ultimate strain recorded on top surface (compression) is 30% higher than the predicted compressive yield point (2,103 micro-strain), and on the bottom surface (tension) it is 10% higher than the *P. radiata* tensile strain capacity (3,969 micro-strain).

4.4.3.3 Bending stiffness EI

Table 4.8 represents bending stiffness *EI* for all investigated panels under four-point bending tests, obtained from strain, $(EI)_{SG}$, and deflection, $(EI)_\delta$, readings (explained in the methodology section). There are differences between *EI*s calculated using strain and deflection methods. The differences between the three SG readings are due to the difference along the width of section. While, the differences between LVDT readings (deflections) are due to the variations along the length. Average and COVs from each method are characterized in Table 4.8. COVs of the deflection method are lower than those of the strain method. However, since the deflections used to calculate the bending stiffness were very small (just within the tolerance limit of the LVDT), the authors believe that the *EI*s calculated using strain gauges, $(EI)_{SG}$, are more accurate, and are used in the discussions herein.

The PCS panels displayed higher bending stiffness than the BCS panels. Largest *EI* amongst PCS panels is PCS-S-F#3 with an average value of 132.9 N.mm^2, which is 58% greater than the largest *EI* of all BCS panels, (BCS-S-F* panel with 84 N.mm^2). Bending stiffness of the double-layer bamboo or peeler core panels are not larger than the single-layer panels. However, comparing the *EI* values obtained from SG1, SG2 and SG3 along the width of the panels, it can be seen that COVs are significantly lower in double-layer panels in both BCS and PCS panels. This suggests that in the double-layer panel, the outer plywood skin is more uniformly stressed over its width. From Table 4.8, the optimum bending stiffness results correspond to PCS-TH-F#1 and PCS-TH-F#2 with *EI* of 143.63 N.mm^2 and 138.36 N.mm^2, respectively. The bending stiffness of the PCS-TH-F#1 panel is 60% and 19.8 % higher than the BCS-S-F* and PCS-S-F#3 panels, respectively.

Table 4.8 Bending stiffness of the panels obtained from the four-point bending test results.

Sample	$EI \times 10^9$ (N.mm^2) (SG$_1$)	$EI \times 10^9$ (N.mm^2) (SG$_2$)	$EI \times 10^9$ (N.mm^2) (SG$_3$)	$(EI)_{SG} \times 10^9$ (N.mm^2) AVG.(COV)	$EI \times 10^9$ (N.mm^2) (δ_1)	$EI \times 10^9$ (N.mm^2) (δ_2)	$EI \times 10^9$ (N.mm^2) (δ_3)	$(EI)_\delta \times 10^9$ (N.mm^2) AVG.(COV)	w_2/w_1 Eq. (4.8)
BCS-S-F	60.68	83.01	56.04	66.58 (21.65%)	68.06	68.66	68.09	68.27 (0.50%)	0.04
BCS-S-F*	93.16	69.13	89.80	84.03 (15.48%)	65.87	67.02	62.04	64.98 (4%)	0.42
BCS-D-F*	62.33	57.46	69.65	63.15 (9.72%)	65.05	60.28	63.03	62.79 (3.81%)	0.42
PCS-S-F #1	91.58	104.51	114.9	103.66 (11.27%)	95.77	100.55	95.66	97.31 (2.87%)	0.15
PCS-S-F #2	96.42	103.79	84.42	94.88 (10.30%)	81.77	83.19	75.79	80.25 (4.89%)	0.28
PCS-S-F #3	143.07	135.72	119.93	132.90 (8.90%)	107.70	109.22	107.64	108.19 (0.83%)	0.41
PCS-D-F	66.36	68.76	70.17	68.43 (2.81%)	73.49	75.64	71.12	73.42 (3.08%)	0.06
PCS-TH-F #1	151.85	138.26	139.68	143.26 (5.22%)	118.13	117.31	127.80	121.08 (4.82%)	0.26
PCS-TH-F #2	143.52	127.95	143.63	138.36 (6.52%)	124.65	112.01	127.16	121.27 (6.70%)	0.25
CL3/75-F #1	218.82	212.51	188.26	206.53 (7.81%)	172.27	147.41	146.69	155.46 (9.37%)	0.43
CL3/75-F #2	216.05	202.50	135.28	184.61 (23.43%)	155.88	158.97	186.42	167.09 (10.06%)	0.46

Eq. 4.8 was used to calculate the shear stiffness (GA) of the panels, using EIs from average strain gauge readings (column 5 of Table 4.8). Using the calculated GA, the shear to flexure deflection ratios (w_2/w_1) of the panels in four-point bending tests are calculated and summarised in Table 4.8. Large variations in shear to flexure ratios are observed in BCS and PCS panels, and are due to the disparities in measured EIs. However, in PCS-TH panels, contribution of shear to the total deformation is very consistent and is about a quarter.

4.4.4 Shear tests

Shear force (V) versus mid-span deflections of three-point shear test results are shown in Figure 4.11. The displacement Δ is the average of the neutral axis deflections (Δ_1 and Δ_2) on either sides of the panels. The shear forces are plotted against mid-span tensile strains (ε) and core shearing strains (γ) of the panels in Figure 4.12 and Figure 4.13, respectively. The results collected from the shear tests are summarized in Table 4.9. The shear stress at the interface ($\tau_{interface}$) between core and plywood skins are calculated using Eq. 4.9.
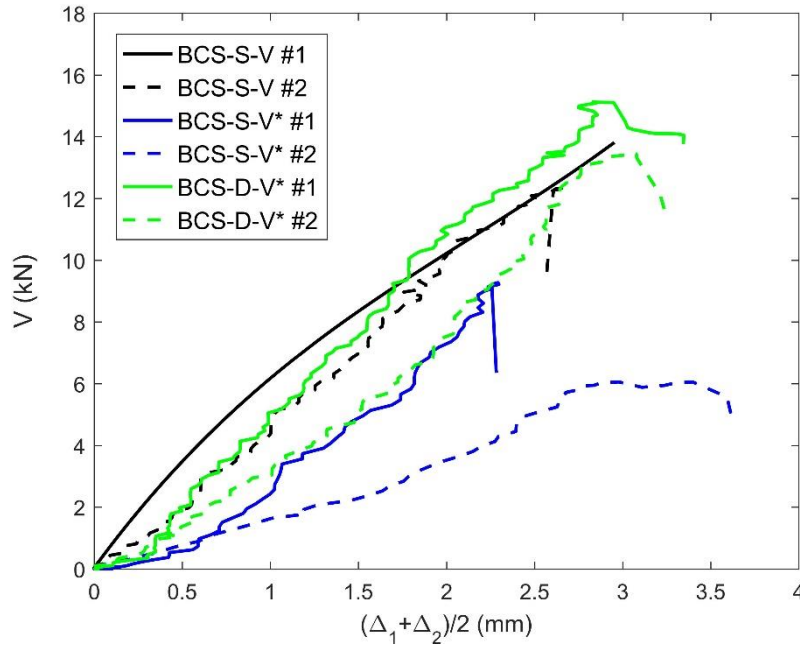
(a)
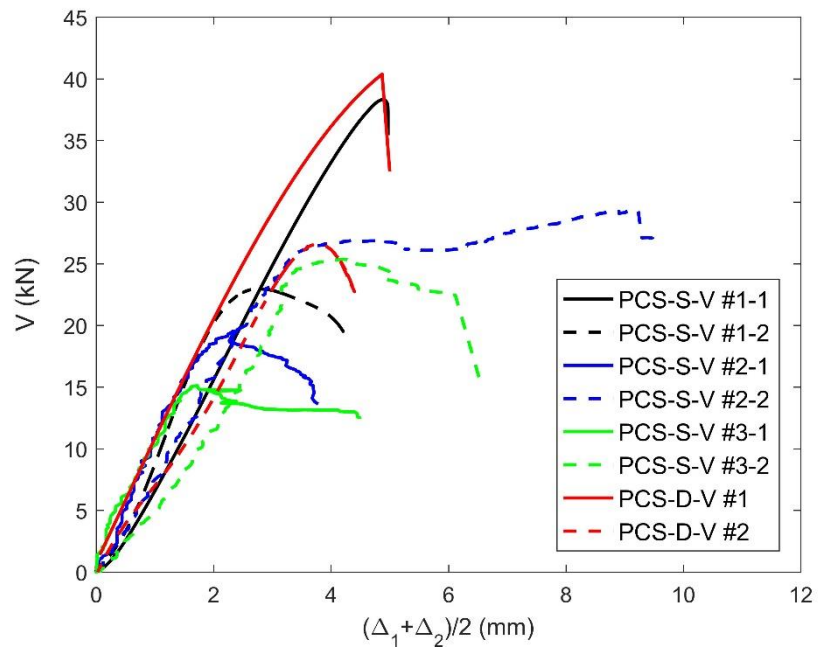
(b)
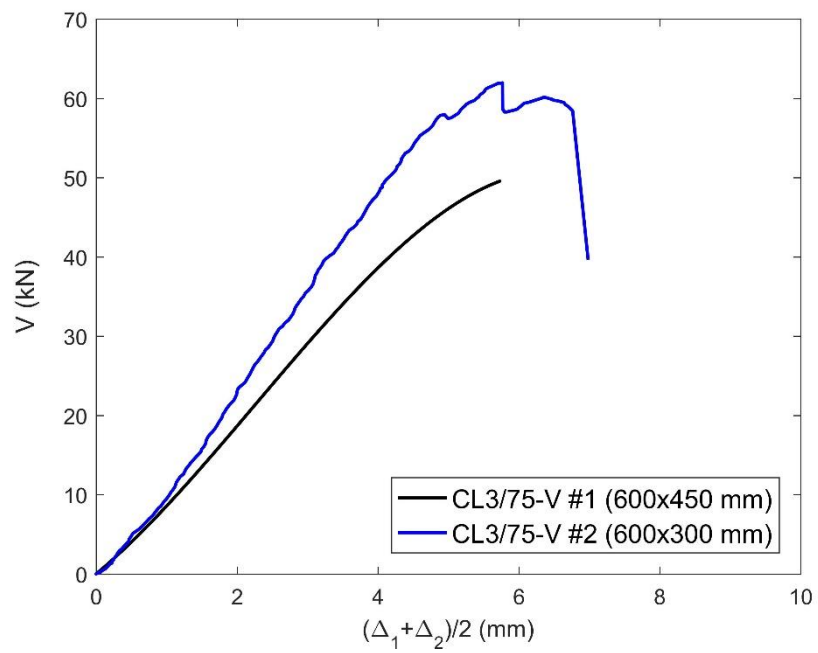
(c)

Figure 4.11 Three-point shear test results; (a) single and double-layer BCS, (b) single and double-layer PCS, and (c) CLT panels.
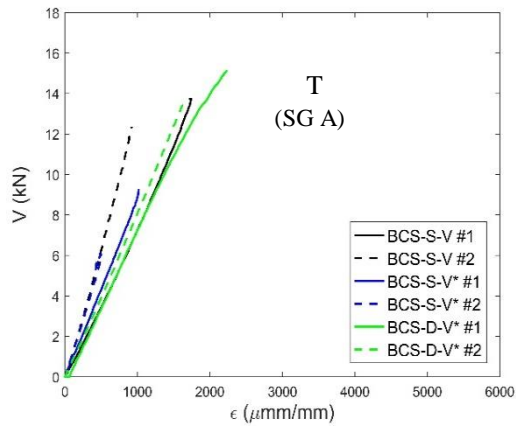
(a)
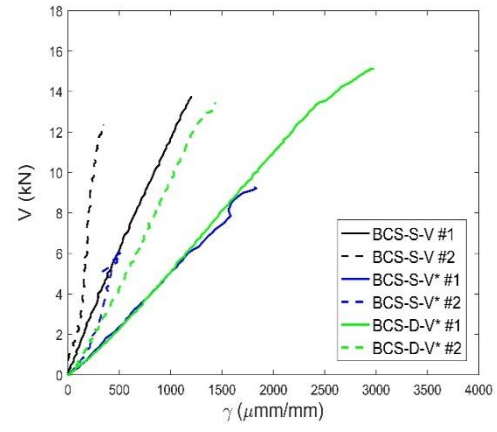
(a)
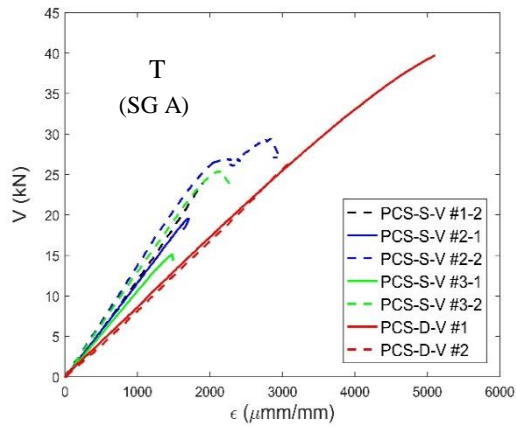
(b)
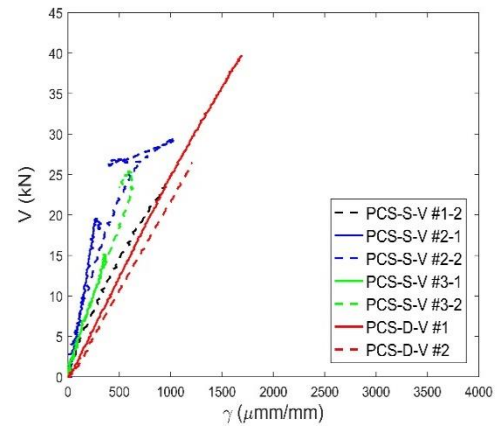
(b)
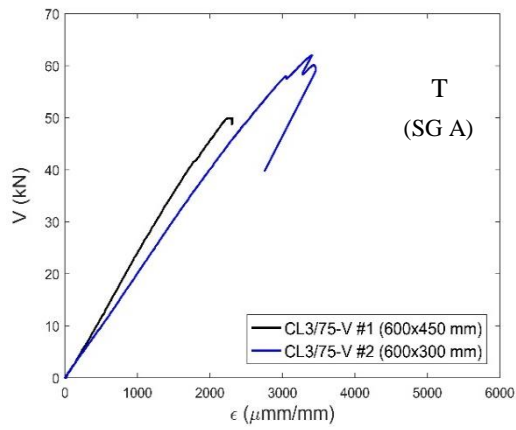
(c)
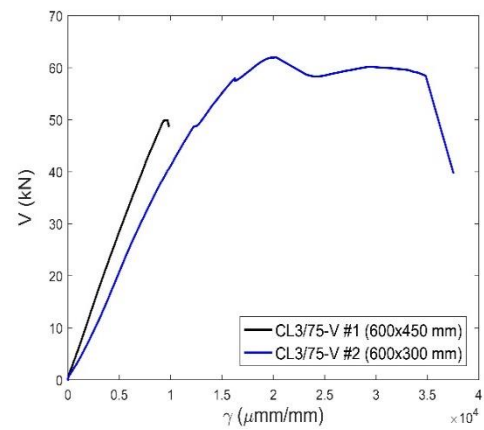
(c)

Figure 4.12 Shear force versus tensile strain response of the panels under three-point (shear) tests.

Figure 4.13 Shear force versus core shearing strain response under three-point (shear) tests.

BCS-S-V #1   BCS-S-V* #1   BCS-D-V* #1

BCS-S-V #2   BCS-S-V* #2   BCS-D-V* #2
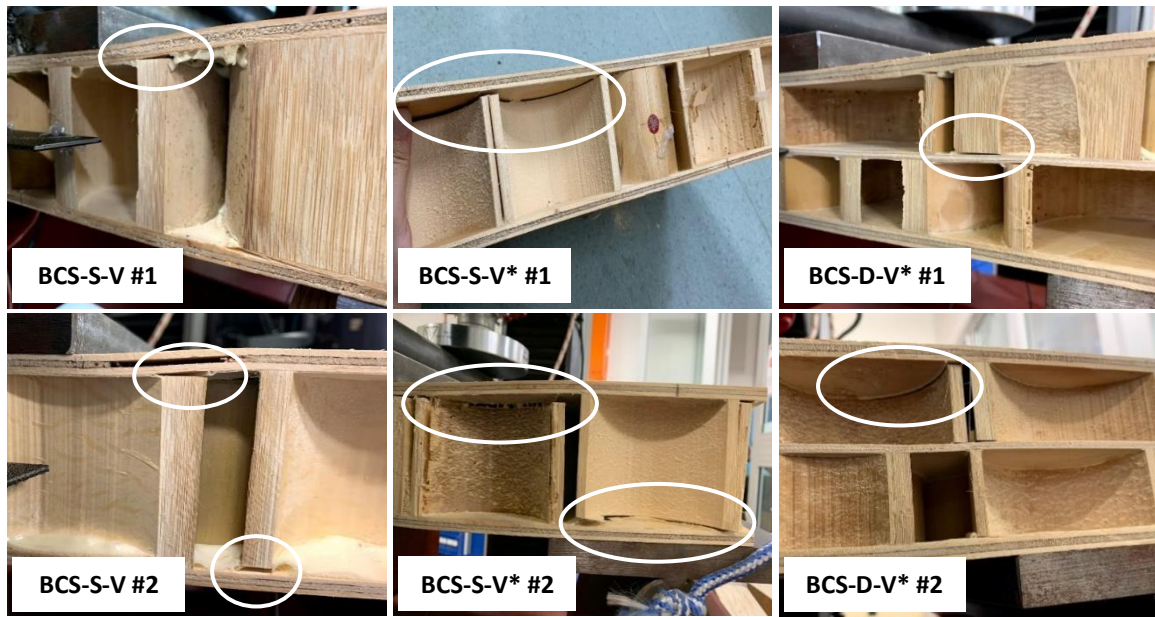
(a)
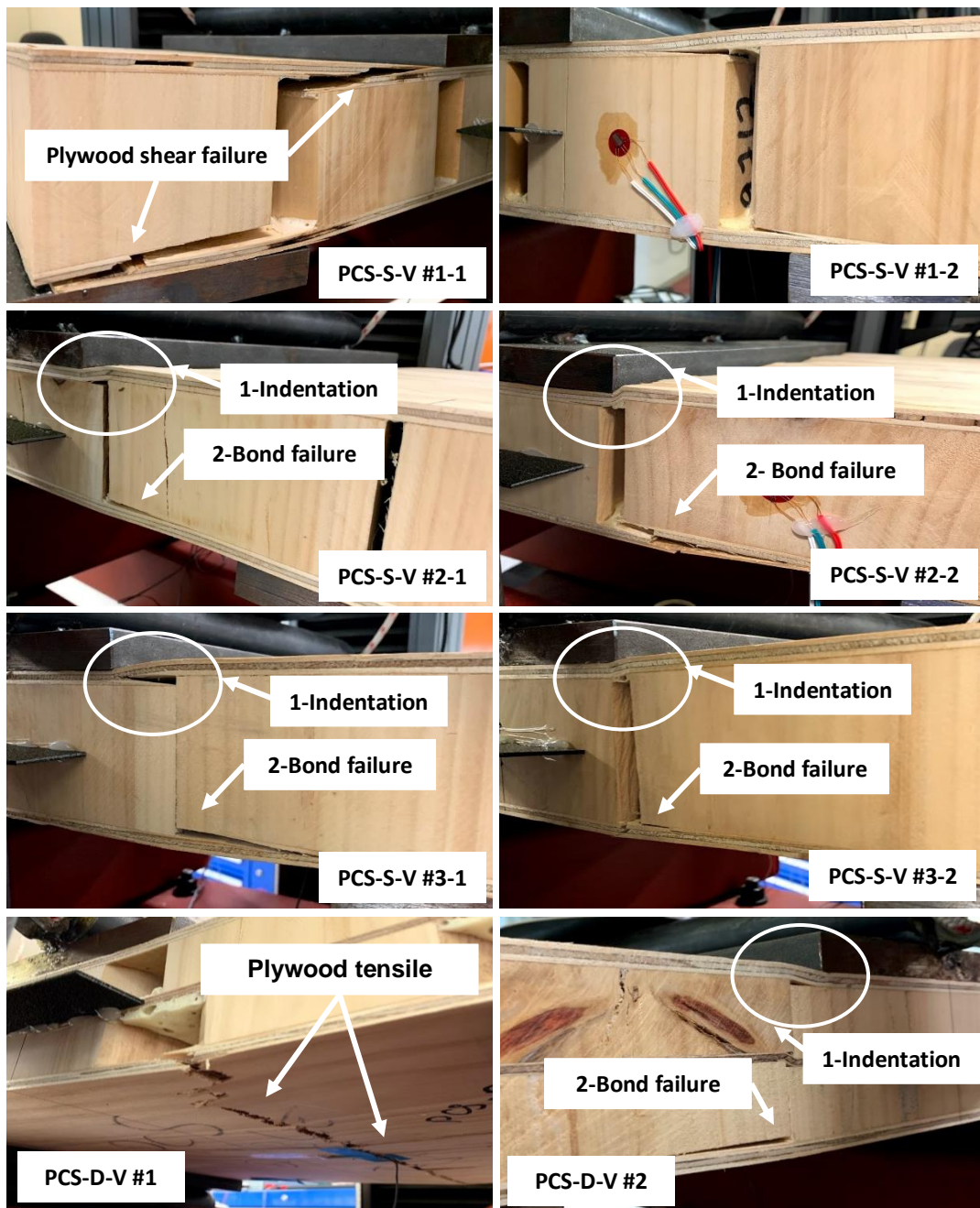
(b)
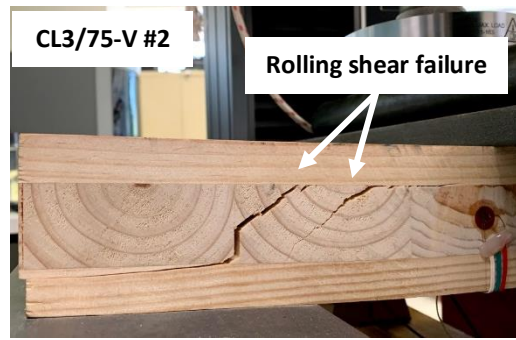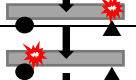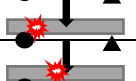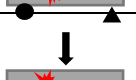
(c)

Figure 4.14 Three-point (shear) test results showing the failure modes in: (a) single and double-layer BCS, (b) single and double-layer PCS and (c) CLT panels.

As shown in shear force-displacement responses of the BCS panels in Figure 4.11 (a), the single-layer bamboo panels depict sporadic behaviour. The ultimate shear forces (V_{ult}) in Table 4.9, show that the bamboo borer has a significant effect in reducing the shear capacity of BCS panels (*). In the double-layer bamboo panels, the force-deflection slope is more consistent. Comparison between the average ultimate shear capacities (V_{ult}) of the double-layer and single-layer bamboo panels (neglecting the * panels), in Table 4.9 suggests that double-layer core geometry can increase the shear capacity by 9%. Comparison between Figure 4.12 (a) and Figure 4.13 (a), shows that at almost similar tensile strains in their skins, the BCS panels experience different core shear strains. Interestingly, the stiffest shear-strain response belongs to BCS-S-V#2. This suggests that in absence of local interface defects, the single-layer bamboo panels can be as strong as the double-layer ones. Tensile strain results (ε_{tu}) in Table 4.9 are much lower than the predicted ultimate strains of plywood in bamboo panels. The failure modes in Figure 4.14 (a) clearly show shear interface failure. This can be explained based on the calculated interface shear stresses ($\tau_{interface}$) in Table 4.9 (calculated from Eq. 4.9), which exceed the shear bond capacity (0.99 MPa) for glue spread rate of 180 g/m^2 in Table 4.6. In double-layer panel BCS-D-V*#1, which depicts the largest ultimate shear capacity, the interface failure occurs at the centre of the panel.

Table 4.9 Three-point (shear) test results.

Sample	V_{ult} (kN)	$\epsilon_{tu}^{exp}/\epsilon_{tu}$	$\tau_{interface}$ (MPa) Eq. 4.9	$\tau^{ult}/\tau_{CLT}^{ult}$	γ_{ult} (Rosette) (µmm/mm)	Failure mode	Location of failure
BCS-S-V#1	13.7	0.33	1.15	1.10	1,230	Shear interface	
BCS-S-V#2	12.3	0.18	1.07	0.98	374	Shear interface	
BCS-S-V*#1	9.3	0.20	0.75	0.66	1,830	Interface due to mold attack	
BCS-S-V*#2	6.1	0.10	0.50	0.43	500	Interface due to mold attack	
BCS-D-V*#1	15.1	0.55	1.54	0.89	2,980	Shear interface	
BCS-D-V*#2	13.4	0.41	1.35	0.79	1,440	Shear interface	
PCS-S-V#1-1	38.3	-	0.81	0.85	-	Skin shear failure	
PCS-S-V#1-2	24.1	0.37	0.53	0.53	1,000	Skin failure	
PCS-S-V#2-1	19.5	0.33	0.45	0.44	2,650	Indentation/ bond failure	
PCS-S-V#2-2	29.4	0.54	0.67	0.67	1,060	Indentation/ bond failure	
PCS-S-V#3-1	15.1	0.29	0.35	0.34	351	Indentation/ bond failure	
PCS-S-V#3-2	25.3	0.43	0.57	0.58	665	Indentation/ bond failure	
PCS-D-V#1	39.7	1.29	1.30	0.57	1,690	Plywood tensile failure	
PCS-D-V#2	26.4	0.78	0.84	0.38	1,210	Indentation/ bond failure	
CL3/75-V#1	49.8	0.31	N.A	-	9,847	N.A	
CL3/75-V#2	62.0	0.46	N.A	1.0	34,837	Rolling shear failure	

110

As shown in Figure 4.11 (b), the single-layer PCS panels depict ductile response and considerable post-ultimate load bearing capacity, whereas the double-layer peeler core panels show a sudden drop at the ultimate shear capacity. Compared to the bamboo core panels, the peeler core panels have relatively more consistent stiffness. Interface shear stresses in the PCS panels represented in Table 4.9, are well below the shear bond capacity (0.99 MPa). Comparison between Figure 4.12 (a) and (b) shows that at similar loads, the tensile strains in the skin of BCS and PCS panels are not much different. However, the shear strains in the peeler cores are much lower than those of the bamboo cores (see Figure 4.13 (a) and (b)). Most favourable shear response is observed in the double-layer PCS-D-V#1 sample, where the panel fails in the tensile rupture of the plywood skin (Figure 4.14 (b)). Other PCS panels have lower shear capacities which correspond to initiation of an indentation failure localised at the interface gap between the peeler cores, followed by a bond failure at the core-skin interface (see Figure 4.14 (b)). This type of failure is observed both in single and double-layer PCS panels.

4.4.5 Comparison between sandwich panels and CLT

A comparison has been made between the bending and shear responses of the manufactured sandwich panels and commercial CLT panels, CL3/75 *(XLam 2016)*. Total of four CLT panels, two in four-point bending and two in three-point shear, were tested similar to the test procedures described previously.

The load versus mid-span displacement of CL3/75-F#1 and CL3/75-F#2 under four-point bending test is shown in Figure 4.8 (a). Both panels exhibited similar initial elastic stiffness, while the ultimate load (P_{ult}) of CL3/75-F #1 panel exceeded that of the CL3/75-F #2 panel by 11.21%. In CL3/75-F#1 panel, a slight drop in the load was observed at P=32 kN, and was due to initiation of a crack at an inclined angle in the middle layer (rolling shear) and adjacent to a knot in the bottom layer. As the load increased, the crack propagated within the board interface surface and resulted in a catastrophic failure outside the pure bending zone, as shown in Figure 4.10 (d). The failure in CL3/75-F#2 panel initiated as a vertical crack in the middle layer and propagated through the board interface surface followed by tensile rupture of the bottom layer. Differences in the failure modes of the tested CLT panels in bending is evident in the curvature response of Figure 4.8 (b). The ultimate curvature of the CL3/75-F#2 panel was 0.98×10^{-4}

mm^{-1} and was 38% higher than the ultimate curvature of CL3/75-F#1. As can be seen from Figure 4.9 (k), plastic behaviour is observed in the compression face of CL3/75-F#2 at M=10.32 kN.m.

Bending rigidities of the CLT panels are represented in Table 4.8. There is some difference in EIs calculated from strain gauges and those calculated from LVDTs (deflections). This is probably because of the differences in the mechanical properties of the boards used to manufacture the CLT panel. Adopting the strain gauge readings, the average EI from SGs in CL3/75-F#1 is 12% higher than CL3/75-F#2 panel. The minimum shear to flexure contribution (w_2/w_1) of the CLT panels is 0.43, and is greater than all of the sandwich panels.

Figure 4.11 (c) shows the shear force versus average mid-span displacement response of the CLT panels in three-point shear tests. CL3/75-V#1 panel with a width of 450 mm was initially tested, but did not fail before P=100 kN (capacity of the Instron machine). Thus, CL3/75-V#2 was trimmed to 300 mm wide. The CL3/75-V #2 panel failed in rolling shear as shown in Figure 4.14 (c). Two shear cracks initiated in the cross layer at angles of 45°, and one propagated to the glue line between middle and bottom layers. The recorded ultimate tensile strain and core shearing strain of both CLT panels are shown in Figure 4.12 (c) and Figure 4.13 (c). For sake of comparison shear force (V) of CL3/75-V#2 is multiplied by the width ratio (450/300). CL3/75-V#2 shows a plateau at ultimate shear force, which is related to the initiation and propagation of the rolling shear crack (Figure 4.14 (c)). The recorded tensile strain in CL3/75-V#2 panel is 3,442 micro-strain and it is only half the capacity of the CLT external laminates (7,412 micro-strain). Using Eq. 4.12, the maximum shear stress (in the neutral-axis) at the ultimate shear load of CL3/75-V#2 is equal to 2.48 MPa, and is greater than the rolling shear strength of CLT (between 1 to 2 MPa) (Sikora, McPolin & Harte 2016). The maximum shear stresses (in the neutral-axis) at the ultimate shear capacity of all panels are normalised to that of CL3/75-V#2 (2.48 MPa), and are represented in Table 4.9. It can be seen that the cores of almost all sandwich panels are less stressed compared to the CLT panel. Comparison between the shear stress ratios of single-layer and double-layer bamboo and peeler cores in Table 4.9, shows that at similar shear capacities, core of the double-layer panel is less stressed. This indicates that less number of bamboo or peeler core rings could have been used in the double-layer panels.

Test results of all panels are summarised in Figure 4.10. Ultimate shear and bending capacity and stiffness correspond to the average values for each panel type, and are normalised to the corresponding average values of the CLT panel. It should be noted that in flexural design, stiffness is more important than the ultimate capacity (Karacabeyli & Gagnon 2019). Amongst all sandwich panels, the best stiffness-to-weight ratio belongs to PCS-TH. At almost similar weight, the stiffness-to-weight ratio of PCS-TH panel is 0.77 times the CLT. The lightest panels are single-layer bamboo core panels (BCS-S), which weigh slightly over half of the CLT, and have ultimate moment capacity about one-third of the CLT. The normalised stiffness-to-weight ratio of the BCS-S panels is 72% of the CLT. No particular benefit is observed in the results of the double-layer bamboo core panels compared to the single-layer ones. Single and double-layer peeler core panels depict better shear performances, however, no significant improvements are seen in the bending performance of the peeler core panels with thin skins (PCS-S and PCS-D), compared to other sandwich panels.

Table 4.10 Comparison between the average test results of the panels.

Panel	w (Kg/m^2)	w/w$_{CLT}$	M$_{ult}$/M$_{CLT}$	EI/EI$_{CLT}$	V$_{ult}$/V$_{CLT}$	(EI/EI$_{CLT}$)/(w/w$_{CLT}$)
CL3/75	35.56	1.0	1.0	1.0	1.0	1.0
BCS-S	19.13	0.54	0.34	0.39	0.21	0.72
BCS-D	20.14	0.57	0.40	0.32	0.23	0.57
PCS-S	35.38	1.00	0.49	0.56	0.41	0.57
PCS-D	36.33	1.02	0.40	0.35	0.53	0.34
PCS-TH	33.29	0.94	0.79	0.72	-	0.77

4.5   Conclusions and recommendations

Sandwich panels were manufactured from plywood skins and bamboo/peeler core rings. Experimental tests were conducted to evaluate: (1) the interface core/skin strength, (2) bending strength and stiffness, and (3) shear strength. Results were compared to test results of commercial CLT panels of almost similar depth.

Shear bond tests showed that increasing the glue spreading rate does not enhance the interface strength significantly. However, using larger adhesive spread rates showed more consistent shear bond results. In the three-point shear

tests, the dominant shear failure modes of the BCS and PCS panels were shear interface and indentation/bond failure, respectively. The double-layer peeler core (PCS-D) panels outperformed all other sandwich panels, and reached 64% of the shear capacity of the CLT panel.

Almost all bamboo core (BCS) and peeler core (PCS) panels failed due to the tensile skin failure observed within the pure bending zone, under four-point bending test. No major improvement in the bending capacity of the double-layer sandwich panels were observed in comparison with the single-layer panels. The peeler core panel with thick faces (PCS-TH) depicted ultimate moment capacity as high as 79% of the CLT panel. Moreover, the PCS-TH panel showed curvature at ultimate moments larger than the CLT panels. With a weight 6% lower than the CLT panel, the PCS-TH panel achieved bending stiffness (EI) as large as 72% of the CLT. The normalised weight-to-stiffness ratio of the BCS-S panels showed to be as high as 72% of the CLT.

A better manufacturing strategy and optimum face-thickness and core layout may enable production of BCS and PCS panels that can outperform the CLT panels in bending and shear strength and stiffness.

5 Load bearing sandwich timber walls with plywood faces and bamboo core

STATEMENT OF CONTRIBUTION TO CO-AUTHORED PUBLISHED PAPER

This chapter includes a co-authored paper. The bibliographic details of the co-authored paper, including all authors, are:

Darzi, S, Karampour, H, Gilbert, BP, Bailleres, H, & Fernando, D. Load bearing sandwich timber walls with plywood faces and bamboo core, *Structures*, (Submitted 6th February 2020, under review).

My contribution to the paper involved: literature review, analytical study, numerical modelling, run analyses, discussion of the results and writing and editing.

(Signed) _____ Date: 16/03/2020

PhD Candidate: **Siavash Darzi**

(Countersigned) _____ Date: 16/03/2020

Principle Supervisor/ Corresponding author of paper: **Dr. Hassan Karampour**

(Countersigned) _____ Date: 16/03/2020

Associate Supervisor: **Associate Professor Benoit P. Gilbert**

(Countersigned) _____ Date 16/03/2020

External Supervisor: **Dr. Henri Bailleres**

Load bearing sandwich timber walls with plywood faces and bamboo core

Abstract

Novel light timber sandwich panels (referred to as BCS panels herein) are manufactured by gluing plywood faces to bamboo core rings. The panels are tested in compression and in bonding shear (between bamboo and plywood). A finite element model is developed and validated against the experimental results, and is used to capture the responses of the BCS panels under axial and combined axial and bending actions. A probabilistic approach is adopted in the finite element analysis (FEA) to investigate the effect of plywood material properties. Moreover, effect of different core configurations, face thickness, core layers and initial imperfection shapes on the axial compressive capacity of the panels are investigated. Where possible, results are compared against theoretical predictions. Current test results show that under axial compressive action, the ultimate capacity to weight ratio of the BCS panels are up to 27.3% higher than a conventional CLT panel of the same dimension. At large slenderness ratios, the proposed BCS panels have ultimate axial capacities close to the conventional CLT panels. Under combined axial and bending loading, the BCS panels outperform a CLT panel of similar size.

5.1 Introduction

Sandwich structures with high stiffness-to-weight and strength-to-weight ratios, are widely used in automotive, aerospace, marine and industrial applications. Typically, a sandwich panel is made up of two outer skins (also known as faces) which are connected using a light-weight core. The skins are normally made of steel (Sohel & Liew 2011; Zhang et al. 2018), fibre reinforced composites (Manalo, AC et al. 2010) and sometimes reinforced concrete (Shams et al. 2015). Common material used in the core are balsa wood (Dawood, Ballew & Seiter 2011), polymeric and metallic foams (Mamalis et al. 2008; Reyes 2008), fibre reinforced polymer (FRP) (Fam & Sharaf 2010) and metallic alloys (Crupi, Epasto & Guglielmino 2012).

The majority of studies on sandwich structures are focused on flexural behaviour under out-of-plane loading including static, shock, impact and blast resistance (Mastali, Valente & Barros 2017; Wang, Zhihua et al. 2011). With the advancement of fabrication technology, manufacturing of sandwich panels with various core configurations are made possible. Hence, recent studies are focused on axial compressive and bending responses of sandwich panels with different core materials and formations. Budiansky (1999) and Wicks and Hutchinson (2001) performed theoretical investigations of compressive response of metallic sandwich panels with metal foam and lattice cores, respectively. The results demonstrated that hat-stiffened panels are a better alternative compared to metal foam core sandwich columns in terms of axial performance and stiffness-to-weight. Cote et al. (2007) and Biagi and Bart-Smith (2012) showed that pyramidal truss core and extruded aluminium corrugated core sandwich columns outperform the conventional hat-stiffened panels in compression. Mozafari et al. (2015) and Mozafari et al. (2016) studied the in-plane compressive responses of foam-filled aluminium honeycombs and observed much stronger load bearing capacity than single honeycombs. Paik, Thayamballi and Kim (1999) investigated the strength characteristics of aluminium honeycomb sandwich panels with different cell thicknesses, core heights and panel aspect ratio through axial compression tests. More recently, Sun et al. (2016) experimentally and numerically investigated the compressive strength, stiffness, energy absorption and collapse modes of honeycomb sandwich panels, and examined the effects

of core heights, honeycomb-wall thickness and face-sheet thickness on the critical buckling loads of the sandwich structures.

Sandwich panels are used in construction industry in flooring, roofing, and wall applications (Karlsson & TomasÅström 1997). With the recent global trend towards mid-rise to high-rise timber buildings, more attention is given to light-weight and sustainable wood products. Existing mass timber buildings commonly use cross-laminated-timber (CLT) floor diaphragms and load-bearing walls (Reynolds, Casagrande & Tomasi 2016). The current authors previously proposed the Bamboo Core Sandwich (BCS) panel, and examined its theoretical flexural performance compared to CLT (Darzi et al. 2018a, 2018b). Single layer (BCS-S) and double-layer (BCS-D) panels are depicted in Figure 5.1 and are comprised of vertically aligned hollow bamboo rings (core) and commercial plywood laminates (skins). The hollow bamboo rings are bonded to the face skins using commercial adhesive. Bamboo is used in the core of the proposed sandwich panel due to: (1) its being a recyclable and sustainable natural material, (2) its rapid harvest (3-4 years from the time of planting), and (3) its outstanding stiffness-to-weight ratio. The current paper aims to complement the previous theoretical flexural study (Darzi et al. 2018b), and investigates the capacity and failure modes of the BCS panels under axial compressive load as well as combined bending and axial compression actions. This is done through experimental, numerical and simplified analytical approaches. The paper is concluded with a comparison between the axial compressive and combined compression and bending performances of the proposed BCS and conventional CLT panels.

5.2 Materials and manufacturing

5.2.1 Samples

In order to investigate the feasibility of the concept, two types of BCS panels: (a) single-layer (BCS-S) shown in Figure 5.1 (a), and (b) double-layer (BCS-D) shown in Figure 5.1 (b) were manufactured and tested. As shown in Figure 5.1 (a), the BCS-S panel is comprised of a single layer bamboo core sandwiched between two 7.2 mm structural plywood skins. The BCS-D panel (Figure 5.1 (b)) has two layers of bamboo rings sandwiched between 7.2 mm plywood skins, with bamboo rings separated by a 3 mm plywood laminate. The structural plywood laminates were commercially available and were manufactured to Australia/New

Zealand Standard (*AS/NZS 2269.0:2012 Plywood-Structural Part 0: Specifications* 2012) from softwood veneers of plantation pine (*Pinus radiata*). The selected plywood IDs were 7-24-3 and 4-14-3. The numbering sequence in the ID gives from left to right: the nominal plywood thickness, the face veneer thickness multiplied by 10, and the number of plies in the assembly. For example, plywood ID 7-24-3, describes a 7 mm thick plywood, with 2.4 mm thick veneers on the top and bottom, and a total number of 3 veneer layers.
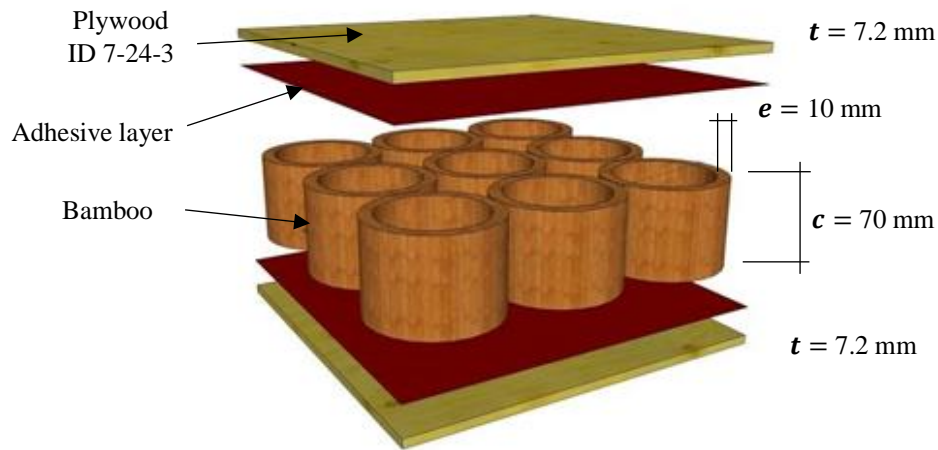
(a)
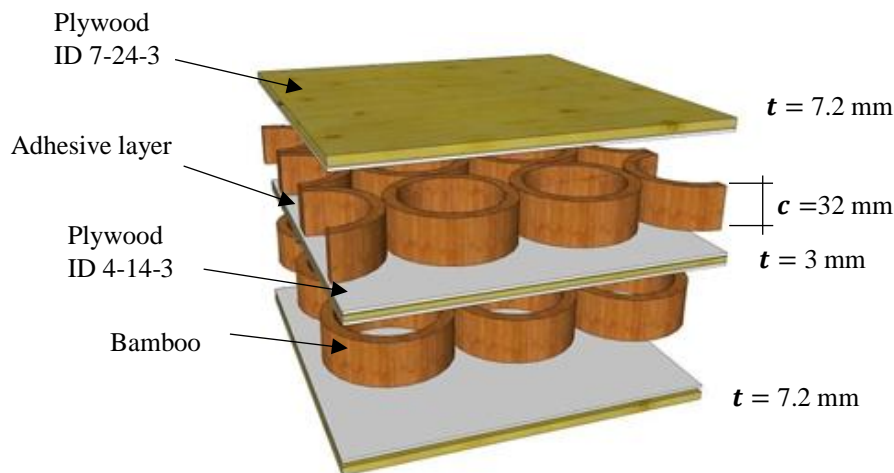
(b)

Figure 5.1 Schematic illustrations of: (a) the single-layer panel (BCS-S), and (b) double-layer panel (BCS-D).

5.2.2 Manufacturing

To fabricate the BCS panels, mature *Moso* bamboo (*Phyllostachys pubescens*) culms with an average diameter of 100 ± 20 mm and a wall thickness (*e*) of 10 mm were selected. The bamboo culms were initially dried to a nominal 12% MC (moisture content), and were then cut to rings with nominal heights of 70 mm for the BCS-S, and 32 mm for the BCS-D panels, respectively. Then, a timber frame with dimensions slightly smaller than the aspired panel dimensions was made. The timber frame was filled with the bamboo cores, adjusting the arrangement such that to keep the bamboo rings packed as closely as possible. A liquid single-component polyurethane adhesive (*PURBOND HB S709*) was applied to one side of the plywood skin, using the recommended spread rate (180 *g/m²*). Prior to the application of the adhesive, the plywood surface was moistened with a light water spray. Then, the timber frame packed with bamboo rings was placed on top of the plywood skin and was cold pressed at a pressure of 0.8 MPa, for a period of 120 minutes. Prior to the installation of the second side of the BCS panel, the first side was passed through the belt sander to even out the bamboo rings. The manufactured BCS panel was then left in the open air for 24 hours to reach the balanced moisture content.

Two panels (one BCS-S and one BCS-D panel) with length of (*a*=2,070 mm), width of (*b*=570 mm) and nominal depths of (*h*= 85 mm) were manufactured for the compression study. To investigate the shear bond strength (the bond between the bamboo rings and the plywood faces), 12 BCS-S panels with length of (300 mm), width of (300 mm) and nominal depths of (85 mm) were manufactured.

5.2.3 Material properties (Probabilistic approach)

Due to the large variation in the mechanical properties of the *Pinus radiata* used in the commercial plywood, a probabilistic approach was used to estimate the modulus of elasticity (MOE) in the parallel-to-grain direction (E_L) and the compressive strength in the parallel-to-grain direction (σ_{cu}) of the *Pinus radiata* veneers (Dahl 2009). The cumulative log-normal distribution function (CDF) is

$$CDF = \frac{1}{2} + \frac{1}{2} erf\left[\frac{\ln x - \mu}{\sqrt{2}\sigma}\right]$$

(5.1)

where the two parameters μ and σ are the mean and standard deviation of the set of data values, respectively. By adopting recommended mean and standard

deviation for E_L and σ_{cu} (*Wood Handbook: Wood as an Engineering Material* 2010a), the elastic material properties of *Pinus radiata* are represented in Table 5.1 for the 30th, 50th and 70th percentiles. The corresponding CDF curves (Eq. 5.1) are plotted in Figure 5.2. The material properties of bamboo cores were taken as the average values of *Moso* bamboo reported in (Chung, Yu & Chan 2002), and are represented in Table 5.1.

Table 5.1 Material properties of bamboo and pine (*Pinus radiata*) used in the BCS panels.

Material	E_L (MPa)	E_T (MPa)	E_R (MPa)	G_{LT} (MPa)	G_{TR} (MPa)	G_{LR} (MPa)	v_{LT}	v_{TR}	v_{LR}
Moso Bamboo	10,500	1,260	1,260	630	630	630	0.3	0.3	0.3
Species pine (*radiata*) – 30th	9,993	450	740	530	100	550	0.4	0.3	0.4
Species Pine (*radiata*) – 50th	11,220	505	830	595	112	617	0.4	0.3	0.4
Species Pine (*radiata*) – 70th	12,590	566	932	667	126	692	0.4	0.3	0.4
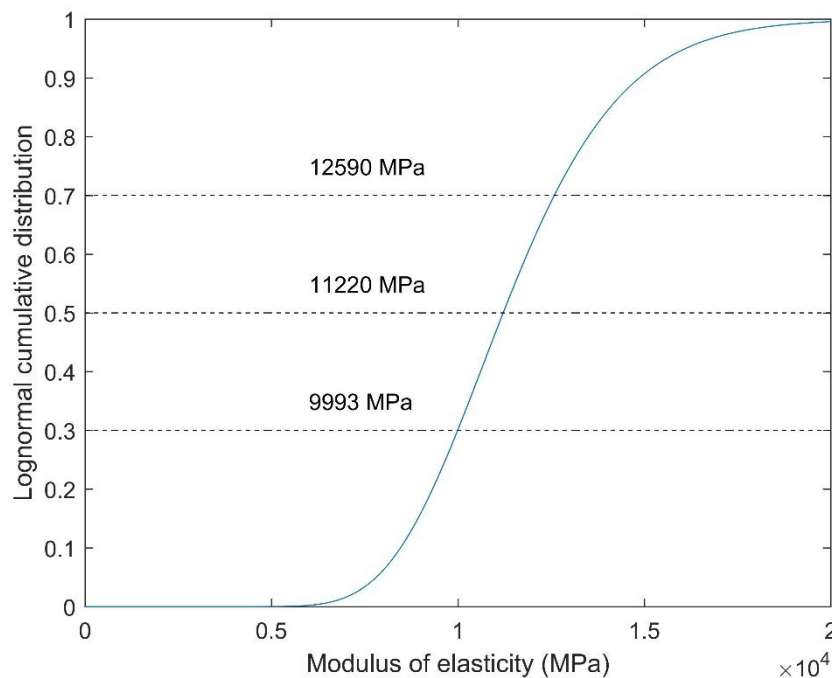
(a)
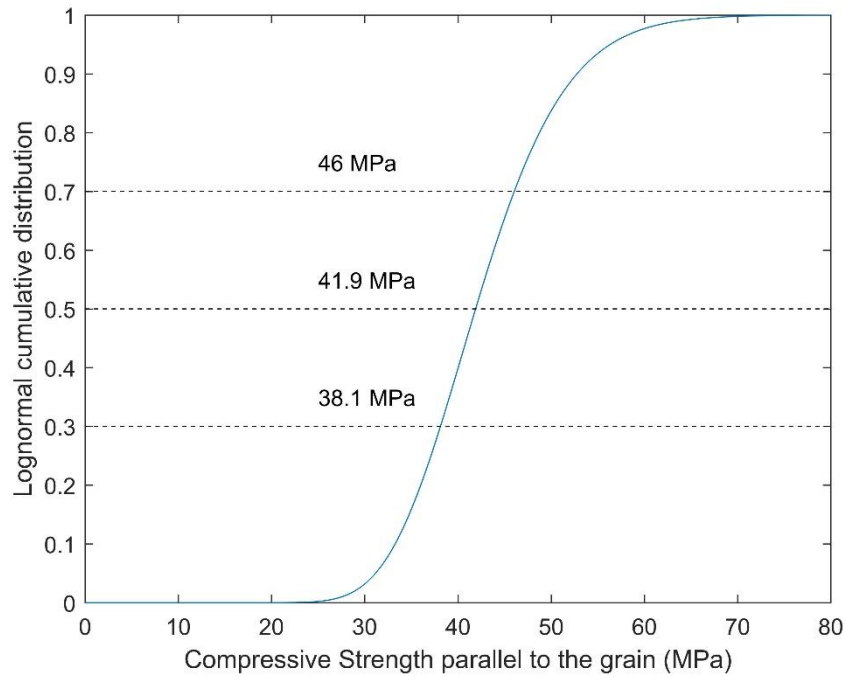
(b)

Figure 5.2 Cumulative distribution function (CDF) of: (a) MOE parallel-to-grain (E_L), and (b) compressive strength parallel-to-grain (σ_{cu}) for *radiata* veneers of plywood.

5.3   Experiments

5.3.1   Shear bond tests

Adhesive spread rate study was conducted to evaluate the shear strength between bamboo and *Pinus radiata* plywood. To accomplish this, adhesive shear block testing was performed in adhesive spread rates of 180, 360 and 540 *g/m²* for the BCS-S panel. For each adhesive spread rate, four BCS-S panels with dimensions of 300 mm × 300 mm and depth of 85 mm were manufactured (Figure 5.3). The panel dimensions were selected such that 3 intact bamboo rings could fit in the panel in each direction. Two timber planks were glued to the top and bottom surfaces of the panel. Using a 100 kN Instron machine, a lateral displacement was imposed on the top plank, while the bottom plank was fixed in the machine's jaw. The shear bond strength was calculated as the failure load divided by the total wall-thickness area of the 9 bamboo rings.

Plywood

Adhesive

1, 2 and 3 × standard spread

100 ± 20 mm

Bamboo

70 mm

300 mm

300 mm

Force

Fixed support
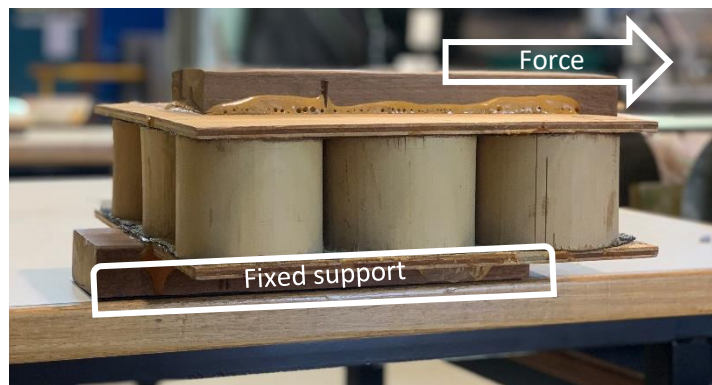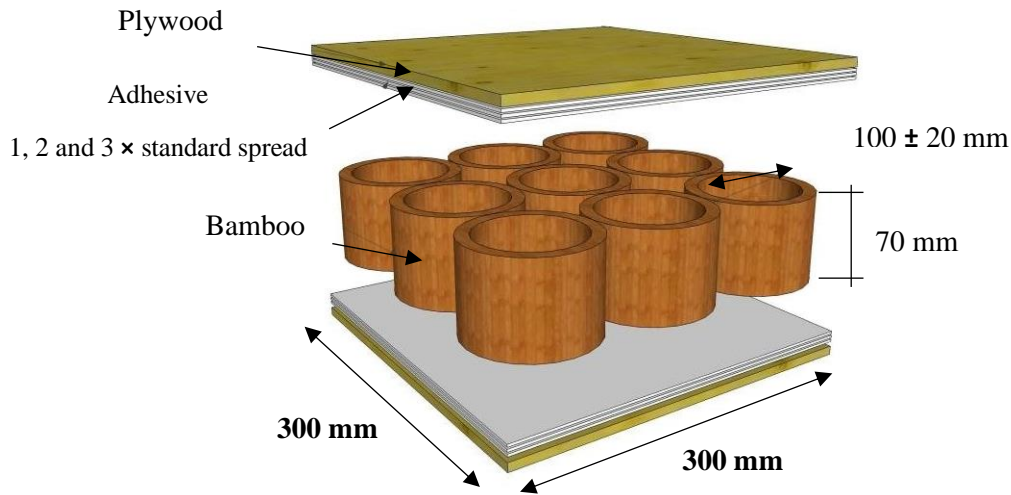
Figure 5.3 Shear bond strength tests (BCS-S panels).

5.3.2 Axial compressive tests

BCS-S and BCS-D panels (2,070 mm height × 570 mm width × 85 mm depth) were tested using a 500 kN MTS universal testing machine. The test set-up and the boundary conditions are shown in Figure 5.4. Solid steel shafts (rollers) were inserted between the BCS panel and the hydraulic jack on top and the base plate at the bottom. The shafts restrained the out of plane translation (in y and z directions shown in Figure 5.4), and thus allowed buckling of the panel about its minor axis (y-axis). The top platen was lowered at a constant rate of 1 mm/min, and the corresponding compressive load was recorded. A 3D Digital Image Correlation (DIC) system from Correlated Solutions Inc. (Correlated SOLUTIONS 2019) was used to measure the displacement and strain contours in the in-plane and out-of-plane directions. To do so, the entire panel surface on one side was brushed using a specific roller to provide the desired speckled pattern. A 2 camera/tripod assembly was located at a distance about 9 meters away from the panel, and was used to capture images of the speckle pattern during the axial

123

loading. LED lights were placed in the vicinity of the panel to provide the required contrast. The DIC was synchronised with the MTS machine to provide the displacement and strain fields at any given load.
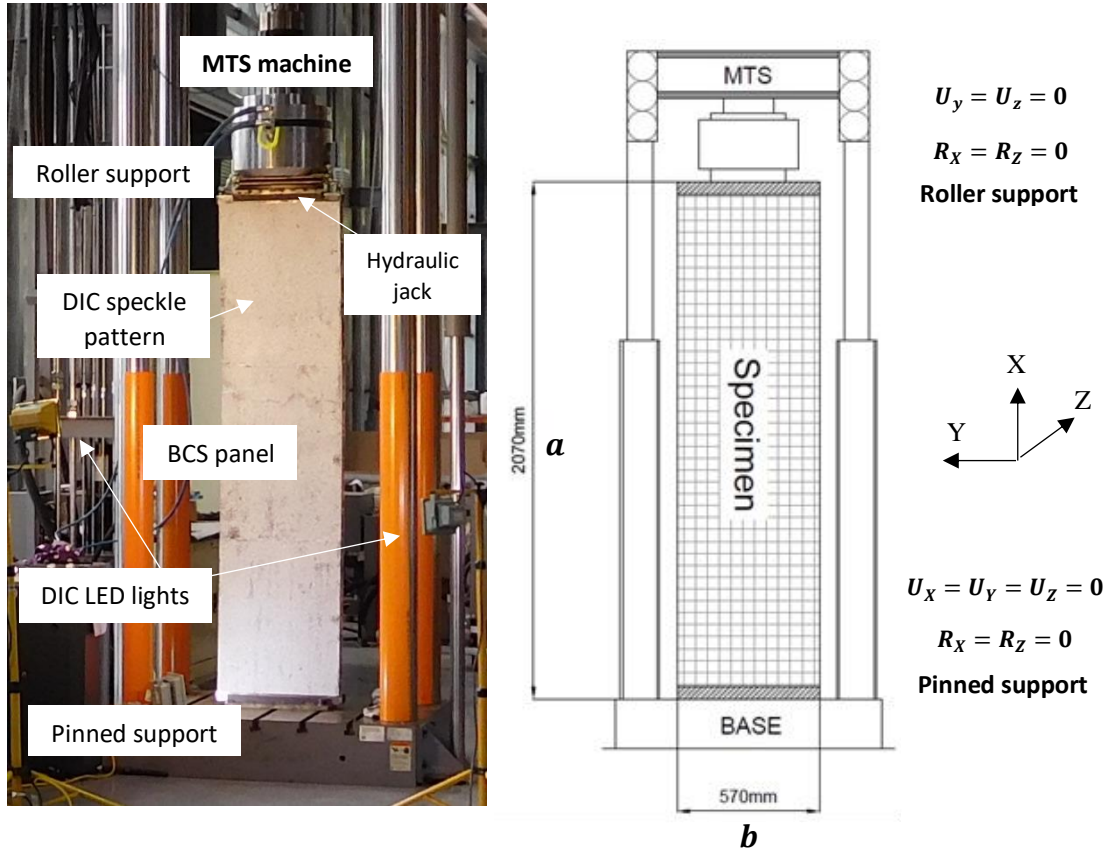
Figure 5.4 Axial compression test setup showing the BCS panel, test machine and the adopted boundary conditions.

5.4 Analytical and numerical models

5.4.1 Axial capacity of the BCS

The Euler's expression of the critical elastic buckling load (P_E) for the simply supported BCS panel with length of a is given by

$$P_E^{BCS} = \frac{\pi^2 (EI)_{eq.}}{a_e^2} \tag{5.2}$$

where $(EI)_{eq}$ is the equivalent stiffness of the composite cross-section. a_e is the effective length of the panel, and is equal to a for the existing simply supported boundary conditions. The equivalent stiffness is calculated based on the properties of the transformed cross-section of the panel. Denoting the ratio

E_{skin} / E_{core} of the two moduli of elasticity by N, the transformed section is developed by replacing the skin material (plywood) with the core material (bamboo). The equivalent stiffness for the BCS panel becomes

$$(EI)_{eq.} = E_{core}\left[\frac{b_c c^3}{12} + I_{Skin-trans.}\right] \tag{5.3}$$

where E_c is the modulus of elasticity of bamboo in the radial direction and c is the core height (see Figure 5.1). In a BCS panel, at any given cross-section cut along the span, the width of the bamboo core (b_c) is almost equal to $2en_b$, where e is the nominal bamboo wall-thickness and n_b is the number of bamboo rings across the width of the panel. The moment of inertia of the transformed skin ($I_{skin-trans.}$) can be expressed as

$$I_{skin-trans.} = 2\left(\frac{1}{12}bNt^3 + (bNt)(\frac{c}{2}+\frac{t}{2})^2\right), \quad b_{trans.} = bN, \quad N = \frac{E_{skin}}{E_{core}} \tag{5.4}$$

where E_{skin} is the modulus of elasticity of the plywood skin in the parallel-to-grain direction. To derive the mechanical properties of plywood skins from orthotropic properties of each veneer, a classical laminate theory tool (*OSULaminates* developed by *Oregon State University*) was utilised (Nairn 2015). Material properties of the plywood skins obtained from *OSULaminates*, comprised of *Pinus radiata* veneers with properties listed in Table 5.1 for the corresponding percentiles, are presented in Table 5.2.

In derivation of the elastic buckling capacity of the BCS panel (P_{EV}^{BCS}), the shear deformation needs to be considered

$$P_{EV}^{BCS} = \frac{P_E^{BCS}}{1 + \dfrac{kP_E^{BCS}}{(AG)_{eq}}} \tag{5.5}$$

The current authors derived analytical expressions for the equivalent shear stiffness ($AG)_{eq.}$ and the Timoshenko shear coefficient (κ) of a BCS panel (Darzi et al. 2018b). For the sake of brevity, the expressions are shown here, and the avid reader is referred to (Darzi et al. 2018b) for the complete derivation of the equations.

$$(AG)_{eq} = (b_c d)G_c + (bt_{mid-ply})G_{mid-ply}$$

(5.6)

$$\kappa = \frac{c}{(EI)_{eq}} \left(E_{skin} \frac{btd}{2} + \frac{E_{core}(b_c)}{4} \left(\frac{c^2}{4} \right) \right)$$

The second term in the RHS of $(AG)_{eq}$ in Eq. 5.6, corresponds to the BCS-D panel, where $t_{mid\text{-}ply}$ and $G_{mid\text{-}ply}$ are the thickness and shear modulus of the middle plywood in the BCS-D panel (see Figure 5.1 (b)).

The compression capacity of a stub BCS panel P_r^{BCS} is

$$P_r^{BCS} = \sigma_Y^{plywood}.A_{plywood} + \sigma_Y^{bamboo}.A_{bamboo}$$

(5.7)

where $A_{plywood}$ is the sum of all cross-sectional areas of layers running parallel to the load, and σ_Y is the yield strength parallel to the fibre direction.

Table 5.2 The material properties of the BCS panel plywood skins calculated from the classical laminate theory (Nairn 2015)

Plywood ID	Pine (*Radiata*) veneer grade	E_L	E_T	G_{LT}	v_{LT}	Layer's thickness (mm) and lay-up
7-24-3	30th	6,862	3,657	530	0.03	2.4 / 2.4 / 2.4
7-24-3	50th	7,704	4,106	595	0.03	2.4 / 2.4 / 2.4
7-24-3	70th	8,645	4,608	667	0.05	2.4 / 2.4 / 2.4

5.4.2   Axial capacity of the CLT

The elastic buckling capacity of a CLT panel (*CSA O86:2019, Engineering design in wood* 2019), considering the shear deformation is

$$P_{EV}^{CLT} = \frac{P_E^{CLT}}{1 + \frac{kP_E^{CLT}}{(AG)_{eff}}}$$

(8)

where P_E is the Euler buckling load (Eq. 5.2), and $E=E_{05}$ and $I=I_{eff}$ are determined based on the properties of the layers oriented parallel to the axial load direction, only. E_{05} is the modulus of elasticity for design of compression members, and is equal to $0.82E$ for machine stress-rated (MSR) lumbers(*CSA O86:2019, Engineering design in wood* 2019). For rectangular cross-sections the shear

126

factor *k* of 1.2 is adopted (*CSA O86:2019, Engineering design in wood* 2019). The effective bending stiffness $(EI)_{eff}$ (similar to $(EI)_{eq}$ in Eq. 5.2) and the shear stiffness $(AG)_{eff}$ of a CLT panel with alternating orthogonal layers can be determined via the shear analogy method (Blass & Fellmoser 2004; Darzi et al. 2018b).

$$(EI)_{eff} = \sum_{i=1}^{n} E_i.b_i.\frac{h_i^3}{12} + \sum_{i=1}^{n} E_i.A_i.z_i^2$$

(5.9)

$$(AG)_{eff} = \frac{d_a^2}{\left[\left(\dfrac{h_1}{2.G_1.b}\right) + \left(\sum_{i=2}^{n-1} \dfrac{h_i}{G_i.b_i}\right) + \left(\dfrac{h_n}{2.G_n.b}\right)\right]}$$

where E_i is the modulus of elasticity of layer *i*, and b_i, h_i and A_i are the width, thickness and cross-sectional area of each individual layer, respectively. The distance between the centroid of each layer and the centroid of the total cross-section of the CLT panel is z_i. Subscripts 1 and *n* correspond to the top and bottom layers, respectively. As recommended in (*CSA O86:2019, Engineering design in wood* 2019), in the transverse layers, the modulus of elasticity E_i is multiplied by 1/30. The shear modulus of the laminations (G_i), normally taken as E_i/16 for the longitudinal layers. To account for the rolling shear effect, the shear modulus in the transverse direction is divided by 10. Based on the recommendations of the Canadian Standards Association (CSA) (*CSA O86:2019, Engineering design in wood* 2019), the unfactored compressive design capacity of the CLT panel P_r^{CLT} is

$$P_r^{CLT} = f_c A_{eff} K_{Zc} K_C$$

(5.10)

where f_c is the specified strength in compression parallel to the grain of the laminations oriented parallel to the axial load. A_{eff} is the effective cross-sectional area of the panel accounting only for the layers with laminations oriented parallel to the axial load. K_{zc} and K_c are the size and slenderness factors, respectively (*CSA O86:2019, Engineering design in wood* 2019)

$$K_{Zc} = 6.3\left(\sqrt{12}r_{eff}a\right)^{-0.13} \leq 1.3 \quad , \quad K_C = \left[1.0 + \frac{f_c K_{Zc} C_C^3}{35E_{05}}\right]$$

(5.11)

where r_{eff} and C_c are the effective radius of gyration and the slenderness ratio of a simply supported CLT panel with length a, respectively.

$$r_{eff} = \sqrt{\frac{I_{eff}}{A_{eff}}} \quad , \quad C_C = \frac{a_e}{\sqrt{12}r_{eff}} \tag{5.12}$$

5.4.3 Capacity of the CLT panel under combined bending and axial compression actions

CLT panels subject to combined out-of-plane bending and compressive axial load should satisfy the following interaction equation (*CSA O86:2019, Engineering design in wood* 2019)

$$\frac{P}{P_r^{CLT}} + \frac{M}{M_r^{CLT}} \left[\frac{1}{1 - \dfrac{P}{P_{EV}^{CLT}}} \right] \leq 1 \tag{5.13}$$

where P and M are the applied compressive axial load and applied bending moment, respectively. M_r^{CLT} is the unfactored out-of-plane bending moment design resistance of the CLT panel

$$M_r^{CLT} = f_b S_{eff} K_{rb} \quad , \quad S_{eff} = \frac{2(EI)_{eff}}{Eh} \tag{5.14}$$

where f_b is the specified bending strength of laminations in the longitudinal layers. S_{eff} is the effective out-of-plane section modulus of CLT panel. E and h are the modulus of elasticity of laminations in the longitudinal layers and thickness of the panel, respectively. The adjustment factor for bending moment resistance of CLT panels, K_{rb} is equal to 0.85 (*CSA O86:2019, Engineering design in wood* 2019).

5.4.4 Finite element analysis (FEA)

Finite element analysis (FEA) was conducted using ANSYS 19.0 (ANSYS 19.0 Release) to calculate the compressive capacities of the BCS panels with different lengths and core configurations. In the FEA, the diameter and wall-thickness of all bamboo rings were identical (Figure 5.1). Moreover, to fit in intact bamboo rings, the width of the panel was taken as 600 mm (was 570 mm in the experiment). The plywood veneers and the bamboo rings were meshed using eight node solid elements SOLID186 (ANSYS 19.0 Release). The experimental

results (will be discussed later) did not show any de-bonding between bamboo rings and plywood faces in the pre-buckling (ultimate capacity) stage. Therefore, in the FEA, no-slip contact model was adopted between the core and the faces. However, in the FEA, the stresses in the contact elements at each loading were compared to the shear bond test results. Plywood veneers had one element along the veneer thickness and the bamboo core was discretised with two and seven elements along the wall-thickness (*e*) and core height (*c*), respectively.

Figure 5.5 (a) shows the FEA mesh and boundary conditions of a BCS-S panel. In order to replicate the experimental boundary conditions (Figure 5.4), thick steel discs were attached to either ends of the BSC panel in the FE model. The discs on the top and bottom were restrained about translation in *y* and *z* directions and rotation about *x* and *z* directions, to mimic simply supported bending about minor axis. The bottom disc was fixed in the *x* direction, while the top disc could freely move in the longitudinal direction.

(a) (b)
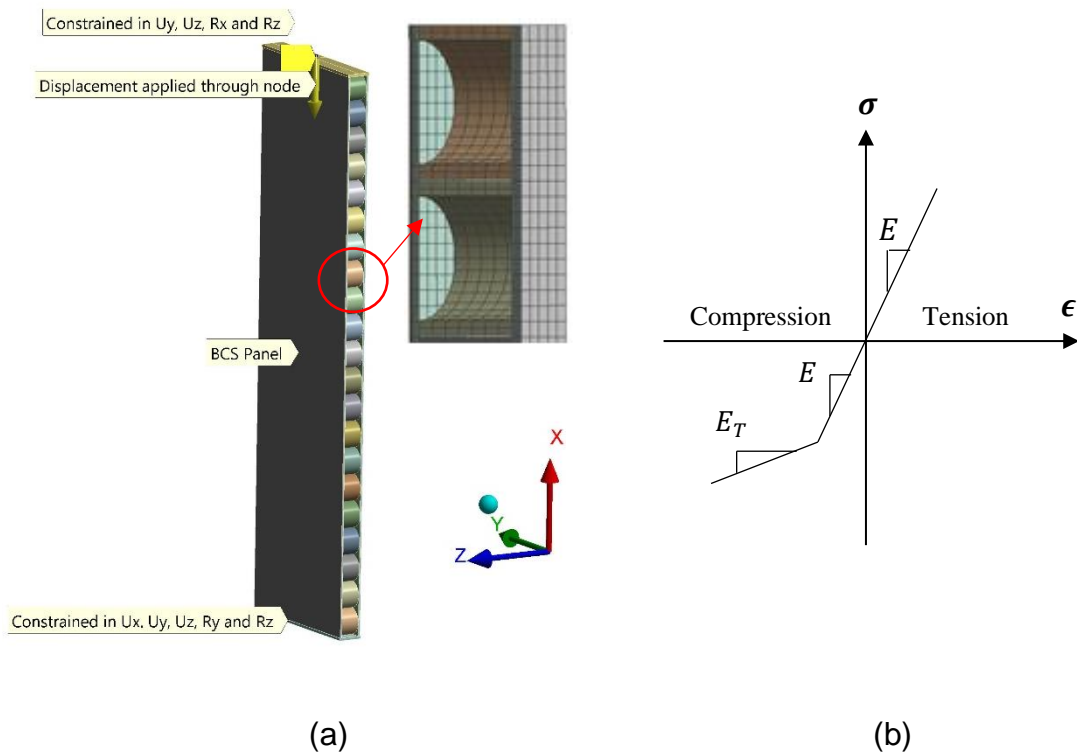
Figure 5.5 (a) The mesh, and (b) the adopted stress-strain relationship model of plywood veneers used in the FEA.

To account for the plastic behaviour of the plywood in compression, the Hill's orthotropic bilinear hardening (Hill 1998) definition was adopted in the FEA. The stress potential in the Hill criterion is expressed as

129

$$\sigma_e = \sqrt{F_{RR}\left(\sigma_x - \sigma_y\right)^2 + F_{LL}\left(\sigma_y - \sigma_z\right)^2 + F_{TT}\left(\sigma_z - \sigma_x\right)^2 + 2N_{LT}\tau_{xy}^2 + 2N_{TR}\tau_{yz}^2 + 2N_{RL}\tau_{xz}^2}$$

(5.15)

F and N are constants obtained from material tests conducted in different orientations

$$F_{ij} = \left[\frac{\left(\sigma_0\right)^2}{2}\right]\left[\frac{1}{\left(\sigma_{jj}^y\right)^2} + \frac{1}{\left(\sigma_{kk}^y\right)^2} - \frac{1}{\left(\sigma_{ii}^y\right)^2}\right] = \frac{1}{2}\left[\frac{1}{R_{jj}^2} + \frac{1}{R_{kk}^2} - \frac{1}{R_{ii}^2}\right]\begin{Bmatrix} i = L,T,R \\ j = T,R,L \\ k = R,T,L \end{Bmatrix} \qquad \text{(5.16a)}$$

$$N_{ij} = \frac{3}{2}\left[\frac{\left(\tau_0\right)^2}{\sigma_{ij}^y}\right] = \frac{3}{2}\left[\frac{1}{R_{ij}^2}\right] \quad (i \neq j = L,T,R) \qquad \text{(5.16b)}$$

and σ_{ii}^y and σ_{ij}^y correspond to the normal and shear yield stresses, where subscripts L, T and R, are associated with the longitudinal, tangential and radial directions, respectively. R_{ij} are the yield ratios which relate the yield level for stress components σ_{ij}^y, to the reference yield stress σ_0 of the material. The yield ratios are

$$R_{ij} = \begin{cases} \dfrac{\sigma_{ij}^y}{\sigma_0}, & \text{if } i = j \\[2mm] \dfrac{\sigma_{ij}^y}{\tau_0}, & \text{if } i \neq j \end{cases} \qquad \text{(5.17a)}$$

$$\tau_0 = \frac{\sigma_0}{\sqrt{3}} \qquad \text{(5.17b)}$$

and are represented in Table 5.3 for different percentiles. Tangent modulus (E_T) of 345 MPa is adopted (Alam 2004). The elastic-plastic stress-strain relationship of timber in compression used in the FEA is shown in Figure 5.5 (b). The material properties of the bamboo rings were assigned using local cylindrical coordinate systems. Since the current study investigates the buckling capacity of the wall panels (not the post-buckle response), elastic behaviour was assumed for plywood in tension.

130

The ultimate buckling capacities of the panels are sensitive to the shape of the geometric imperfections. To acquire the geometric imperfect shapes, linear Eigenvalue buckling analyses were performed and the first two buckling mode shapes (mode Ⅰ and mode Ⅱ) were developed. These buckling modes were then imposed as initial imperfections to the model, and nonlinear FEA were conducted. Normalised amplitude of the initial imperfection adopted in all models was equal to $\delta/a=2\times10^{-4}$. In the axial compressive study, firstly, the imperfection was imposed to the FEA model, and then an axial shortening displacement was applied to the top disc through a master node.

Table 5.3 The Hill yield constants for *Radiata* veneers of plywood skins in FE model of BCS panels

Material	$\sigma_{cu}^{\parallel}$ (MPa)	$\sigma_{cy}^{\parallel}$ (MPa)	R_{LL}	R_{TT}	R_{RR}	R_{LT}	R_{TR}	R_{LR}
Species pine (*Radiata*) – 30th	38.1	28.6	1	0.18	0.19	0.67	0.48	0.67
Species Pine (*Radiata*) – 50th	41.9	31.4	1	0.17	0.18	0.60	0.44	0.6
Species Pine (*Radiata*) – 70th	46.0	34.5	1	0.15	0.16	0.55	0.40	0.55

In the combined loading study, two load paths were investigated. The first load path was axial compressive force followed by bending, $p \rightarrow w$. The axial load was maintained as a fraction of the axial capacity found in the axial compressive study. Then a lateral wind pressure (w) was gradually applied to the panel in the transverse direction, until buckling was observed. In the second load path, the lateral wind pressure of w=2 kPa (typical design wind pressure in non-cyclonic regions of East coast Australia (*AS/NZS 1170.2:2011 Structural design actions Part 2: Wind actions* 2011)) was maintained while the axial shortening was induced, $w \rightarrow p$. The axial force corresponding to the initiation of the buckle was calculated.

In all of the FEA results, the capacity of the panel corresponds to the minimum load associated with one of these failure modes: (1) onset of yield in the plywood skins using the Hill's criteria (Eq. 5.15), (2) the bond stress between the plywood and the bamboo core exceeding the bond strength measured in the experiment (section 5.1), and (3) global buckling of the panels or local buckling of the skin.

5.5 Results and discussion

5.5.1 Shear bond strength

The ultimate loads at failure of the shear bond tests are represented in Table 5.4. The shear strength at the bond is found by dividing the ultimate load by the bamboo wall-thickness area. It can be seen that doubling or tripling the glue spread rate, does not translate into a significant increase in the bond strength. Hence, in the manufacturing of the panels, the recommended spread rate 180 g/m^2 was adopted. At this spread rate, the average shear strength at the bamboo-plywood contact is 0.99 MPa.

Table 5.4 Summary of adhesive shear block tests in BCS panels.

Specimen	Spread rate of adhesive (g/m^2)	Bamboo wall-thickness area (mm^2)	Failure load (kN)	Shear bond strength (MPa)
BCS 1-1		19,330	25.4	1.31
BCS 1-2	180	23,458	26.7	1.14
BCS 1-3		24,174	17.8	0.74
BCS 1-4		19,695	15.8	0.80
Avg(COV)		21,664 (11%)	21.4 (25%)	0.99 (27%)
BCS 2-1		18,715	22.4	1.20
BCS 2-2	360	23,421	27.1	1.16
BCS 2-3		21,365	26.6	1.25
BCS 2-4		17,697	19.3	1.09
Avg(COV)		20,299 (13%)	23.8 (16%)	1.17 (5%)
BCS 3-1		24,913	27.7	1.11
BCS 3-2	540	20,963	25.0	1.19
BCS 3-3		26,089	31.7	1.21
BCS 3-4		20,113	25.4	1.26
Avg(COV)		23,019 (13%)	27.4 (11%)	1.19 (5%)

5.5.2 Axial compression

5.5.2.1 Comparison between experimental, analytical and FEA results

The first two buckling mode shapes (I and II) of the BCS-S and BCS-D panels obtained from finite element Eigen buckling analyses are shown in Figure 5.6. The first modes (mode I) in either panels are the classic Euler mode shape. Mode

II of the BCS-S is the classical double-curved sinusoidal shape, whereas, in the BCS-D panel, mode II is local buckling of the plywood skin.
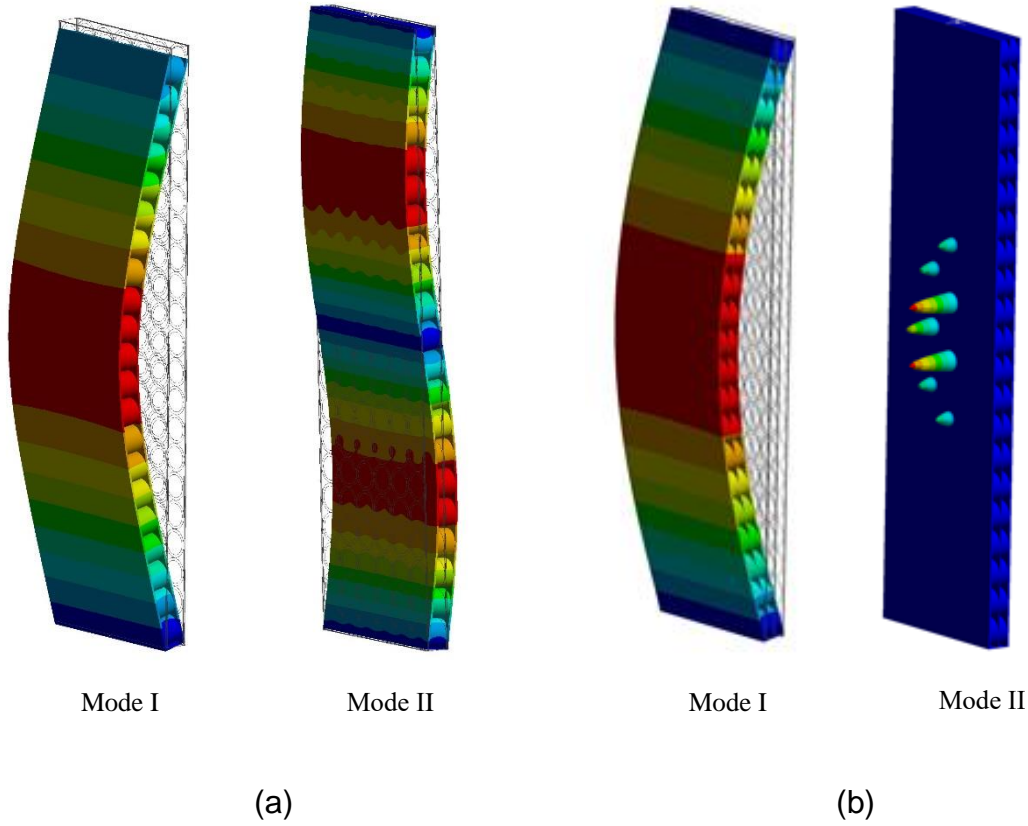
Figure 5.6 FEA results showing buckling mode shapes Ⅰ and Ⅱ in (a) the BCS-S panel, and (b) BCS-D panel.

Figure 5.7 and Figure 5.8 compare the load vs. lateral displacement and longitudinal strains at the mid-height of the BCS-S and BCS-D panels, respectively, obtained from the experimental and FEA results. The analytical axial compressive capacity of the BCS panels (P_{EV}^{BCS}) from Eq. 5.5 are also shown in the figure for comparison. The failed samples are shown in Figure 5.9.

As shown in Figure 5.7 (a), in the BCS-S panel the load increases monotonically with negligible lateral displacement. At the onset of buckling, the lateral displacement grows significantly as the axial load drops. Similar trend is observed in the load-strain response of Figure 5.7 (b). The ultimate capacity of the BCS-S panel obtained from the experiment is 179 kN. The analytical formulation (Eq. 5.5) does not include geometric imperfections and material nonlinearities and provides upper bounds of capacities. As seen in Figure 5.7 (a), the analytical

133

predictions using the 30th percentile, overestimates the experimental result by 12.1%.
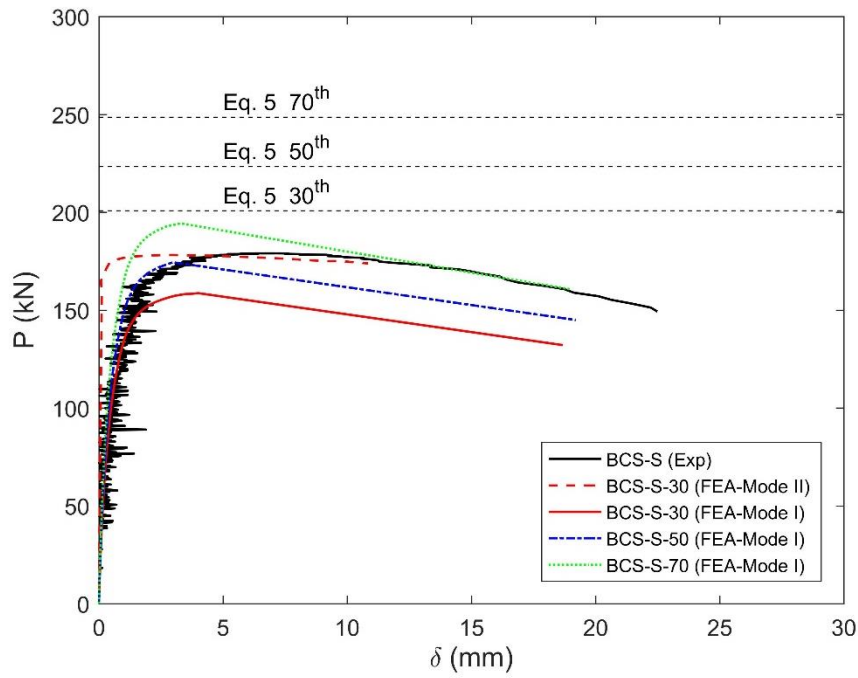
(a)
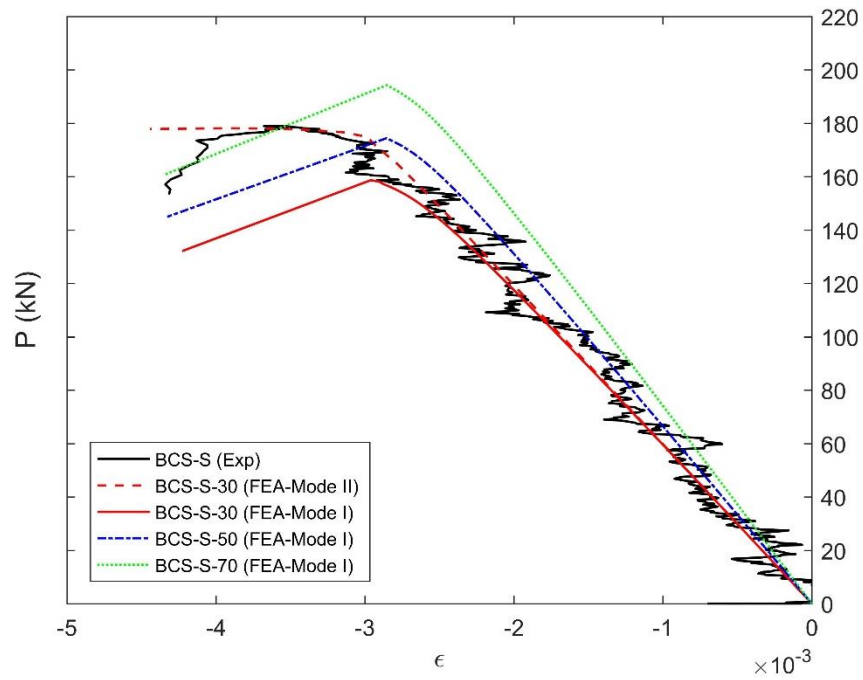
(b)

Figure 5.7 Comparison between experimental and FEA results: (a) load vs. mid-lateral displacement, and (b) load vs. longitudinal strain curves in BCS-S panels with various MOE and MOR percentiles (30th, 50th and 70th).
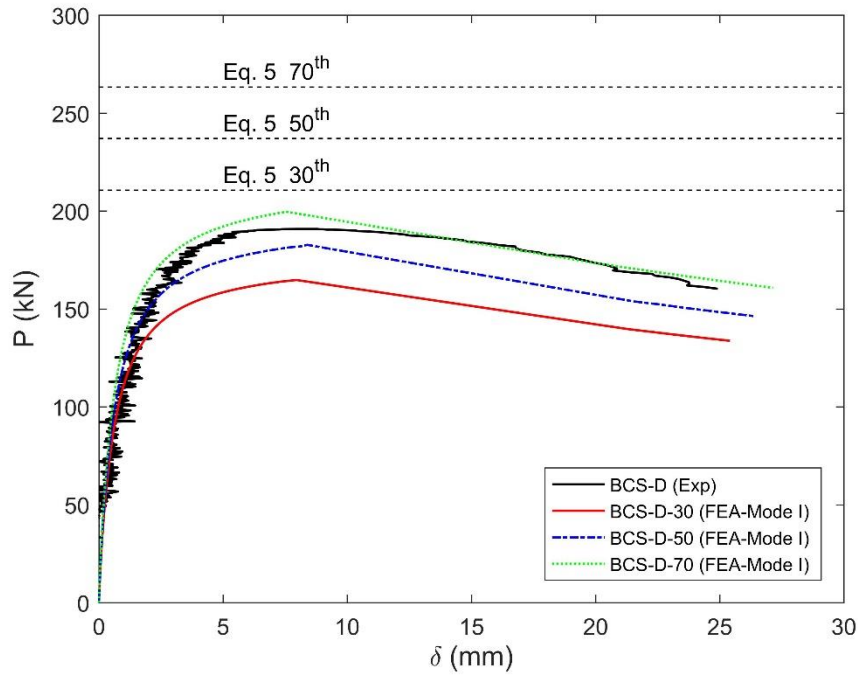
(a)
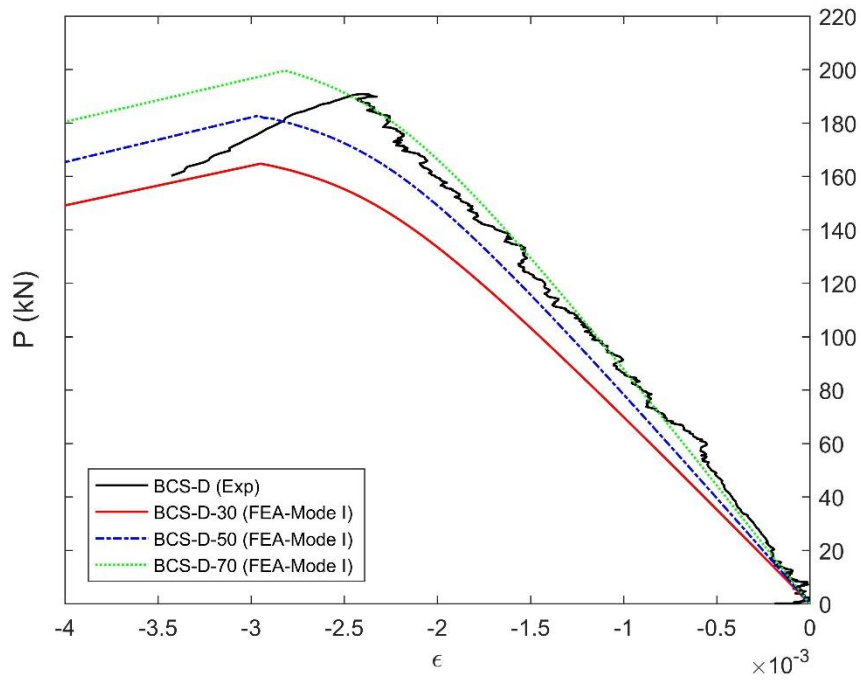
(b)

Figure 5.8 Comparison between the experimental and FEA results: (a) load vs. mid-lateral displacement, and (b) load vs. longitudinal strain in BCS-D panels with various MOE and MOR percentiles (30th, 50th and 70th).

In order to capture the FEA response of the BCS-S panels, models with different MOE and MOR percentiles (30th, 50th and 70th) and with mode Ⅰ and Ⅱ imperfections (Figure 5.6 (a)) are produced. As shown in Figure 5.7 (a), using mode Ⅰ imperfections, ultimate capacities of 158.7 kN, 174.4 kN and 194.3 kN corresponding to 30th, 50th and 70th percentiles, respectively, are calculated. As shown in Figure 5.7 (b), the linear load-strain response of the FEA-Mode Ⅰ with 30th percentile matches with the experimental response. However, the ultimate capacity of the FEA- is 11.36% lower than the experimental observation. Whereas, when buckling mode shape Ⅱ (Figure 5.6 (a)) is used as the initial imperfection (with 30th material), the load displacement/strain response matches the experimental response, and the ultimate load is only 0.48% lower than the experiment. Moreover, using the FEA Mode Ⅱ-30th model, similar plateaus are observed in the load displacements/strains at the ultimate load, as those seen in the experiment. The plateau is associated with the yield in compression of the plywood faces. The failed BCS-S panel is shown in Figure 5.9 (a), and the local failure points are circled. It can be seen that the local failure points of the physical test are not at the mid-span, and are closer to the maximum lateral displacement/strain contours suggested by the FEA.

Figure 5.8 shows results of the BCS-D panels. The ultimate capacity of the BCS-D panel is 190.8 kN, and it is 6.6% higher than the BCS-S panel. The analytical predictions are larger than the experimental results. Amongst the FEA results, those of the FEA-Mode Ⅰ-70th are in a good agreement with the experimental results with 4.6% difference in the peak load. The snap-through buckle response of Figure 5.8 (b) corresponds to the buckling failure shown in Figure 5.9 (b). Unlike the deformed shape at failure of the FEA, the location of the failure in the tested BCS-D panel is not exactly in the middle. That may be related to local material imperfections and explains the differences between the ultimate loads between the FEA and the experiment.

(a)   (b)
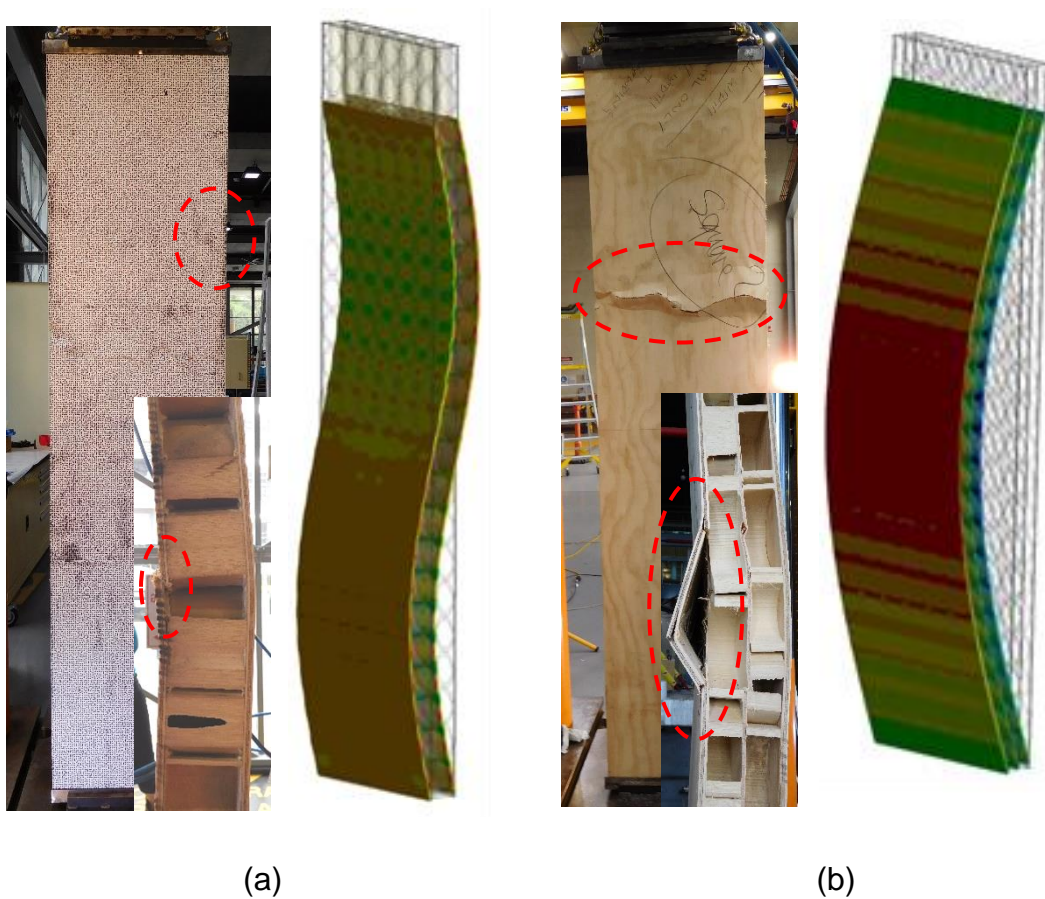
Figure 5.9 Experimental and exaggerated FEA failure modes of the BCS panels subjected to compressive axial load; (a) BCS-S panel with FEA-Mode II-30th, and (b) BCS-D panel with FEA-Mode I-70th. FEA results show the longitudinal strain contours.

5.5.2.2 Optimised core configuration

The FEA results in the previous section showed good agreement with the experimental results. Using the validated FEA, an effort is made to optimise the core configuration in the BCS panels. Assumed core configurations are depicted in Figure 5.10 (a). All panels have similar depth of 84.4 mm (same as the physical model). Using the validated FEA, and assuming buckling mode shape Ⅰ (shown in Figure 5.6) imposed as the initial imperfection, with 50th percentile material properties, the load-axial displacement response of each configuration is calculated and is plotted in Figure 5.10 (b). To benchmark, results of the BCS-S and BCS-D panels are also shown.

The most superior stiffness and ultimate capacity correspond to a single layer design with the plywood thickness doubled (BCS-S1). This sample can be manufactured by gluing a 3-strand commercial plywood to the existing skins. The capacity of BCS-S1 is 79.5% higher than the BCS-S, and 71.4% larger than the BCS-D panels. By using identical plywood thickness (BCS-D1), the stiffness and ultimate capacity of the BCS-D panel is increased by 62.15% and 6.85%, respectively. Moreover, as seen in the response of BCS-D1 in Figure 5.10 (b), using identical plywood thickness stabilises the post-bucking response of the panel. Tripling the core layers (BCS-T) increases the ultimate capacity by 20% and stiffness by 26.7%, compared to BCS-D panel. By adding a gap between the bamboo cores (68 mm along the width of the panel) in a single layer concept (BCS-S2), the number of bamboo core decreases by 33.3%, while no significant change in stiffness and ultimate capacities are observed. In the BCS-S2 (-30%) panel, the mechanical properties of the bamboo are reduced by 30%. No significant change in stiffness and buckling capacity is observed between this panel and the BCS-S2 panel.

$t = 7.2$ mm

$t = 7.2$ mm

$c = 70$ mm

BCS-S

$t = 14.4$ mm

$t = 14.4$ mm

$c = 55.6$ mm

BCS-S1

$t = 7.2$ mm

$t = 7.2$ mm

$c = 70$ mm

68 mm

BCS-S2

$t = 7.2$ mm

$t = 3$ mm

$t = 7.2$ mm

$c = 33.5$ mm

$c = 33.5$ mm

BCS-D

$t = 7.2$ mm

$t = 7.2$ mm

$t = 7.2$ mm

$c = 31.4$ mm

$c = 31.4$ mm

BCS-D1

$c = 16$ mm

$c = 32$ mm

$c = 16$ mm

$t = 7.2$ mm

$t = 3$ mm

$t = 3$ mm

$t = 7.2$ mm

BCS-T
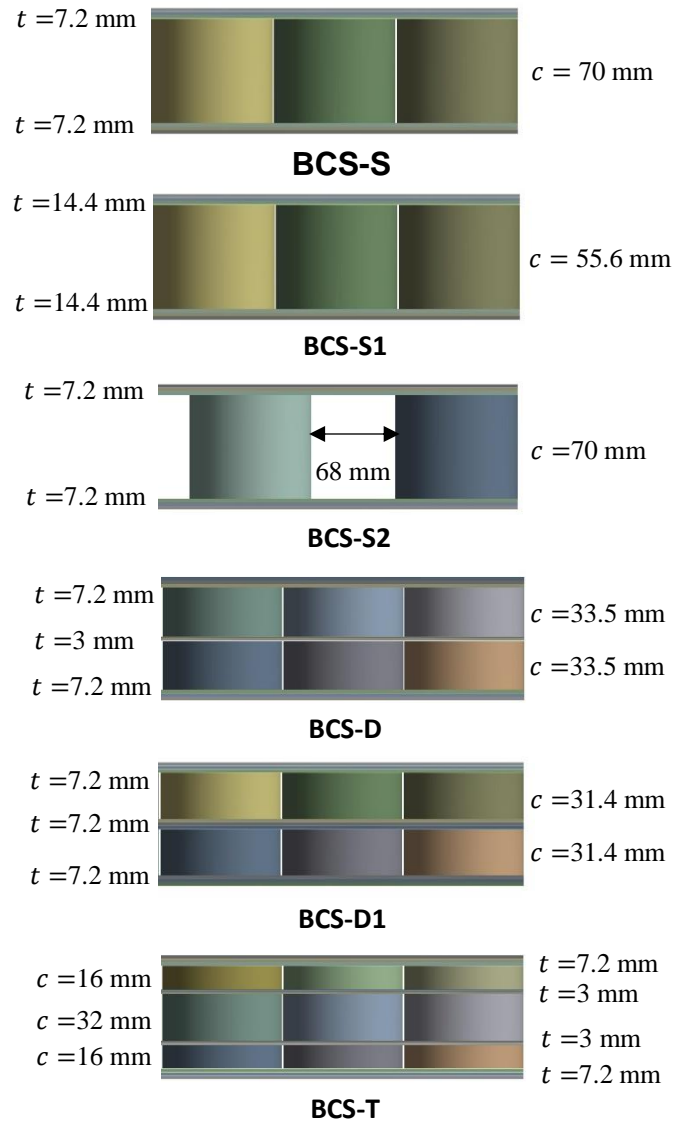
(a)
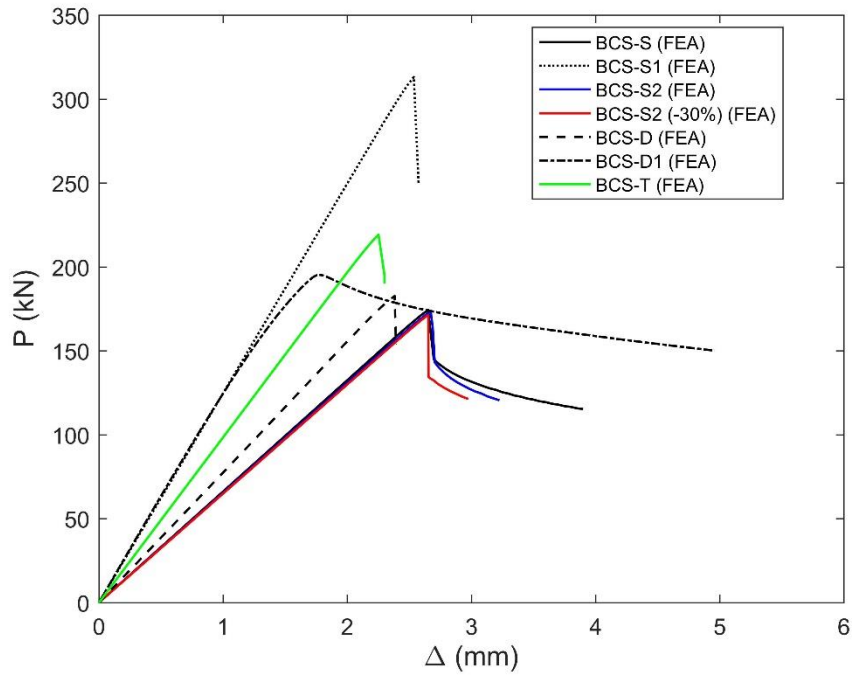
(b)

Figure 5.10 Optimised core configuration study showing: (a) assumed core configurations in the BCS panels, and (b) corresponding load vs. axial displacement from the FEA.

5.5.3 Comparison between BCS and CLT panels

5.5.3.1 Axial compression

Ultimate capacities of BCS-S and BCS-D panels at different lengths are calculated using FEA with mode shapes Ⅰ and Ⅱ imperfections. Results are shown in Figure 5.11, where the ultimate load (P) is normalised to the corresponding compressive capacity of the panel (P_r), given in Eq. 5.7 to give the strength index SI ($SI = P/P_r$). All panels have similar width (600 mm), and depth (84.4 mm). Lengths of the panels vary between 300 mm and 3000 mm, hence the non-dimensional slenderness ratio ($\lambda_{BCS} = \sqrt{12}a/d$) changes from 12.3 to 123.1.
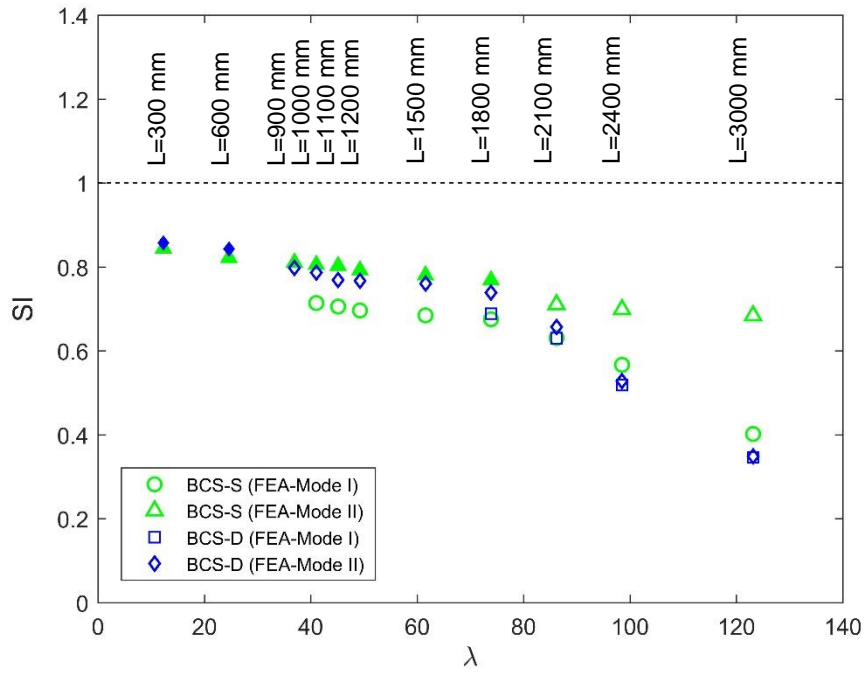
(a)
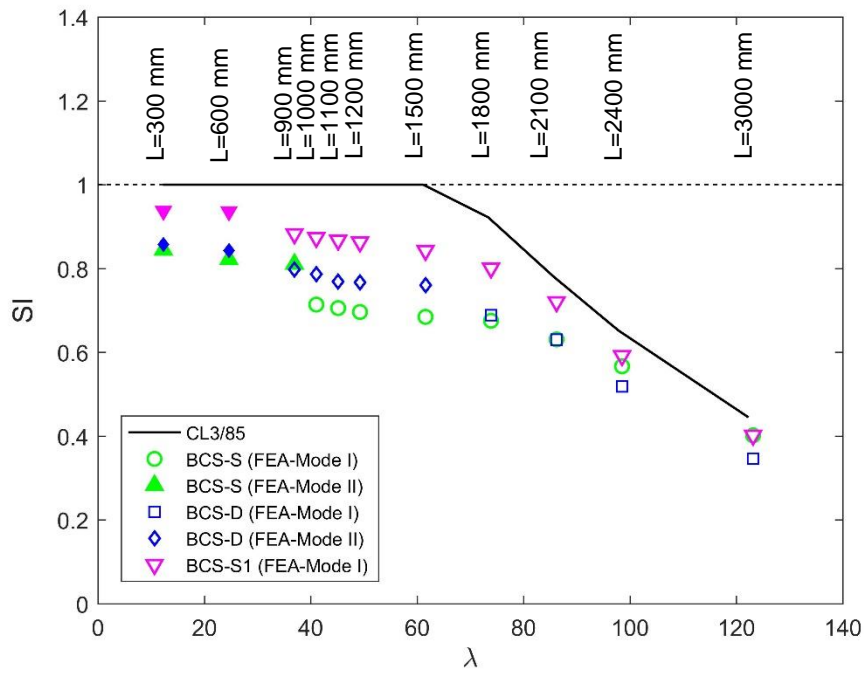
(b)

Figure 5.11 Axial compressive capacity of the BCS panels, (a) effect of the initial imperfection mode shapes, and (b) slenderness curves based on minimum capacities found from Figure 5.11 (a).

In all FEA models, and at different load stages, failure in (1) buckling, (2) yield of plywood (Eq. 5.15), and (3) shear bond failure were checked. All samples failed either in buckling or in shear bond failure. None of the samples showed a pre-buckle yield failure in plywood. The data points shown in solid fill correspond to the shear bond (interface) failure. The interface failure is assumed to occur when the shear stress between bamboo cores and plywood skins exceeds 0.99 MPa, (tested shear bond strength in Table 5.4). As shown in Figure 5.11 (a), there is a significant difference in ultimate capacity of BCS-S panels between Mode Ⅰ and Mode Ⅱ imperfections. At large slenderness ratios (λ>100), the capacity of the BCS-S panel from Mode Ⅰ is substantially lower than the Mode Ⅱ. This suggests that the axial capacity of the BCS-S panel is very sensitive to the fabrication tolerances. Axial capacity of the BCS-D panel is not as sensitive to the initial imperfection mode. All the BCS-S (Mode Ⅰ) panels experience failure in global buckling. However, in BCS-S (Mode Ⅱ) shear interface failure is observed at panel lengths a<1800 mm. The two short BCS-D panels (a=300 mm and a=600 mm) experience shear interface failure, while the remaining panels fail in overall buckling.

Slenderness curves are developed for the BCS panels based on the minimum capacity (calculated from the FEA with respective initial imperfection mode, shown in Figure 5.11 (a)), and are plotted in Figure 5.11 (b). The slenderness curve of the panel with the optimum core configuration (BCS-S1) is plotted as well. In all panels, 50th percentile material properties are incorporated into the FEA.

For sake of comparison, the slenderness curve of a *CL3/85 XLam* CLT product (XLam 2016) is shown as well. The *CL3/85* panel consists of three layers of sawn boards with a total thickness of 85 mm (20 mm/ 45 mm/ 20 mm). The two outermost layers (1 and 3) are aligned in the span direction (parallel to axial compressive load), and the middle layer is perpendicular to the span direction. The unfactored compressive design capacity of the CLT panels under axial load is calculated from Eq. 5.10, based on the material properties of the CLT laminations listed in Table 5. The parallel to grain modulus of elasticity (E_L), bending strength (f_b) and compressive strength (f_c) are taken from *XLam* design guide (XLam 2016). The unfactored compressive design capacity of the *CL3/85*

142

(Eq. 5.10) with length of 2,070 mm (and width of 570 mm) and based on the material properties of Table 5.5, is 326.2 kN.

In Figure 5.11 (b), to calculate the strength index SI of the CLT panels, the unfactored compressive design capacity P_r from Eq. 5.10, is normalised to the corresponding compressive capacity of a short CLT panel (assuming K_{zc} and K_c are equal to one in Eq. 5.10).

As shown in Figure 5.11 (b), the CLT curve is an upper bound for all BCS panels. The next best is the BCS-S1 panel. However, it can be seen that at large slenderness ratios (λ>100), which is within the typical column lengths in a building (L=3 m), the BCS panels achieve strength indexes (SI) close to the CLT panel. The shear interface failure mode only occurs in stubby BCS panels (λ<40). The governing failure mode in all BCS panels with (λ>40) is the Euler column buckle mode.

Table 5.5 Material properties of the CLT laminations.

	MOE (parallel to span) (MPa)	MOE (perpendicular to span) (MPa)	Shear Modulus (parallel to span) (MPa)	Shear Modulus (perpendicular to span) (MPa)	Compression strength f_c (parallel to span) (MPa)	Bending strength f_b (parallel to span) (MPa)
External laminations	8,000	267	500	50	18	14
Internal laminations	6,000	200	375	37.5	15	10

5.5.3.2 Combined axial compression and bending (p → w load path)

Capacity of the BCS panels with length (a=2,100 mm) under combined loading is studied using FEA with 50th percentile material properties. The FEA is conducted in two load steps. In the $p \rightarrow w$ load path, and in the first load step, the axial force in the panel is maintained at 30%, 50% and 70% of the axial capacity of the corresponding panel calculated from pure compression FEA study in the previous sections. In the second load step, a uniform lateral wind pressure w is applied to one face of the plywood, and is increased until the failure is observed. Lateral wind pressures w for each panel at the predetermined axial load are represented

in Table 5.6 and are plotted in Figure 5.12. Combined loading results of the *CL3/85* are also shown in Figure 5.12. In the CLT panel, the moment at failure *M* is calculated from the interaction equation (Eq. 5.13), and the equivalent lateral load *w* is found assuming simply supported boundary conditions ($w = 8M/a^2$).

A shown in Figure 5.12 and represented in Table 5.6, at small normalised axial loads (30%), lateral capacity of the BCS-S1 panel is 47.6% and 83.6% larger than those of the BCS-D and BCS-S panels, respectively. The difference gets smaller as the axial load approaches the full capacity of the panel in compression. Normalised capacity of the CLT panel is closer to the capacity of the BCS-S panel. The failure modes of all BCS panels are shear interface failure (due to excessive bending) as represented in Table 5.6.
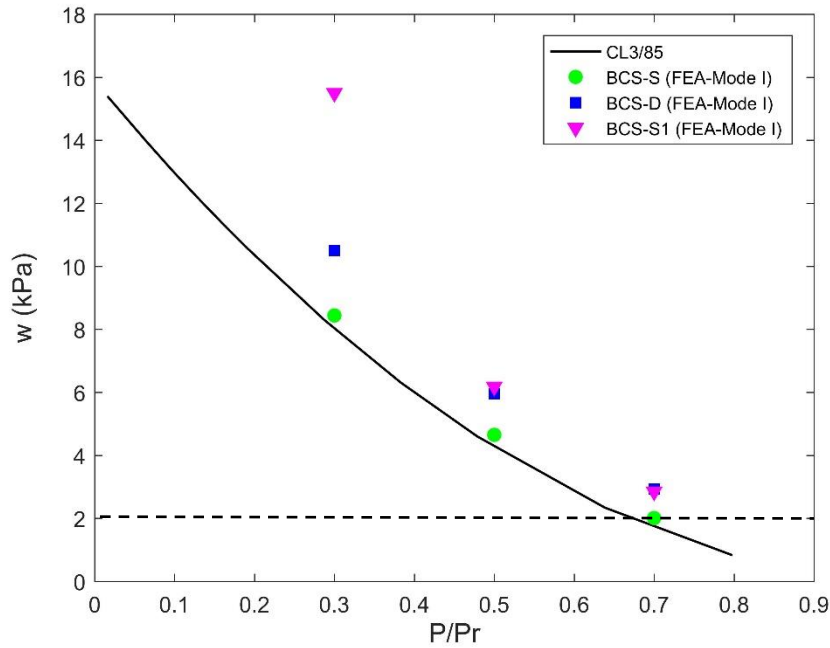
Figure 5.12 Combined loading results of the BCS-S, BCS-D and BCS-S1 panels, compared to *CL3/85* (p → w load path).

Table 5.6 Combined loading results BCS-S, BCS-D and BCS-S1 panels with length of 2.1 m and using 50th percentiles.

	Nominal loading			BCS-S			BCS-D				BCS-S1			
	P	w (kPa)	P_r (kN)	w_{ult} (kPa)	P/P_r	Failure mode	P_r (kN)	w_{ult} (kPa)	P/P_r	Failure mode	P_r (kN)	w_{ult} (kPa)	P/P_r	Failure mode
$p \rightarrow w$ load path	30% P_r	-		8.44		interface		10.50		interface		15.5		interface
	50% P_r	-	174.4	4.65	-	interface	195.7	5.96	-	interface	315.3	6.18	-	interface
	70% P_r	-		2.01		interface		2.93		interface		2.85		interface
$w \rightarrow p$ load path	-	2 kPa	-	-	0.81	buckling	-	-	0.74	buckling	-	-	0.77	buckling

5.5.3.3 Combined axial compression and bending (w → p load path)

In this load path, a 2 kPa lateral wind pressure (typical design wind pressure in non-cyclonic regions of East coast Australia) is applied, and the axial shortening is imposed until failure is observed. Results are presented in Table 5.6. All BCS panels fail in Euler column buckling mode. The normalised load capacity of the BCS-S, BCS-D, and BCS-S1 panels are 0.81, 0.74 and 0.77 of the axial compressive capacity under pure compression in each panel, respectively. The corresponding normalised load capacity of the *CL3/85* is 0.67 (see Figure 5.12).

5.6 Conclusions

Novel timber panels with commercial plywood faces and bamboo ring cores were manufactured and tested in axial compression and in the shear bond strength. In the shear bond tests, square panels with width of 300 mm and depth of 85 mm were manufactured and tested. Shear bond strength test results showed that increasing the polyurethane adhesive spread rate, does not enhance the shear bond strength significantly. Therefore, a spread rate of 180 g/m^2 with shear strength at the bamboo-plywood contact of 0.99 MPa was adopted in the manufacturing of large panels.

Two types of panels were tested in axial compression, a single-layer (BCS-S) and a double-layer (BCS-D). The panels had length of 2,070 mm, width of 570 mm, and depth of 85 mm. The axial test capacities of the BCS-S and BCS-D panels, were shown to be 179.0 kN and 190.8 kN, respectively. At similar dimensions, the unfactored axial compressive design capacity (*CSA O86:2019, Engineering design in wood* 2019) of a CLT panel (*CL3/85*) is 326.2 kN. However, the BCS-S and BCS-D panels weigh 19.42 kg/m^2 and 20.15 kg/m^2, which is 55.7% and 54% less than the CLT panel (with a nominal weight of 43.85 kg/m^2), respectively. Therefore, the ultimate capacity to weight ratio of BCS-S and BCS-D panels are 24% and 27.3% higher than a conventional CLT panel (*CL3/85*), respectively.

The FEA study with probabilistic material definitions and different initial geometric imperfections revealed that the buckling capacity of the BCS panels are significantly affected by the plywood material properties. Effect of geometric imperfection (imposed as Eigen buckling mode shapes in the FE models) was shown to be more substantial in the capacity of the BCS-S panel. The parametric

FEA study with various core configurations revealed that the highest axial stiffness and capacity is gained using a single-layer panel with the plywood thickness doubled (BCS-S1). While, a BCS-D panel with identical plywood thicknesses showed a more stabilised post-buckling response. Reducing the material properties of bamboo by 30% did not affect the stiffness and buckling capacity of the panels.

In order to study the length effect, slenderness curves were developed for the BCS and CLT panels. Short BCS-S and BCS-D depicted failure in bond between the bamboo rings and the plywood faces. Whereas, column buckling failure was observed in long wall panels. The slenderness curve of the CLT panel was shown to be an upper bound of BCS panels at all slenderness ratios. However, at large slenderness ratios (λ>100), which is within the typical column lengths of a building (a=3 m), the BCS panels achieved normalised axial capacities close to the CLT (*CL3/85*) panel.

In the combined loading studies, two different load paths were considered: (1) compression then lateral wind, and (2) lateral wind then compression. In the first load path ($p \rightarrow w$), the axial loads in the panels were maintained at fractions of the panel's ultimate axial load capacity. Then the lateral wind load was gradually increased until failure occurred. All BCS panels failed in shear bond strength. It was understood that at small axial loads, the BCS panels have larger capacity compared to the CLT panel. The difference almost vanished as the axial load approached the full capacity. In the second load path ($w \rightarrow p$), initially a 2 kPa lateral wind pressure was applied, then axial force was imposed until failure occurred. All the BCS panels failed in global buckling. The normalised axial capacity of the BCS-S and BCS-D panels were 20.9% and 10.45% larger than the CLT panel, respectively. The BCS-S1 panel (with optimised core configuration) showed 14.92% increase in the combined capacity compared to the CLT panel.

6 Conclusions

6.1 Thesis findings

The successful implementation of the BCS and PCS panels requires that the structural properties of such panels be comparable to products that are already commercially viable. The structural sandwich panels discussed in this study are an attempt to develop products that reduce the use of resources, while utilizing affordable and sustainable local timber and wood waste. The potential uses of such panels using bamboo and peeler core in the building industry, as a replacement for solid panels would greatly reduce the demand on timber resources.

The first phase of this research is based on numerical analyses to study the flexural responses of the proposed BCS and PCS panels covering a range of aspect ratios (*a/b*) in one-way and two-way bending configurations. A modified Ritz method is developed to study the flexural stiffness of the panels. This method unlike previous formulations of sandwich orthotropic plates, accounts for the local bending stiffness of the faces (thick face) and the flexural rigidity of the cores (thick-stiff core) of the BCS and PCS panels. The results obtained from the modified Ritz method reveal that only panels with double plywood skins can be a better alternative to commercial CLT panels, while the total depth and weight of the panels can be up to 8% thinner and 40% lighter than CLT. The PCS panels are in average 10% stiffer than the BCS panels. The Timoshenko beam coefficients of the BCS and PCS panels are found to be 0.817 and 0.815, respectively, which are much smaller than the coefficient 1.2 for the CLT panels. The ultimate capacity of the PCS panel is found to be 27% larger than the capacity of the BCS panel. However, the PCS panel is 30% heavier than the BCS panels. The ultimate capacity of the panels (panels with double plywood skins) in one-way bending are investigated using a validated FEA. The FEA results indicate that in BCS and PCS panels failure occurs in tension parallel to the grain while the compressive plywood skin reaches its yield capacity.

The second phase of this research is based on a series of experimental tests to investigate the bending and shear performances of single-layer and double-layer BCS and PCS panels. Results are compared to test results of commercial CLT panels of almost similar depth. The optimum adhesive spread rate is also identified through conducting shear bond tests in the single-layer BCS panels, since the single-layer BCS panels are more susceptible to shear interface failure. Four-point bending tests are carried out according to the recommendations of BS EN 16351:2015, to measure the bending strength and stiffness of the panels. Tensile skin failure within the pure bending zone is observed as the main mode failure in most sandwich panels. Three-point shear tests are conducted in accordance with ANSI/APA PRG 320-2019.The BCS panels failed due to the loss of shear interface contact between bamboo core rings and the plywood skins, whereas PCS panels showed local indentation/ bond failure between the peeler core rings and the plywood skins. No significant improvements are observed in the double-layer panels compared to single-layer panels in bending. However, in shear, double-layer panels show more consistent capacities. Based on the stiffer response of the PCS panels compared to the BCS panels, as numerically determined in Chapter 3, and experimentally tested in Chapter 4, a more efficient PCS panel with thicker plywood skins and a fewer number of peeler cores (PCS-TH) is manufactured and is tested under four-point bending. It is shown that the PCS-TH panels achieves 0.77 times the bending stiffness-to-weight ratio of the commercial CLT panel. The PCS-TH panels also display a better ductile performance in bending and shear in comparison with CLT suggesting it could be a preferred product choice in some building applications. Furthermore, unlike common sandwich panels in the building industry (e.g. SIPs), no core shear failure and localised punching or flatwise crushing of the core have been observed within the BCS and PCS panels.

To get insight into axial performances of the panels, single and double-layer BCS panels are studied under axial compressive load as well as combined bending and axial compression actions, through experimental, numerical, and simplified analytical approaches. Based on the experimental test results in Chapter 4, the BCS panels are selected as they display comparable ductile performance to the PCS-TH panels, while the BCS panels weigh 41% less than the PCS-TH panels. The test results show that under axial compressive action, the ultimate capacity

to weight ratio of the BCS panels are up to 27.3% higher than a commercial CLT panel of same dimension. At large slenderness ratios (typical column lengths of a building), the proposed BCS panels have ultimate axial capacities close to the conventional CLT panels. From combined loading studies, the BCS panels outperform a CLT panel of similar size.

6.2   Recommendations for future research

Mechanical performance testing of the BCS and PCS panels have shown that utilisation of low value and small diameter timber to produce structural components in the building industry is technically feasible. However, there are several manufacturing issues that need to be addressed in future studies to improve the performance of the BCS and PCS panels.

These can be summarized as listed below:

(1) A better manufacturing strategy: Gluing the top and bottom surfaces of bamboo core rings prior to panel manufacturing may contribute to a better contact surface between plywood skins and bamboo cores within the panel. This action may prevent the premature interface failure, particularly in BCS panels in shear.

(2) Optimum face-thickness and core layout: this may enable production of more efficient panels that can outperform the CLT in bending and shear strength and stiffness. For instance, in PCS panels, the slight interface gap among the peeler core rings under the loading head caused the localised indentation/ bond failure. Preventing the gap by using solid timber products may increase the capacity of the peeler core panels.

(3) Addition of timber boards between face and core: this can improve fire performance of the panels. Moreover, removing the gap in between bamboo rings/peeler cores and making core blocks with different aspect ratio can enhance the shear performance and fire resistance.

Reference List

Ahmad, M & Kamke, F 2011, 'Properties of parallel strand lumber from Calcutta bamboo (Dendrocalamus strictus)', *Wood Science and Technology*, vol. 45, no. 1, pp. 63-72.

Aicher, S, Hirsch, M & Christian, Z 2016, 'Hybrid cross-laminated timber plates with beech wood cross-layers', *Construction and building materials*, vol. 124, pp. 1007-18.

Alam, P 2004, 'The reinforcement of timber for structural applications and repair', University of Bath.

Allen, HG 1969, *Analysis and design of structural sandwich panels*, Pergamon Press, Oxford.

Amada, S, Ichikawa, Y, Munekata, T, Nagase, Y & Shimizu, H 1997, 'Fiber texture and mechanical graded structure of bamboo', *Composites Part B: Engineering*, vol. 28, no. 1-2, pp. 13-20.

ANSI/APA PRG 320-2019 Standard for Performance-Rated Cross-Laminated Timber, APA – The Engineered Wood Association, Tacoma, WA 98466, <https://www.apawood.org/ansi-apa-prg-320>.

ANSYS 17.0 Mechanical User's Guide, Ansys, Inc. Canonsburg, PA 15317.

ANSYS 19.0 Release ANSYS Inc. 275 Technology Drive, Canonsburg, PA 15317.

APA—The Engineered Wood Association 2018, 'ANSI/APA PRG 320: 2018: Standard for performance-rated cross-laminated timber', *American National Standard. Tacoma, WA: APA-The Engineered Wood Association*, vol. 246.

AS 1720.1:2010 Timber structures Part 1: Design methods, 2010, Standards Australia Limited.

AS/NZS 1080.1:2012 Timber-Methods of test, Method 1: Moisture content, 2012, Standards Australia Limited.

AS/NZS 1170.2:2011 Structural design actions Part 2: Wind actions, 2011, Standards Australia Limited.

AS/NZS 2269.0:2012 Plywood-Structural Part 0: Specifications, 2012, Standards Australia Limited/Standards New Zealand.

ASTM D2718-18, Standard Test Methods for Structural Panels in Planar Shear (Rolling Shear), 2018, ASTM International, West Conshohocken, PA, <http://www.astm.org/cgi-bin/resolver.cgi?D2718>.

ASTM D3500 - 14, Standard Test Methods for Structural Panels in Tension, 2014, ASTM International, West Conshohocken, PA, <http://www.astm.org/cgi-bin/resolver.cgi?D3500>.

ASTM D5456-19, Standard Specification for Evaluation of Structural Composite Lumber Products, 2019, ASTM International, West Conshohocken, PA, <http://www.astm.org/cgi-bin/resolver.cgi?D5456>.

Awad, ZK, Aravinthan, T, Zhuge, Y & Gonzalez, F 2012, 'A review of optimization techniques used in the design of fibre composite structures for civil engineering applications', *Materials & Design*, vol. 33, pp. 534-44.

Awad, ZK, Aravinthan, T, Zhuge, Y & Manalo, A 2013, 'Geometry and restraint effects on the bending behaviour of the glass fibre reinforced polymer sandwich slabs under point load', *Materials & Design*, vol. 45, pp. 125-34.

Bart-Smith, H, Hutchinson, J & Evans, A 2001, 'Measurement and analysis of the structural performance of cellular metal sandwich construction', *International journal of mechanical sciences*, vol. 43, no. 8, pp. 1945-63.

Biagi, R & Bart-Smith, H 2012, 'In-plane column response of metallic corrugated core sandwich panels', *International Journal of Solids and Structures*, vol. 49, no. 26, pp. 3901-14.

Blass, HJ & Fellmoser, P 2004, 'Design of solid wood panels with cross layers', *8th world conference on timber engineering*, vol. 2, pp. 543-8.

Bodig, J & Jayne, BA 1982, *Mechanics of wood and wood composites*, vol. 712, Van Nostrand Reinhold New York.

Brancheriau, L & Baillères, H 2002, 'Natural vibration analysis of clear wooden beams: a theoretical review', *Wood Science and Technology*, vol. 36, no. 4, pp. 347-65.

Brandner, R, Flatscher, G, Ringhofer, A, Schickhofer, G & Thiel, A 2016, 'Cross laminated timber (CLT): overview and development', *European Journal of Wood and Wood Products*, vol. 74, no. 3, pp. 331-51.

BS EN 16351 : 2015 Timber Structures- Coss Laminated Timber- Requirements, 2015, British Standards Institution, <https://infostore.saiglobal.com/en-us/Standards/BS-EN-16351-2015-286674_SAIG_BSI_BSI_663613/>.

Budiansky, B 1999, 'On the minimum weights of compression structures', *International Journal of Solids and Structures*, vol. 36, no. 24, pp. 3677-708.

Cao, Y, Street, J, Li, M & Lim, H 2019, 'Evaluation of the effect of knots on rolling shear strength of cross laminated timber (CLT)', *Construction and building materials*, vol. 222, pp. 579-87.

Ceccotti, A 2002, 'Composite concrete-timber structures', *Progress in Structural Engineering and Materials*, vol. 4, no. 3, pp. 264-75.

Chiniforush, AA, Akbarnezhad, A, Valipour, H & Xiao, J 2018, 'Energy implications of using steel-timber composite (STC) elements in buildings', *Energy and Buildings*, vol. 176, pp. 203-15.

Chung, K & Yu, W 2002, 'Mechanical properties of structural bamboo for bamboo scaffoldings', *Engineering structures*, vol. 24, no. 4, pp. 429-42.

Chung, K, Yu, W & Chan, S 2002, 'Mechanical properties and engineering data of structural bamboo'.

CIRAD 2012, *BINGÒ (Beam Identification by Nondestructive Grading) software*, <https://www.picotech.com/library/application-note/non-destructive-testingof-wood>.

CoDyre, L & Fam, A 2016, 'The effect of foam core density at various slenderness ratios on axial strength of sandwich panels with glass-FRP skins', *Composites Part B: Engineering*, vol. 106, pp. 129-38.

Correlated SOLUTIONS 2019, *VIC-3D Testing Guide*, <http://correlatedsolutions.com/>.

Cote, F, Biagi, R, Bart-Smith, H & Deshpande, VS 2007, 'Structural response of pyramidal core sandwich columns', *International Journal of Solids and Structures*, vol. 44, no. 10, pp. 3533-56.

Crocetti, R, Sartori, T & Tomasi, R 2014, 'Innovative timber-concrete composite structures with prefabricated FRC slabs', *Journal of Structural Engineering*, vol. 141, no. 9, p. 04014224.

—— 2015, 'Innovative timber-concrete composite structures with prefabricated FRC slabs', *Journal of Structural Engineering*, vol. 141, no. 9, p. 04014224.

153

Crupi, V, Epasto, G & Guglielmino, E 2012, 'Collapse modes in aluminium honeycomb sandwich panels under bending and impact loading', *International Journal of Impact Engineering*, vol. 43, pp. 6-15.

CSA O86:2019, Engineering design in wood, 2019, the Canadian Standards Association, CSA Group, Mississauga, Ontario, Canada L4W 5N6.

Dahl, KB 2009, 'Mechanical properties of clear wood from Norway spruce'.

Dai, J & Hahn, HT 2003, 'Flexural behavior of sandwich beams fabricated by vacuum-assisted resin transfer molding', *Composite structures*, vol. 61, no. 3, pp. 247-53.

Daniel, IM & Abot, JL 2000, 'Fabrication, testing and analysis of composite sandwich beams', *Composites Science and Technology*, vol. 60, no. 12, pp. 2455-63.

Darzi, S, Karampour, H, Gilbert, BP & Bailleres, H 2018a, 'Flexural behaviour of a novel bamboo-plywood sandwich composite panel', paper presented to 2018 World Conference on Timber Engineering (WCTE 2018), Seoul, Republic of Korea.

—— 2018b, 'Numerical study on the flexural capacity of ultra-light composite timber sandwich panels', *Composites Part B: Engineering*, vol. 155, pp. 212-24.

Dawood, M, Ballew, W & Seiter, J 2011, 'Enhancing the resistance of composite sandwich panels to localized forces for civil infrastructure and transportation applications', *Composite structures*, vol. 93, no. 11, pp. 2983-91.

Dawood, M, Taylor, E, Ballew, W & Rizkalla, S 2010, 'Static and fatigue bending behavior of pultruded GFRP sandwich panels with through-thickness fiber insertions', *Composites Part B: Engineering*, vol. 41, no. 5, pp. 363-74.

Dawood, M, Taylor, E & Rizkalla, S 2010, 'Two-way bending behavior of 3-D GFRP sandwich panels with through-thickness fiber insertions', *Composite structures*, vol. 92, no. 4, pp. 950-63.

Ehrhart, T, Brandner, R, Schickhofer, G & Frangi, A 2015, 'Rolling shear properties of some European timber species with focus on cross laminated timber (CLT): test configuration and parameter study'.

Fam, A & Sharaf, T 2010, 'Flexural performance of sandwich panels comprising polyurethane core and GFRP skins and ribs of various configurations', *Composite structures*, vol. 92, no. 12, pp. 2927-35.

Fellmoser, P & Blaß, HJ 2004, 'Influence of rolling shear modulus on strength and stiffness of structural bonded timber elements', in *CIB-W18 Meeting*, vol. 37.

2010, *Massive Timber Construction Systems Cross-laminated Timber (CLT)*, by FWPA, Technical Design Guide, Forest and Wood Products Australia.

Gatóo, A, Sharma, B, Bock, M, Mulligan, H & Ramage, MH 2014, 'Sustainable structures: bamboo standards and building codes', in *Proceedings of the Institution of Civil Engineers-Engineering Sustainability*, vol. 167, pp. 189-96.

George, T, Deshpande, VS, Sharp, K & Wadley, HN 2014, 'Hybrid core carbon fiber composite sandwich panels: fabrication and mechanical response', *Composite structures*, vol. 108, pp. 696-710.

Ghavami, K 2005, 'Bamboo as reinforcement in structural concrete elements', *Cement and concrete composites*, vol. 27, no. 6, pp. 637-49.

Giongo, I, Piazza, M & Tomasi, R 2012, 'Out of plane refurbishment techniques of existing timber floors by means of timber to timber composite structures', in *WCTE 2012–World Conference on Timber Engineering*.

Goad, P & Snape, D 2015, 'Library at the Dock', *Architecture Australia*, vol. 104, no. 1, p. 92.

2011, *Putting a price on pollution: What it means for Australia's property and construction industry*, by Green Building Council Australia, Green Building Council Australia.

Green, M & Taggart, J 2020, *Tall wood buildings: Design, construction and performance*, Birkhäuser.

Grenestedt, JL & Bekisli, B 2003, 'Analyses and preliminary tests of a balsa sandwich core with improved shear properties', *International journal of mechanical sciences*, vol. 45, no. 8, pp. 1327-46.

Gutkowski, R, Brown, K, Shigidi, A & Natterer, J 2008, 'Laboratory tests of composite wood–concrete beams', *Construction and building materials*, vol. 22, no. 6, pp. 1059-66.

Hassanieh, A, Valipour, H & Bradford, M 2016, 'Experimental and numerical study of steel-timber composite (STC) beams', *Journal of Constructional Steel Research*, vol. 122, pp. 367-78.

Herrmann, AS, Zahlen, PC & Zuardy, I 2005, 'Sandwich structures technology in commercial aviation', in *Sandwich structures 7: Advancing with sandwich structures and materials*, Springer, pp. 13-26.

Hill, R 1998, *The mathematical theory of plasticity*, vol. 11, Oxford university press.

Hindman, DP & Bouldin, JC 2014, 'Mechanical properties of southern pine cross-laminated timber', *Journal of Materials in Civil Engineering*, vol. 27, no. 9, p. 04014251.

I.S. EN 1995-1-1: 2005, Eurocode 5: Design of timber structures - Part 1-1: General - Common rules and rules for buildings, 2005, European Committee for standization: CEN/TC 250

ISO 22157:2019, Bamboo structures — Determination of physical and mechanical properties of bamboo culms — Test methods, 2019, the International Organization for Standardization, <https://www.iso.org/standard/65950.html>.

Janssen, JJ 1981, 'Bamboo in building structures', Technische Hogeschool Eindhoven.

Jensen, K, Al-Rubaye, S, Thomas, RJ & Maguire, M 2020, 'Mechanics-Based model for elastic Bending, Axial, thermal Deformations, and asymmetry of concrete composite sandwich wall panels', *Structures*, vol. 23, pp. 459-71.

Kabir, K, Vodenitcharova, T & Hoffman, M 2014, 'Response of aluminium foam-cored sandwich panels to bending load', *Composites Part B: Engineering*, vol. 64, pp. 24-32.

Karacabeyli, E & Gagnon, S 2019, *Canadian CLT Handbook*, 2019 edn, vol. 1, FPInnovations.ca.

Karlsson, KF & TomasÅström, B 1997, 'Manufacturing and applications of structural sandwich components', *Composites Part A: Applied Science and Manufacturing*, vol. 28, no. 2, pp. 97-111.

Khorsandnia, N, Valipour, HR & Crews, K 2012, 'Experimental and analytical investigation of short-term behaviour of LVL–concrete composite connections and beams', *Construction and building materials*, vol. 37, pp. 229-38.

Kim, J & Swanson, SR 2001, 'Design of sandwich structures for concentrated loading', *Composite structures*, vol. 52, no. 3, pp. 365-73.

Kim, JH, Lee, YS, Park, BJ & Kim, DH 1999, 'Evaluation of durability and strength of stitched foam-cored sandwich structures', *Composite structures*, vol. 47, no. 1, pp. 543-50.

Kreuzinger, H 1995, 'Mechanically jointed beams and columns', *Timber Engineering-STEP*, vol. 1, pp. 1-8.

Kreuzinger, H 1999, 'Flaechentragwerke – platten, scheiben und schalen – ein Berechnungsmodell fuer gaengige Staikprogramme (in German)', *Bauen mit Holz. S*, vol. 1, no. 1, pp. 34-9.

Lakreb, N, Bezzazi, B & Pereira, H 2015, 'Mechanical behavior of multilayered sandwich panels of wood veneer and a core of cork agglomerates', *Materials & Design (1980-2015)*, vol. 65, pp. 627-36.

Lee, AW, Bai, X & Peralta, PN 1996, 'Physical and mechanical properties of strandboard made from moso bamboo', *Forest Products Journal*, vol. 46, no. 11/12, p. 84.

Li, H-t, Chen, G, Zhang, Q, Ashraf, M, Xu, B & Li, Y 2016, 'Mechanical properties of laminated bamboo lumber column under radial eccentric compression', *Construction and building materials*, vol. 121, pp. 644-52.

Li, X 2004, 'Physical, chemical, and mechanical properties of bamboo and its utilization potential for fiberboard manufacturing'.

Li, X, Ashraf, M, Li, H, Zheng, X, Al-Deen, S, Wang, H & Hazell, PJ 2020, 'Experimental study on the deformation and of parallel bamboo Strand Lumber under drop-weight penetration impact', *Construction and building materials*, vol. 242, p. 118135.

Li, Y, Shen, H, Shan, W & Han, T 2012, 'Flexural behavior of lightweight bamboo–steel composite slabs', *Thin-Walled Structures*, vol. 53, pp. 83-90.

Liew, JR & Sohel, K 2010, 'Structural performance of steel-concrete-steel sandwich composite structures', *Advances in Structural Engineering*, vol. 13, no. 3, pp. 453-70.

Loss, C & Davison, B 2017, 'Innovative composite steel-timber floors with prefabricated modular components', *Engineering structures*, vol. 132, pp. 695-713.

M. Reis, E & H. Rizkalla, S 2008, 'Material characteristics of 3-D FRP sandwich panels', *Construction and building materials*, vol. 22, no. 6, pp. 1009-18.

Mahdavi, M, Clouston, P & Arwade, S 2010, 'Development of laminated bamboo lumber: review of processing, performance, and economical considerations', *Journal of Materials in Civil Engineering*, vol. 23, no. 7, pp. 1036-42.

Mahfuz, H, Islam, MS, Rangari, VK, Saha, MC & Jeelani, S 2004, 'Response of sandwich composites with nanophased cores under flexural loading', *Composites Part B: Engineering*, vol. 35, no. 6, pp. 543-50.

Malo, K, Abrahamsen, R & Bjertnæs, M 2016, 'Some structural design issues of the 14-storey timber framed building "Treet" in Norway', *European Journal of Wood and Wood Products*, vol. 74, no. 3, pp. 407-24.

Mamalis, A, Spentzas, K, Manolakos, D, Ioannidis, M & Papapostolou, D 2008, 'Experimental investigation of the collapse modes and the main crushing characteristics of composite sandwich panels subjected to flexural loading', *International journal of crashworthiness*, vol. 13, no. 4, pp. 349-62.

Manalo, A, Aravinthan, T, Karunasena, W & Islam, M 2010, 'Flexural behaviour of structural fibre composite sandwich beams in flatwise and edgewise positions', *Composite structures*, vol. 92, no. 4, pp. 984-95.

Manalo, A, Aravinthan, T, Karunasena, W & Ticoalu, A 2010, 'A review of alternative materials for replacing existing timber sleepers', *Composite structures*, vol. 92, no. 3, pp. 603-11.

March, H 1955, *Effects of shear deformation in the core of a flat rectangular sandwich panel: 1. Buckling under compressive end load. 2. Deflection under uniform transverse load*, Madison, Wis.: US Dept. of Agriculture, Forest Service, Forest Products Laboratory.

Martakos, G 2016, 'Enhanced Performance of Sandwich Structures by Improved Damage Tolerance', Aalborg University.

Mastali, M, Valente, IB & Barros, JA 2017, 'Flexural performance of innovative hybrid sandwich panels with special focus on the shear connection behavior', *Composite structures*, vol. 160, pp. 100-17.

McCormack, T, Miller, R, Kesler, O & Gibson, L 2001, 'Failure of sandwich beams with metallic foam cores', *International Journal of Solids and Structures*, vol. 38, no. 28, pp. 4901-20.

McGavin, RL, Leggate, W, Bailleres, H, Hopewell, G & Fitzgerald, C 2019, *A guide to the rotary veneer processing of coconut palms*, Australian Centre for International Agricultural Research (ACIAR) 2019.

Melo, RRd, Menezzi, D, Soares, CH, Pavan, BE & Rodolfo Júnior, F 2014, 'Rotary peeling yield of Schizolobium amazonicum (Leguminosae-Caesalpinioideae)', *Acta Amazonica*, vol. 44, no. 3, pp. 315-20.

MGB Architecture and Design 2012, *The case for tall wood buildings*, viewed 19/09/2017.

Mostafa, A, Shankar, K & Morozov, E 2013, 'Insight into the shear behaviour of composite sandwich panels with foam core', *Materials & Design*, vol. 50, pp. 92-101.

Mousa, MA & Uddin, N 2009, 'Experimental and analytical study of carbon fiber-reinforced polymer (FRP)/autoclaved aerated concrete (AAC) sandwich panels', *Engineering structures*, vol. 31, no. 10, pp. 2337-44.

Mozafari, H, Khatami, S, Molatefi, H, Crupi, V, Epasto, G & Guglielmino, E 2016, 'Finite element analysis of foam-filled honeycomb structures under impact loading and crashworthiness design', *International journal of crashworthiness*, vol. 21, no. 2, pp. 148-60.

Mozafari, H, Molatefi, H, Crupi, V, Epasto, G & Guglielmino, E 2015, 'In plane compressive response and crushing of foam filled aluminum honeycombs', *Journal of Composite Materials*, vol. 49, no. 26, pp. 3215-28.

Mullens, MA & Arif, M 2006, 'Structural insulated panels: Impact on the residential construction process', *Journal of construction engineering and management*, vol. 132, no. 7, pp. 786-94.

Nairn, JA 2015, *OSU Laminates*, 6.0 edn, OSU Oregan State UNIVERSITY, <http://www.cof.orst.edu/cof/wse/faculty/Nairn/OSULaminates.html>.

Nia, AA & Sadeghi, M 2010, 'The effects of foam filling on compressive response of hexagonal cell aluminum honeycombs under axial loading-experimental study', *Materials & Design*, vol. 31, no. 3, pp. 1216-30.

Nugroho, N & Ando, N 2001, 'Development of structural composite products made from bamboo II: fundamental properties of laminated bamboo lumber', *Journal of wood science*, vol. 47, no. 3, p. 237.

Paik, JK, Thayamballi, AK & Kim, GS 1999, 'The strength characteristics of aluminum honeycomb sandwich panels', *Thin-Walled Structures*, vol. 35, no. 3, pp. 205-31.

Panjehpour, M, Ali, A, Abdullah, A & Voo, YL 2013, 'Structural Insulated Panels: Past, Present, and Future', *Journal of Engineering, Project & Production Management*, vol. 3, no. 1.

Pardue, JR 2011, *Double skin composite hybrid structural insulated panel*, Google Patents.

Patrick, J 2007, *Fundamental characteristics of 3-D GFRP pultruded sandwich panels.(MS), North Carolina State University, Raleigh, NC.*

Perotti, LE 2011, 'Modeling the behavior of fiber reinforced sandwich structures subjected to underwater explosions', California Institute of Technology.

Raftery, GM & Harte, AM 2013, 'Nonlinear numerical modelling of FRP reinforced glued laminated timber', *Composites Part B: Engineering*, vol. 52, pp. 40-50.

Ramanathan, M 2008, 'Hong Kong–bastion of bamboo scaffolding', in *Proceedings of the Institution of Civil Engineers-Civil Engineering*, vol. 161, pp. 177-83.

Reddy, J 1987, 'A generalization of two-dimensional theories of laminated composite plates', *International Journal for Numerical Methods in Biomedical Engineering*, vol. 3, no. 3, pp. 173-80.

REIS, EM 2005, 'CHARACTERISTICS OF INNOVATIVE 3-D FRP SANDWICH PANELS', Doctor of Philosophy thesis, North Carolina State University.

Reyes, G 2008, 'Static and low velocity impact behavior of composite sandwich panels with an aluminum foam core', *Journal of Composite Materials*, vol. 42, no. 16, pp. 1659-70.

Reynolds, T, Casagrande, D & Tomasi, R 2016, 'Comparison of multi-storey cross-laminated timber and timber frame buildings by in situ modal analysis', *Construction and building materials*, vol. 102, pp. 1009-17.

Saikia, P, Dutta, D, Kalita, D, Bora, JJ & Goswami, T 2015, 'Improvement of mechano-chemical properties of bamboo by bio-chemical treatment', *Construction and building materials*, vol. 101, pp. 1031-6.

Shams, A, Stark, A, Hoogen, F, Hegger, J & Schneider, H 2015, 'Innovative sandwich structures made of high performance concrete and foamed polyurethane', *Composite structures*, vol. 121, pp. 271-9.

Sharaf, T, Shawkat, W & Fam, A 2010, 'Structural performance of sandwich wall panels with different foam core densities in one-way bending', *Journal of Composite Materials*, vol. 44, no. 19, pp. 2249-63.

Sharma, B, Gatoo, A, Bock, M, Mulligan, H & Ramage, M 2014, 'Engineered bamboo: state of the art', *Proceedings of the Institution of Civil Engineers-Construction Materials*, vol. 168, no. 2, pp. 57-67.

Sharma, B, Gatóo, A, Bock, M & Ramage, M 2015, 'Engineered bamboo for structural applications', *Construction and building materials*, vol. 81, pp. 66-73.

Sikora, KS, McPolin, DO & Harte, AM 2016, 'Effects of the thickness of cross-laminated timber (CLT) panels made from Irish Sitka spruce on mechanical performance in bending and shear', *Construction and building materials*, vol. 116, pp. 141-50.

Sinha, A, Way, D & Mlasko, S 2013, 'Structural performance of glued laminated bamboo beams', *Journal of Structural Engineering*, vol. 140, no. 1, p. 04013021.

Smith, RE 2010, *Prefab architecture: A guide to modular design and construction*, John Wiley & Sons.

Sohel, K & Liew, JR 2011, 'Steel–Concrete–Steel sandwich slabs with lightweight core—Static performance', *Engineering structures*, vol. 33, no. 3, pp. 981-92.

Song, Z-z, Cheng, S, Zeng, T, Yang, F, Jing, S-d & Fang, D-n 2015, 'Compressive behavior of C/SiC composite sandwich structure with stitched lattice core', *Composites Part B: Engineering*, vol. 69, pp. 243-8.

Spacone, E & El-Tawil, S 2004, 'Nonlinear analysis of steel-concrete composite structures: State of the art', *Journal of Structural Engineering*, vol. 130, no. 2, pp. 159-68.

Steeves, CA & Fleck, NA 2004, 'Material selection in sandwich beam construction', *Scripta materialia*, vol. 50, no. 10, pp. 1335-9.

Steiger, R, Gülzow, A & Gsell, D 2008, 'Non destructive evaluation of elastic material properties of crosslaminated timber (CLT)', in *Conference COST E*, vol. 53, pp. 29-30.

Styles, M, Compston, P & Kalyanasundaram, S 2007, 'The effect of core thickness on the flexural behaviour of aluminium foam sandwich structures', *Composite structures*, vol. 80, no. 4, pp. 532-8.

Sun, Z, Shi, S, Guo, X, Hu, X & Chen, H 2016, 'On compressive properties of composite sandwich structures with grid reinforced honeycomb core', *Composites Part B: Engineering*, vol. 94, pp. 245-52.

Timoshenko, SP & Woinowsky-Krieger, S 1959, *Theory of plates and shells*, McGraw-hill.

Triantafillou, TC & Gibson, LJ 1987, 'Failure mode maps for foam core sandwich beams', *Materials Science and Engineering*, vol. 95, pp. 37-53.

Trujillo, DJA, Ramage, M & Chang, W-S 2013, 'Lightly modified bamboo for structural applications', *Proceedings of the Institution of Civil Engineers-Construction Materials*, vol. 166, no. 4, pp. 238-47.

Tuwair, H, Hopkins, M, Volz, J, ElGawady, MA, Mohamed, M, Chandrashekhara, K & Birman, V 2015, 'Evaluation of sandwich panels with various polyurethane foam-cores and ribs', *Composites Part B: Engineering*, vol. 79, pp. 262-76.

Valipour, HR & Crews, K 2011, 'Efficient finite element modelling of timber beams strengthened with bonded fibre reinforced polymers', *Construction and building materials*, vol. 25, no. 8, pp. 3291-300.

Van Erp, G & Rogers, D 2008, 'A highly sustainable fibre composite building panel', in *Proceedings of the international workshop on fibre composites in civil infrastructure–past, present and future*, pp. 1-2.

Vessby, J, Enquist, B, Petersson, H & Alsmarker, T 2009, 'Experimental study of cross-laminated timber wall panels', *European Journal of Wood and Wood Products*, vol. 67, no. 2, pp. 211-8.

Vinson, JR 1999, *The behavior of sandwich structures of isotropic and composite materials*, CRC Press.

Wang, Z, Fu, H, Gong, M, Luo, J, Dong, W, Wang, T & Chui, YH 2017, 'Planar shear and bending properties of hybrid CLT fabricated with lumber and LVL', *Construction and building materials*, vol. 151, pp. 172-7.

Wang, Z, Jing, L, Ning, J & Zhao, L 2011, 'The structural response of clamped sandwich beams subjected to impact loading', *Composite structures*, vol. 93, no. 4, pp. 1300-8.

Wicks, N & Hutchinson, JW 2001, 'Optimal truss plates', *International Journal of Solids and Structures*, vol. 38, no. 30-31, pp. 5165-83.

Wood Handbook: Wood as an Engineering Material 2010a, Centennial Edition edn, vol. 190, Department of Agriculture, Forest Service, Forest Products Laboratory, Madison, WI: U.S.

Wood Handbook: Wood as an Engineering Material 2010b, Centennial Edition edn, Department of Agriculture, Forest Service, Forest Products Laboratory, Madison, WI: U.S.

Wood Solutions design and build 2019, *LifeCycle Tower one - 8 stories of wood-concrete*, <https://www.woodsolutions.com.au/Inspiration-Case-Study/LifeCycle-Tower-One>.

Xiong, J, Ma, L, Wu, L, Li, M & Vaziri, A 2011, 'Mechanical behavior of sandwich panels with hollow Al–Si tubes core construction', *Materials & Design*, vol. 32, no. 2, pp. 592-7.

XLam 2016, *Designing with XLam Cross Laminated Timber*, XLam CROSS LAMINATED TIMBER, <www.xlam.co.nz>.

Xu, B, Bouchaïr, A, Taazount, M & Vega, E 2009, 'Numerical and experimental analyses of multiple-dowel steel-to-timber joints in tension perpendicular to grain', *Engineering structures*, vol. 31, no. 10, pp. 2357-67.

Xu, B, Taazount, M, Bouchaïr, A & Racher, P 2009, 'Numerical 3D finite element modelling and experimental tests for dowel-type timber joints', *Construction and building materials*, vol. 23, no. 9, pp. 3043-52.

Yawalata, D & Lam, F 2011, 'Development of technology for cross laminated timber building systems', *Vancouver, BC: University of British Columbia*.

Zhang, F, Liu, W, Ling, Z, Fang, H & Jin, D 2018, 'Mechanical performance of GFRP-profiled steel sheeting composite sandwich beams in four-point bending', *Composite structures*, vol. 206, pp. 921-32.

Zhou, Q 2013, 'Development of evaluation methodology for rolling shear properties in cross-laminated timber (CLT)', Master's Thesis, the University of New Brunswick, Fredericton, Canada.

Zhou, Q, Gong, M, Chui, YH & Mohammad, M 2014, 'Measurement of rolling shear modulus and strength of cross laminated timber fabricated with black spruce', *Construction and building materials*, vol. 64, pp. 379-86.